UNIVERSITY OF SALFORD

Computational Studies of Hydrogen in Palladium

by

Ian Keith Robinson

A thesis submitted in partial fulfillment for the
degree of Doctor of Philosophy

in the
School of Computing, Science & Engineering
College of Science & Technology
University of Salford
Salford
UK

July 2015

Declaration of Authorship

I, Ian Robinson, declare that this thesis titled, 'Computational Studies of Hydrogen in Palladium' and the work presented in it are my own. I confirm that:

- This work was done wholly or mainly while in candidature for a research degree at this University.
- Where any part of this thesis has previously been submitted for a degree or any other qualification at this University or any other institution, this has been clearly stated.
- Where I have consulted the published work of others, this is always clearly attributed.
- Where I have quoted from the work of others, the source is always given. With the exception of such quotations, this thesis is entirely my own work.
- I have acknowledged all main sources of help.
- Where the thesis is based on work done by myself jointly with others, I have made clear exactly what was done by others and what I have contributed myself.

Signed: Ian Keith Robinson

Date: 4-January, 2015

"There are few laws more precise than those of perfect molecular chaos."

Professor George Porter -The Laws of Disorder

"The probable is what usually happens."

Aristotle

UNIVERSITY OF SALFORD

Abstract

School of Computing, Science & Engineering
College of Science & Technology

Doctor of Philosophy

by Ian Keith Robinson

A series of Monte-Carlo investigations on the Palladium Hydrogen system are presented. It is demonstrated that a simple long-range concentration-dependent attractive force reproduces the form of the pressure-composition isotherms well. Short range pairwise repulsive forces reproduce much of the hydrogen ordering seen within the lattice. A suitable scaling between the long and short range forces has been found which appears to reproduce both the isotherms and the short-range ordering to a reasonable degree.

Programs have been written to generate virtual diffractograms in 1d and 2d in order to observe ordering in the simulations and inform those performing experimental diffraction studies

Studies have been performed of the isotope dependence of absorption taking into account the differing zero point energies of the three hydrogen isotopes.

Acknowledgements

With many thanks to Professor Keith Ross for his quite unreasonable patience and clear guidance.

Contents

List of Figures

List of Tables

Nomenclature

$C_{V,P}$	Heat capacity at constant volume or pressure
C_H	Hydrogen Concentration, interchangeable with r_H
D_t	Tracer Diffusion Coefficient
F	Helmholtz free energy
G	Gibbs Free Energy
$\mathbf{G}$	Reciprocal lattice vector
H	Enthalpy
$\mathcal{H}$	Hamiltonian
J	Particle flux
K_H	Sieverts Constant
N	Number of atoms or sites
P	Total Pressure
P_i	Partial pressure of i^{th} component
Q	Heat
S	Entropy
T	Thermodynamic Temperature
T_c	Critical temperature
U	Internal Energy of a system
V	Interaction potential
Z	Partition Function
d	Differential
f_p	Fugacity
f_t	Tracer Correlation factor
$g(r)$	Pair distribution function
$I(\mathbf{q})$	Coherent Scattering Function
k	Boltzmanns constant
$\mathbf{k}$, $\mathbf{k}'$	Incident and scattered vectors

p	probability
$\mathbf{q}$	Scattering Vector
$\mathbf{r_i}$	position vector of i^{th} atom
t	time
Γ	atomic jump frequency
Ω	Multiplicity of a system
α_{HD}	Separation Factor
α_{WC}	Warren-Cowley short range order parameter
α	(phase) low concentration disordered state
β	(phase) higher concentration ordered state
∂	Partial derivative
δ	delta function
$đ$	Inexact differential
μ	chemical potential
θ	concentration as $\frac{N_H}{0.59N_{Pd}}$ following Lacher [90]

To my wife Tamara who has put up with me staring at a computer screen for most of our marriage. For my boys, Nathan, Saul and Ezra for their enthusiasm which has kept mine up.

Preface

Presented are the results of extensive Monte-Carlo testing of a model of hydrogen in palladium incorporating short-range repulsive pairwise interactions and long-range attraction. The report starts with a discussion of the theoretical background of the Pd-H system. This is followed by an overview of Monte-Carlo simulations of lattice gases. Given that we are attempting to reproduce short-range ordering which is typically investigated using neutron scattering a further section presents how virtual diffraction patterns may be generated from an unknown structure.

Bridging this background with the detail of the simulations Chapter 4 explains in more detail the specifics of the modelling.

Chapter 5 looks at how a suitable scaling between long and short-range forces was found. Given that we are now in a position to produce hopefully meaningful simulations Chapter 6 looks at short-range ordering. The next absorption and desorption from an external gas phase for a single isotope system. Chapter 8 discusses diffusion within the palladium lattice and Chapter 9 discusses modelling systems containing more than one isotope.

Finally brief conclusions and various appendices are presented.

Copies of the code may be downloaded from http://usir.salford.ac.uk
or www.starfishprime.co.uk

Chapter 1

Background Theory

1.1 The Palladium-Hydrogen System

Palladium will readily absorb hydrogen from the gaseous state. At the metal's surface H_2 dissociates into protons with the electrons dispersing into the metallic electron cloud. The proton being much smaller than inter-atomic distances can reside at the inter-metallic interstitial positions and diffuse through the lattice.

Palladium's interaction with hydrogen is particularly interesting, it has been widely studied and has lead to significant applications. It is the only element that will absorb appreciable concentrations of hydrogen at room temperature and the only one which can undergo repeated ab/desorption cycles without pulverising [78]. First identified in 1803, palladium is the least dense of the 'platinum group' metals and a key component in hydrogen sensors, catalytic converters and fuel cells. Its peculiar affinity for hydrogen was first observed by Thomas Graham in 1866. It recently achieved some notoriety for its use in the Fleischmann-Pons cold fusion claims [55]. Palladium will readily adsorb hydrogen at room temperature to a 1:0.7 composition though this can be pushed to 1:1 at higher effective pressures via electrochemical loading. There is some evidence of loading above 1:1 which may result from hydrogen occupying tetrahedral as well as octahedral interstitials though this is controversial. More generally accepted is the formation of extra vacancies in the palladium sub-lattice at high external gas pressure (see section 1.2.3).

Since desorption occurs as readily as absorption the mechanism of hydrogen uptake in palladium is of great interest in the development of materials for hydrogen storage

systems. Hydrogen fuel cells appear to offer one of the better proposals for powering electric vehicles due to hydrogen's high energy density. The development of a suitable safe storage system for hydrogen gas could contribute greatly to widespread application of this technology. Whilst palladium's high price may prohibit widespread bulk applications it will certainly find use as a safe tritium storage medium for a fusion power plant.

As the hydrogen isotopes diffuse at different rates [100] and display differing solubilities [95, 146, 122], palladium membranes have potential in hydrogen isotope separation.

Note: throughout 'hydrogen' refers non-specifically to any hydrogen isotope. 'H', 'D' or 'T' refer to atomic hydrogen generally in the lattice whereas 'HH', 'HD', 'HT' and so on refer to molecular hydrogen in the gas phase.

1.2 Crystal Structure

Palladium forms a face-centred cubic metallic lattice. In the case of Pd-H the consensus appears to be that hydrogen ions reside on the octahedral interstitials distributed around the palladium. These interstitials thus also form an fcc lattice structure – much like rocksalt (fig 1.1). i.e. the palladium lattice structure does not change on hydrogen loading. Hydrogen ions experience electrostatic repulsion and below a critical temperature will tend to form the $I4_1/amd$ (spacegroup 141) structure around $\frac{H}{Pd} \sim 0.6 \rightarrow 0.7$ - the so-called *50K anomaly* (section 1.2.2). Neutron diffraction indicates that in solid pal-

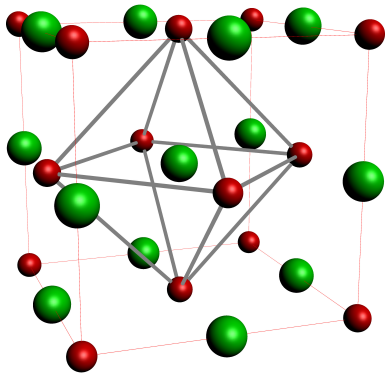

FIGURE 1.1: Pd−H – rocksalt structure, grey lines to octahedral interstitials

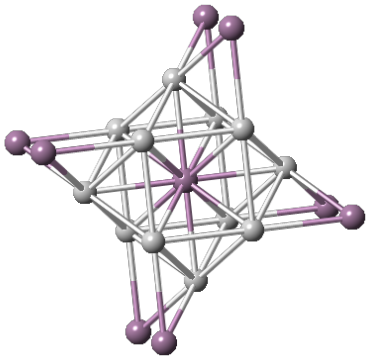

FIGURE 1.2: Ni_4Mo – I4/m structure

bonds drawn for ease of visualisation

ladium hydrogen occupies the octahedral fcc interstitials around the fcc palladium sites

[107]. Pd−H exists in two phases α and β . At room temperature the α phase forms on its own up to a concentration of Pd−$H_{0.02}$ disappearing above Pd−$H_{0.58}$. The resulting phase diagram is dominated by a miscibility gap (a two phase region) with the α low concentration disordered region on one side and a higher concentration ordered β upon the other fig:1.3. Both phases are present until 0 58 where the alpha phase disappears. A key significance of this is that hydrogen undergoes significant ab/desorption at similar constant pressures i.e $\sim$ atmospheric pressure at $\sim$ 420K [78]. This miscibility gap disappears at a critical temperature T_c as reported by Joubert [78] at 566K see fig 1.3.

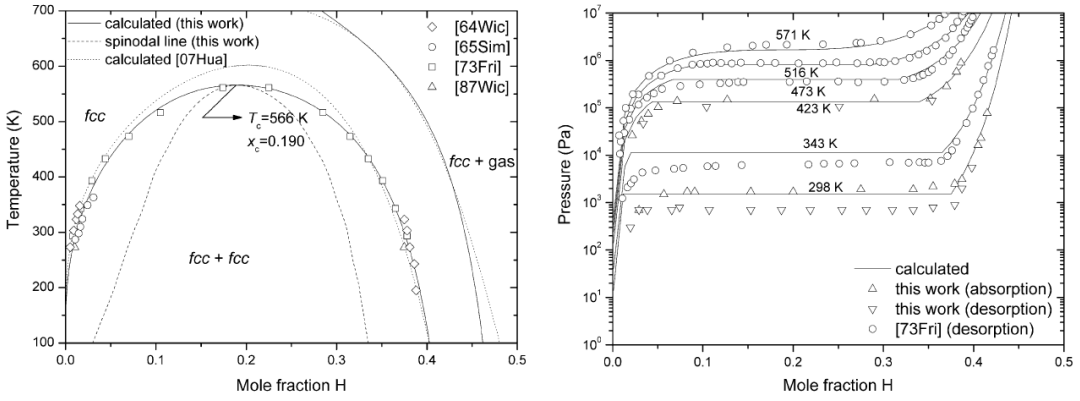

FIGURE 1.3: Miscibility Gap: the left-hand graph represents $p = 1 \times 10^7 Pa$ [78]

McLennan et al. [107] report pure palladium's fcc structure has a lattice parameter of 3.890Å rising to $\simeq$ $4.05\mathring{A}$ at H/Pd of 1.0 with the volume increasing by approx. 11% going from α to β phase. This relatively modest expansion compares to the much larger values seen in other hydrides such as UH_3 where the volume expands by a factor of almost 2 [168]. The mechanical strain in the lattice may be responsible for the observed hysteresis in the absorption and desorption curves. In the case of palladium since the volume expansion is relatively small one could expect hysteresis to be fairly small. Thus absorption/desorption pressures should be similar. If this could be replicated in a cheaper material we may be closer to developing a matrix suitable for commonplace hydrogen storage. Wicke and Blaurock presented a study which indicates that the desorption route represents a 'true strain free equilibrium'. They appear to argue that absorption is associated with the formation of dislocations leading to higher absorption pressures. It may be presumed the desorption pressure is lower due to ions being trapped upon the dislocations [167].

Pitt and Gray [137] report evidence from neutron diffraction experiments that a significant fraction of deuterons (14% in one experiment) may reside at the tetrahedral interstitials around the palladium. One may reasonably assume that this would also be the case for hydrogen. A question being whether the deuterons reside only temporarily in the tetrahedral sites as they necessarily diffuse from *o-site* to *o-site* via *t-site* or whether occupancy is thermodynamically stable. Elsasser et al. [46] argue, on the basis of ab-initio energy calculations, for deuterium and tritium occupancy of tetrahedral interstitials.

1.2.1 Phase Changes

The phase changes during ordering may be characterised as either first or second order. A first order transition presents as a discontinuity in some state variable such as mean site interaction potential and thus a change in enthalpy. A second order will be continuous in energy but characterised by a microscopic ordering change observable by a change in local ordering parameter, in this case such as n.n. or n.n.n occupancy rates.

1.2.2 The 50K Anomaly

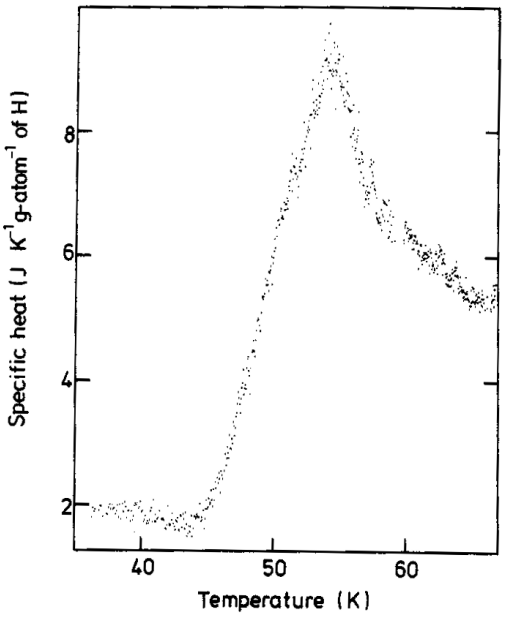

FIGURE 1.4: Temperature dependence of the specific heat for a Pd-H alloy (H/Pd = 0.63) in the 50 K temperature region [45]

Studies of the specific heat of Pd-H by Eichenauer & Schaefer in 1956 showed anomalous behaviour at a temperature of 50K, specifically a time dependent release of heat fig:1.4. Further work by Jacobs and Manchester [73] at C=0.63 H/Pd discounted relaxation of defects and indicated that diffusion leading to a phase transition was the cause. Anomalous behaviour was also observed in measurements of resistivity, Hall effect and internal friction. Anderson et al. [4] in 1978 reported neutron diffraction studies of Pd-D at C=0.64 in which they observed superlattice reflections at $\left(\frac{1}{2}10\right)$ which they interpreted as being due to relatively short-range ordering of D on the octahedral interstitials to a range of at least $25\mathring{A}$ compared to a lattice parameter of $\sim 4\mathring{A}$. Shortly afterwards Ellis and Satterthwaite [45] performed neutron diffraction studies of Pd-H and Pd-D at C=0.78 and T=60K. After an annealing time of up to 2 weeks they reported superlattice reflections at $\left(\frac{4}{5}\frac{2}{5}0\right)$ corresponding to the Ni_4Mo structure, I4/m (space-group 87). This should be apparent as four filled followed by one empty plane in the [420] plane. Here was evidence of a complex concentration as well as a temperature dependent phase structure.

1.2.3 Superabdundant Vacancies

Hydrogen concentrations as high as 1.2 H/Pd have been reported by Fukai et al. [53, 54]. Here Pd and Ni were exposed to hydrogen gas pressures of the order of 2-5 GPa. After removing the hydrogen by heating at a low temperature there remained a residual lattice expansion that was eliminated on annealing at high temperature. This they explained by the formation of Frenkel defects where the Pd atoms were forced to occupy interstitial sites leading to additional vacancies in the metal lattice which could also account for the much higher hydrogen diffusivity reported. It was surmised that these metal vacancies could trap up to 6 deuterons and further that the vacancy-hydrogen cluster could then migrate through the lattice from the surface.

1.3 Some Pertinent Thermodynamic Relationships

Since nanoscale ordering results from systems minimising their free energy it is worth reviewing some basic thermodynamics.

Enthalpy (H) is the total thermodynamic energy of a system being the sum of its internal energy (U) and the energy of formation at constant temperature and pressure, i.e,

that required to displace the surrounding environment (PV).

$$H = U + PV \tag{1.3.1}$$

When hydrogen enters or leaves palladium we may measure the change in enthalpy

$$\Delta U = T\Delta S - P\Delta V \tag{1.3.2}$$

thus as the specific heat capacity

$$C_P = \left(\frac{\delta U}{\delta T}\right)_P = T\frac{\delta S}{\delta T} \tag{1.3.3}$$

$$S = \int_0^T \frac{C_p}{T} dT \tag{1.3.4}$$

In a numerical simulation we should be able to determine the entropy of a large assembly by simply numerically integrating the specific heat, as $C_{V,P} = \frac{\delta E}{\delta T}$ if we have correctly factored in the inter-atomic interactions.

Gibbs Free Energy (G) can be defined as the maximum work which may be obtained from a system, for example by a chemical reaction.

$$G = H - TS \tag{1.3.5}$$

thus

$$G = U + PV - TS \tag{1.3.6}$$

the enthalpy, the internal energy of the system minus TS the energy of formation that is extracted from the surroundings.

Helmholtz Free Energy (F) can be considered as the maximum work which may be obtained from a system at fixed pressure and volume.

$$F = U - TS \tag{1.3.7}$$

Note: since the volume expansion of the Pd-H lattice is relatively small at approx 11% $P\delta V$ is negligible. Thus

$$\delta H = T\delta S + P\delta V \simeq T\delta S \quad (1.3.8)$$

$$\delta U = T\delta S - P\delta V \simeq T\delta S \quad (1.3.9)$$

$$\delta F = -P\delta V - S\delta T \simeq -S\delta T \quad (1.3.10)$$

$$\delta G = V\delta P - S\delta T \quad (1.3.11)$$

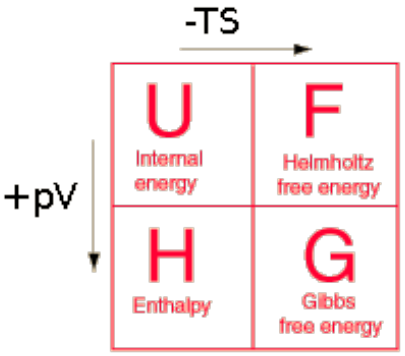

1.3.1 Entropy

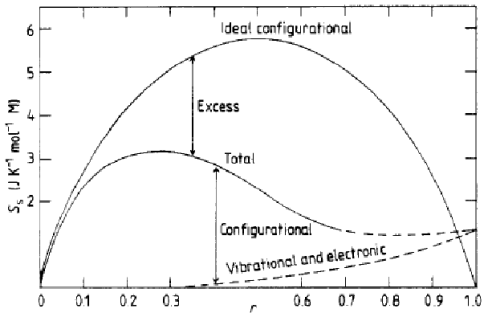

FIGURE 1.5: Contributions to total entropy [87]

Willard Gibbs once referred to entropy as a measure of the 'mixed-up-ness' of a system[1]. However it may be more helpful to regard it as a measure of how evenly energy is distributed within a system and thus how much of the energy is *not available* to do work. Entropy has three components, configurational, electronic, and vibrational (see fig 1.5) where:-

$$S = S_{config} + S_{electronic} + S_{vibrational}$$

In the context of physical systems we have two approaches to defining entropy, the broadly empirical classical thermodynamics of Clausius et. al. and the theoretical statistical approach pioneered by Boltzmann. Starting with the classical view from Clausius we have the macroscopic definition

$$\Delta S = \frac{\Delta Q_{rev}}{T} \quad (1.3.12)$$

where ΔS is the change in entropy and ΔQ_{rev} the reversible energy added to the system.

[1] a fragmentary reference in an incomplete work [61]

Moving to a microscopic statistical definition, the Gibbs Configurational Entropy of a system may be defined as the sum

$$S_{Gibbs} = -k_B \sum_i p_i \ln(p_i) \tag{1.3.13}$$

where p_i is the probability that the system is in the ith microstate. Assuming that all the microstates have equal probability then if $n_{states} = \Omega$ then $p_i = \frac{1}{\Omega}$ giving Boltmann's famous equation

$$S_{config} = k_B \ln \Omega \tag{1.3.14}$$

1.3.1.1 Variation of Configurational Entropy with Concentration

If we have N_v non-interacting vacancies randomly distributed upon a total array of N_L sites then

$$\Omega = \frac{N_L!}{N_v! N_{occupied}!} = \frac{N_L!}{N_v!(N_L - N_v)!} \tag{1.3.15}$$

Applying Stirling's approximation

$$\ln N! = \sum_{k=1}^{N} \ln k = \int_1^N \ln x dx = [x \ln x - x]_1^N = N \ln N - N + 1 \approx N \ln N - N \tag{1.3.16}$$

gives

$$\Delta S = k[N_L \ln N_L - N_v \ln N_v - (N_L - N_v) \ln(N_L - N_v)] \tag{1.3.17}$$

thus

$$\Delta S \simeq k[N_v \ln N_L - N_v \ln N_v] = k \left(N_v \ln \frac{N_L}{N_v} \right) \tag{1.3.18}$$

$$= -k \left(N_v \ln \frac{N_v}{N_L} \right) \tag{1.3.19}$$

The change in Gibbs free energy caused by the addition of a vacancy to a filled lattice is given by

$$\Delta G = \Delta H - T \Delta S \tag{1.3.20}$$

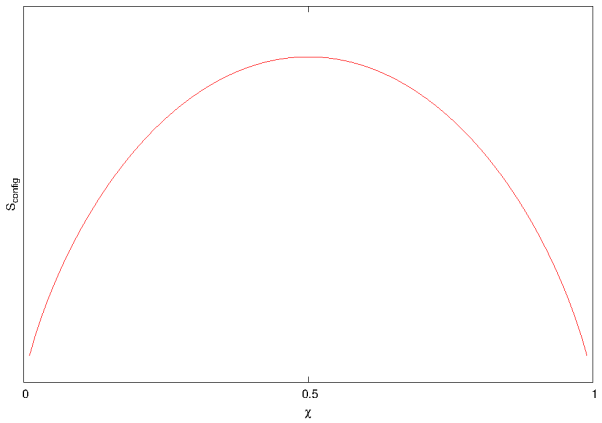

FIGURE 1.6: ΔS_{config} vs r

and the total entropy

$$\Delta S = \Delta S_{config} - \Delta S_{thermal} \tag{1.3.21}$$

where the equilibrium vacancy concentration r occurs when the free energy is minimised. The configurational entropy as a function of vacancy concentration is given by

$$\Delta S_{config} = Nk(r \ln r + (1-r)\ln(1-r)) \tag{1.3.22}$$

i.e.

$$\Delta S = \Delta S_{vacant} + \Delta S_{occupied} \tag{1.3.23}$$

In the case of a binary mixture of A and B in fractional concentrations r_A and r_B. The concentration of empty sites is given by $1-(r_A+r_B)$. Thus fig 1.6.

$$\Delta S_{config} = Nk_B\left(S_A + S_B + S_{Vacant}\right) \tag{1.3.24}$$

$$= Nk_b\left[r_A \ln r_A + r_B \ln r_B + (1-r_A-r_B)\ln\left(1-r_A-r_B\right)\right]. \tag{1.3.25}$$

The chemical potential, μ being the change in entropy per addition of a new atom is

$$\mu_A = \frac{d\left(\frac{S}{Nk_B}\right)}{dr_A} \tag{1.3.26}$$

In a M.C. or molecular dynamics simulation this may be determined via Widom's virtual particle method [170].

1.3.1.2 Vibrational Entropy

Vibrational entropy arises from the quantised lattice vibrations. A complex quantity to determine analytically it may simply be determined experimentally from the heat capacity.

$$\Delta S_{vibrational} = \int_{T_0}^{T} \frac{C_p}{T} dT \tag{1.3.27}$$

1.3.1.3 Electronic Entropy

Electronic entropy arises when electrons are able to occupy higher energy orbitals. In these simulations he hydrogen's electron was assumed to be in the ground state for temperatures $T <\sim 10^3 K$

1.3.2 Chemical Potential

Chemical potential can be a somewhat elusive concept. The definition is simple though being the change in free energy occasioned by the addition or removal of a single particle at fixed volume & temperature.

$$\mu = \left(\frac{\partial F}{\partial N}\right)_{V,T} = -k_B T \ln\left(\frac{Z_{N+1}}{Z_N}\right) \tag{1.3.28}$$

where F is the Helmholtz Free Energy, Z_N is the partition function for N particles and μ is equal to the molar Gibbs Free Energy

$$\mu = G_{mol} = \frac{G}{n_{moles}} \tag{1.3.29}$$

thus from $\mathrm{d}G = V\mathrm{d}P - S\mathrm{d}T$ keeping T constant and varying P gives

$$\mathrm{d}G = V\mathrm{d}P \tag{1.3.30}$$

increasing the pressure from P_1 to P_2

$$G(P_2) - G(P_1) = \int_{P_1}^{P_2} V\mathrm{d}P \tag{1.3.31}$$

$$G(P_2) = G(P_1) + \int_{P_1}^{P_2} V\mathrm{d}P \tag{1.3.32}$$

since for an ideal gas $V = \frac{nRT}{P}$

$$G(P_2) = G(P_1) + \int_{P_1}^{P_2} \frac{nRT}{P} \mathrm{d}P \tag{1.3.33}$$

$$G(P_2) = G(P_1) + nRT \ln\left(\frac{P_2}{P_1}\right) \tag{1.3.34}$$

dividing by n moles and setting P_1 to be some standard pressure p^0gives

$$\frac{G(P_2)}{n} = \frac{G(P_1)}{n} + RT \ln\left(\frac{P_2}{P^0}\right) \tag{1.3.35}$$

therefore

$$\mu_2 = \mu_1 + RT \ln\left(\frac{P_2}{P^0}\right) \tag{1.3.36}$$

The chemical potential of a fluid may be described via two terms, the *ideal* and *excess* potentials

$$\mu = \mu^{\oslash} + \mu^* \tag{1.3.37}$$

where $\mu^{\oslash}$ is the chemical potential of an ideal gas and μ^* the excess chemical potential - the deviation from ideality. This deviation from ideality i.e. the effective pressure is described as the *fugacity* f_p

$$\mu = \mu^{\oslash} + RT \ln\left(\frac{f_P}{P_0}\right) \tag{1.3.38}$$

hence

$$\mu = \mu^{\oslash} + RT \ln\left(\frac{P_{effective}}{P_0}\right) \tag{1.3.39}$$

therefore

$$\mu = \mu^{\oslash} + RT \ln\left(P'\right) \tag{1.3.40}$$

Therefore for an ideal gas where the fugacity is equal to the partial pressure P_i the chemical potential is proportional to the partial pressure $\ln P_i$. The partial pressure of a component of a gaseous mixture is simply the pressure that the specified component would have if all the other components were removed and it was left to fill the volume by itself (see fig1.7).

Thus for a mole fraction of component χ_i of a mixture at pressure P, the partial pressure $P_i = \chi_i P$ and thus the chemical potential

$$\mu_i \propto \ln P_i \propto \ln(r_i P) \tag{1.3.41}$$

The chemical potential μ of a lattice gas thus varies as $\mu = R\ln(\frac{r}{1-r})$ see fig 1.7.

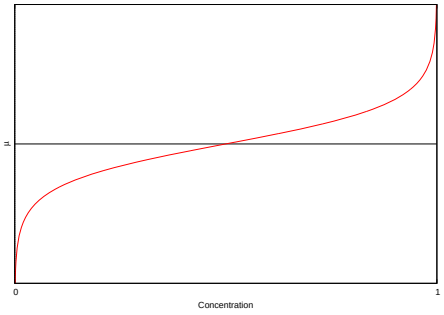

FIGURE 1.7: μ vs r –no interactions theory

1.3.3 Heat Capacity

The heat capacity is of particular significance when considering the behaviour of H in Pd at the 50K anomoly. In the constant volume of the lattice it indicates how energy is partitioned between a system's degrees of freedom. Here quantum effects come into play.

Starting from the definition

$$C_H = \frac{\delta U}{\delta T} \text{ and the classic result for an ideal gas } E_{kinetic} = U_{trans} = \frac{3}{2}k_b T \tag{1.3.42}$$

we have:

$$C = \frac{\delta U}{\delta T} = \frac{3}{2}k_b T \tag{1.3.43}$$

The hydrogen atom sitting at a site however has vibrational energy and thus a contribution to C. Treating H as a simple harmonic oscillator we have as solutions to the Schrödinger equation:

$$E_{vib} = \left(n + \frac{1}{2}\right)\hbar\omega \tag{1.3.44}$$

where n is the vibrational quantum number. This results in equally spaced energy levels at intervals of $\hbar\omega$.

The Einstein model treats each atom simply as a vibrator in a parabolic potential uncoupled to its neighbours.

1.3.4 Thermodynamics of Ab/Desorption

The chemical potential of gaseous atomic hydrogen is half that of the molecular form hence:-

$$\mu_H = \frac{1}{2}\mu_{HH} \tag{1.3.45}$$

$$\mu_H = \mu_H^{\oslash} + kT \ln P_{HH} = \frac{1}{2}\left(\mu_{HH}^{\oslash} + kT \ln r_H P^0\right) \tag{1.3.46}$$

where χ_H is the mole fraction of H, $\mu^{\oslash}$ is the chemical potential at standard pressure P^0 and P_{HH} the partial pressure of H_2. Strictly we should use the fugacity f_P rather than P_{HH} in the case of a non-ideal gas.

This can be rewritten as

$$exp\left(\frac{-\Delta G_f^0(H)}{kT}\right) = \left(\frac{\chi_H}{(P_{HH}/P^0)}\right) \tag{1.3.47}$$

Here $\Delta G_f^0(H)$ is the free energy of formation of hydrogen in the lattice from the gas at standard pressure and temperature.

1.4 Isotope Effects

The Pd-H system displays an unusual *reverse isotope effect*. Simplistically one would assume that Deuterium and Tritium's higher masses and thus lower vibrational frequencies would lead to lower diffusion rates and lower superconducting temperatures than for protium. In reality the inverse is seen. The diffusivity effect is assumed to be due to marked differences in their respective zero point energies in both the gas and solid phases.

Differences can be observed between the different regions on the phase diagram. In the $\alpha + \beta$ mixed phase region adding D causes the total concentration to increase whilst adding D_2 to the β region tends to displace H whilst leaving the concentration unchanged [99]. Understanding this process may give insights into the design of isotope separation systems involving palladium membranes.

Considering the diffusivity within the lattice, it is reasonable to postulate that protium's higher ZPE will raise its energy closer to the energy barrier between sites and thus make site exchanges more probable. One could also argue that since the site exchange rate is likely to be dependent upon the vibrational frequency again the lighter isotope should diffuse more rapidly. Experimentally the diffusion rate is higher for deuterium. Vineyard [163] argued for a more sophisticated approach in which all modes of vibration were considered. Specifically that aligned with the saddle point separating the two sites in question.

It should be simple to model this in a simulation by setting ZPE offsets to be added to the interaction potentials for each site before a jump probability is calculated or conversely setting offsets to the activation energies for the different isotopes.

Looking now at ab/desorption. Taking the values from fig:1.8, the drop in ZPE of H vs D is -0.63 vs. 0.47 eV per atom which should make the solution of H more energetically favoured than D and thus in part account for the greater solubility of H over D. Again this could be factored into the chemical potentials of the molecular isotopes in the gas phase.

Deuterium molecules in the gas phase have a lower zero-point energy than molecular Hydrogen by virtue of their larger mass which leads to lower vibration frequencies. Thus it requires more energy to break the D–D bond vs the H–H bond.

As the energy of a quantum harmonic oscillator is given by

$$E_n = h\nu\left(n + \frac{1}{2}\right) \tag{1.4.1}$$

with

$$\nu \propto \frac{1}{\sqrt{m}} \tag{1.4.2}$$

the frequency ν will vary as approx $\frac{1}{\sqrt{m}}$. Thus doubling the mass from H to D should lead to $E_D \approx \frac{1}{\sqrt{2}}E_H$. It is clear from the values given in fig: 1.8 that hydrogen's potential is anharmonic.

The key questions here are accurately modelling the isotope dependence of adsorption, desorption and diffusion through the lattice.

- The diffusion constant for D in Pd is faster than that of H (3.8×10^{-11} vs. $5.5 \times 10^{-11} m^2 s^{-1}$) at 298K [53]

- In the α phase the solubility of $H > D$ as $T \to \infty$.

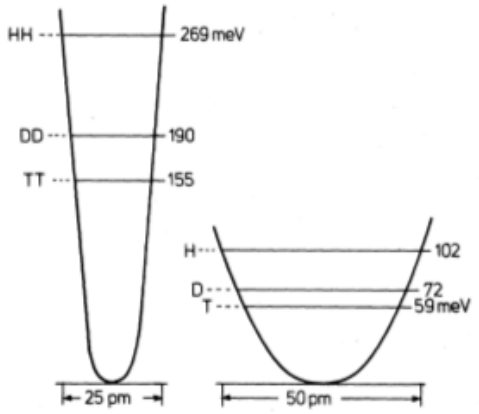

FIGURE 1.8: Potential wells and zero-point energies of the gas (left) and atoms (right) in the octahedral sites of the Pd lattice. The atom zero-point energies are scaled up per atom for the threefold degeneracy and must be counted twice for comparison with molecular energies. [92]

1.4.1 Separation Factor

In a gaseous mixture of H_2 and D_2 some DH will form in equilibrium with the other two molecules. We can define an equilibrium constant initially in terms of the partial pressures P

$$K_{HD} = \frac{P_{HD}^2}{P_{H_2} P_{D_2}} \tag{1.4.3}$$

$$= \frac{\left(\frac{n_{HD}}{n_{total}} P\right)^2}{\left(\frac{n_{H_2}}{n_{total}} P \times \frac{n_{D_2}}{n_{total}} P\right)} \tag{1.4.4}$$

$$= \frac{(n_{HD})^2}{(n_{H_2} \times n_{D_2})} \tag{1.4.5}$$

The separation factor α_{HD} quantifies the differing mix of isotopes between the gas and solid phases. It is commonly defined [53] as:-

$$\alpha_{DH} = \frac{(\chi_g/\chi_s)_D}{(\chi_g/\chi_s)_H} \tag{1.4.6}$$

Thus as the concentration of H in the solid phase increases relative to D, $\alpha_{HD} \to \infty$.

1.5 Basic Theoretical Models of the Pd-H System

1.5.1 The Lacher model

In a seminal paper John Lacher [90] proposed that the two phase region resulted from a long-range attraction between protons. As hydrogen is added the increasing lattice distortion leads to an attractive force via some unknown mechanism. Many studies have shown that the lattice expands approximately linearly with concentration fig:1.9. Furthermore the expansion rates differ between hydrogen isotopes. It is this expansion which is generally accepted leads to a long-range isotopic concentration dependent attraction felt by hydrogen atoms within the lattcie

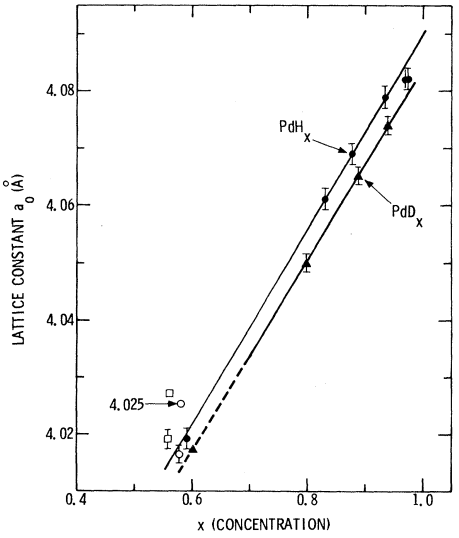

FIGURE 1.9: Expansion of Pd lattice for β-Pd$-$H and β-PdD [151]

As a transition metal palladium possesses overlapping *d* and *s* orbitals accommodating up to 2 and 10 electrons, respectively. With only 10 electrons available these bands are incompletely filled. Measurements of paramagnetic susceptibility against hydrogen concentration suggest that the *d* band is filled at between 0.53 and 0.66 H per Pd and that hydrogen absorption in the *d* band will reach a maximum at a concentration of $C_H \sim 0.6\frac{H}{Pd}$. Thus it is commonly convenient to define a concentration of $\theta = \frac{C_H}{0.6}$. [3] Starting with the assumption that the total average absorption energy of N_H hydrogen atoms within a lattice of N_s sites in their lowest energy states E_0 is given by a Bragg-Williams approximation of

$$< E >= -N_H E_0 - \frac{1}{2}\frac{N_H^2 E_0}{N_s} \tag{1.5.1}$$

Thus

$$\frac{\partial E}{\partial N_H} = -E_0 - \frac{N_H E}{N_s} \tag{1.5.2}$$

ie. the rate of increase of the absorption energy is proportional to C_H.

Through an extended derivation considering the partition function of the hydrogen and Gillespie's vapour pressure equation

$$\Delta H = \int_0^{N_s} k \left(\frac{\partial log_e P^{\frac{1}{2}}}{\partial T^{-1}} \right)_{N_s} \delta N_s \tag{1.5.3}$$

Lacher showed that the heat of adsorption

$$-\Delta H = 8535 n_H + 9443 n_H^2 \text{ Joules per mol} \tag{1.5.4}$$

Of pressure vs. composition it may be shown that

$$log\left(P^{\frac{1}{2}}\right) = log\left(\frac{\theta}{1-\theta}\right) - \frac{\left(\chi_0 - \frac{1}{2}\chi_d + \theta_\chi\right)}{kT} + logA. \tag{1.5.5}$$

As $logA$ varies little with temperature this gives

$$log\left(P^{\frac{1}{2}}\right) = log\left(\frac{\theta}{1-\theta}\right) + 2.3009 - \frac{(445.6 + 986.7\theta)}{T} \tag{1.5.6}$$

From equation 1.5.1 dividing through by N_s gives

$$\frac{< E >}{N_s} = -\frac{M_s E_0}{N_s} - \frac{1}{2}\frac{M_s^2 E}{N_s^2} = \frac{< E >}{N_s} = -\theta E_0 - \frac{1}{2}\theta E \tag{1.5.7}$$

$$\frac{< E >}{N_s} = -\theta E_0 \left(1 - E^{'}\theta\right) \tag{1.5.8}$$

Making the assumption that the increase in energy is proportional to the long-range attractive potential V_{LR} implies that

$$V_{LR} = -k\theta \left(1 - k^{'}\theta\right) \tag{1.5.9}$$

$T_{critical}$	566K	$C_H \simeq 0.29$	[168]
T_1	343K	$C_H \sim 0.025$	[102]
T_2	343K	$C_H \sim 0.58$	[102]

TABLE 1.1: Some key values

the question now becomes how to determine k and $k^{'}$.

1.5.2 The Alefeld Model

In a seminal paper George Alefeld in 1972 [3] proposed a mechanism for long-range attraction in hydrogen-metal systems as a result of expansion of the metal lattice. He suggested that as hydrogen enters the lattice it displaces surrounding metal atoms leading to a long-range displacement around the hydrogen falling off as $1/r^2$ which could be observed as a variation from the expected density of the sample. In the case of the palladium fcc lattice this expansion should be isotropic. Variation in the strain energy should be observed in plots of enthalpy vs concentration, see fig: 5.3. Alefeld suggested that this elastic interaction could be described by an elastic dipole tensor, analogous to an electric dipole tensor used to describe electric dipole moments.

1.5.3 Short-Range Repulsive Forces

Whilst the long-range attraction is responsible for the ab/desorption characteristics it will not impose any significant short-range tendency to order. Here we need to factor in the short-range Coulomb repulsion between the protons. See section 4.4.3.

Chapter 2

The Simulation Models

2.1 The Monte Carlo Method

The Monte-Carlo technique when applied to the Ising model involves the random sampling of a system to determine some numerical solution. It is especially useful for complex systems with many variables which are impractical to solve analytically. Here the approach is to allow atoms to jump between adjacent sites with a probability determined by the difference in potential between the locations. This simulates the random nature of statistical mechanics correctly reproducing entropy effects and energy distributions.

2.1.1 The Lattice Gas Model

Lattice gas models are a class of cellular automata (C.A.) which model the microscopic behaviour of fluids as a set of cells upon a regular lattice. The state of a cell is dependent upon that of its neighbours and a system of cells is typically permitted to evolve over time. One classic example of C.A is the Ising model of ferro-magnetism where each cell may represent atomic spin as a binary state (see fig 2.1).

A lattice gas may be regarded as a form of crystalline gas with particles, atoms or molecules, constrained to sit at specific sites represented by cells. Particles are assumed to move by a series of jumps from filled to vacant sites. A site will typically have some form of potential which may determine whether a jump succeeds. Periodic boundaries will reproduce a larger sample as long as the boundary lengths are much larger than the

coherence length of the system. In the case of Kawasaki dynamics particles exchange between nearest neighbour sites whilst Glauber dynamics permit exchanges over arbitrary ranges (see fig:2.2. It should be apparent that a system will reach equilibrium more quickly with Glauber exchanges especially at low temperatures. However Kawasaki dynamics model more accurately diffusion effects within a lattice.

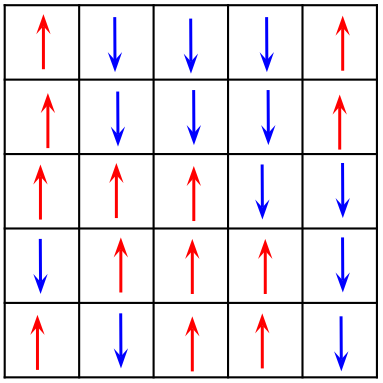

FIGURE 2.1: Ising Model

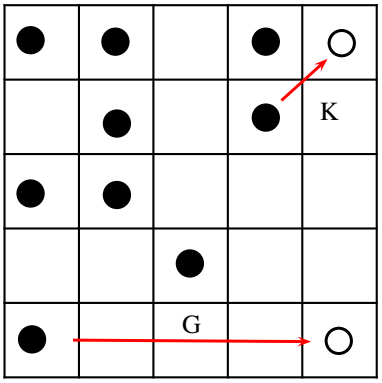

FIGURE 2.2: Kawasaki vs. Glauber

2.1.2 The Metropolis Algorithm

The question arises of how to determine whether a hydrogen atom performs a site exchange (jump). These simulations employed the Metropolis Algorithm [111]. Jumps are probabilistic and jump probabilities are determined from the difference in Hydrogen energies between the two sites in question see fig 2.3. For computational efficiency, transitions down a potential gradient always proceed, only those ascending a potential gradient are probabilistic.

$$P(E_i \rightarrow E_j) = 1 \text{ if } \Delta E \leq 0 \tag{2.1.1}$$

$$P(E_i \rightarrow E_j) = e^{\Delta E_{ij}/k_B T} \text{ if } \Delta E > 0 \tag{2.1.2}$$

with jump probabilities calculated thus:-

$$P(E_i \rightarrow E_j) = \frac{1}{1 + e^{\Delta E_{ij}/k_B T}} \tag{2.1.3}$$

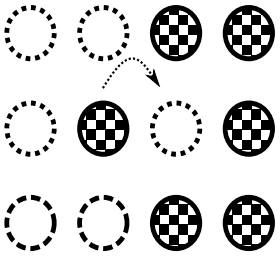

FIGURE 2.3: Metropolis Algorithm

i.e. The probability of successful jump decreases exponentially as the interaction energy difference ΔE increases.

Why?
We are imposing a Boltzmann distribution on the energies of particles in the system, i.e. whilst particles will preferentially tend to a low energy state as the temperature rises there is an increasing probability that they can occupy a higher energy state leaving empty states at lower energies.

Assuming two states i and j and assuming that $E_i > E_j$ the probability $P(E)$ of a particle being at energy E is given by

$$P(E) = e^{E/k_B T} \tag{2.1.4}$$

thus the ratio of particles in the two states is given by

$$\frac{P(E_i)}{P(E_j)} = \frac{e^{-E_i/k_B T}}{e^{-E_j/k_B T}} = e^{-(E_i - E_j)/(k_B T)} \tag{2.1.5}$$

which gives rise to the classic Maxwell-Boltzmann distribution,

Interactions between hydrogen atoms are assumed to be repulsive $(-ve)$ at short-range with a long-range attraction due to the lattice expansion. If we define $\Delta E = V_f - V_i$, then considering a lone atom attempting to jump into a site with many filled n.n. and n.n.n. sites then $\Delta E = -ve$ and the jump is unlikely to occur whilst going the other way$\Delta E = +ve$ and the jump probability will be higher, $P = 1$ in the case of the Metropolis algorithm. Thus jumping 'up' a potential gradient occurs with a probability given by a Maxwell-Boltzmann factor.

2.1.2.1 Modelling an External Bath

The simple model above needs to be modified when atoms are allowed to exchanged with some external bath. This may be achieved simply by setting the energy of the hydrogen atoms in the bath to their chemical potential.

2.1.3 Classes of Ensembles

The term Canonical ensemble describes a system of a fixed number of particles in contact with an external heat bath. Micro-canonical (also little or petite) refers to an entirely isolated system whilst a Grand Canonical ensemble is one in contact with an external heat and particle bath i.e. both the internal energy and the number of particles in the system may change. In this work simulations have either been Canonical Monte Carlo, CMC or Grand Canonical Monte-Carlo GCMC.

2.1.4 Random Walks

Here a particle moves by a series of uncorrelated jumps between sites on a periodic Bravais lattice where the position vector of any lattice point is given by

$$\boldsymbol{R} = n_1\boldsymbol{a_1} + n_2\boldsymbol{a_2} + n_3\boldsymbol{a_3} \tag{2.1.6}$$

where n_1, n_2, n_3 are integers and $\boldsymbol{a_1}, \boldsymbol{a_2}, \boldsymbol{a_3}$ are non-coplanar primitive translation vectors. After N jumps of uniform length l its displacement relative to the starting position is given by

$$\boldsymbol{R} = \sum_{i=1}^{N} l\mathbf{r_i} \tag{2.1.7}$$

where $\boldsymbol{r_i}$ denotes an individual displacement. For perfectly random exchanges at infinite dilution the square mean displacement after n jumps will be

$$< \boldsymbol{r_n^2} >= n\boldsymbol{r_i^2} \tag{2.1.8}$$

where $n = \frac{t}{\tau}$, τ being the mean residence time on a site.

At higher concentrations we have a correlation effect, as some sites are blocked by being occupied. Now there is an enhanced probability of jumping back to the site just left.

$$< \boldsymbol{r^2} >= f\,(1-c)\,t \tag{2.1.9}$$

with f being the concentration dependent correlation factor $0 < f < 1$, t the time in Monte-Carlo cycles and $(1-C)$ being the probability that a site is empty.

2.1.5 Diffusion

One can start with the basic description of mass flow in three dimensions

$$J = -\left(D_{xx}\frac{\partial C}{\partial x} + D_{yy}\frac{\partial C}{\partial y} + D_{zz}\frac{\partial C}{\partial z}\right) = D_{ii}\nabla C_i \tag{2.1.10}$$

where J represents the number particle flux per unit area unit time, C the concentration and D the diffusion coefficients along the principle crystallographic axes. This is usually referred to as *Fick's First Law of Diffusion*. In the case of an isotropic system this simplifies to

$$J = -D\frac{\partial C}{\partial x} \tag{2.1.11}$$

Note that these equations apply only to ideal systems where D is independent of concentration and there is no potential gradient due to e.g. gravitation, electrical or thermal effects. One can now write *Fick's Second Law of Diffusion*

$$\frac{\partial C}{\partial t} = D_{xx}\frac{\partial^2 C}{\partial x^2} + D_{yy}\frac{\partial C^2}{\partial y^2} + D_{zz}\frac{\partial C^2}{\partial z^2} = D_{ii}\nabla^2 C_i. \tag{2.1.12}$$

Again for an isotropic system this may be simplified to

$$\frac{\partial C}{\partial t} = D\frac{\partial C^2}{\partial t^2}. \tag{2.1.13}$$

Consider diffusive flow along a concentration gradient. Assume the number concentration of mobile atoms per unit area at x to be N_x and further along at $x + \Delta x$ the concentration is $N_{x+\Delta x}$. Defining Γ as the mean successful jump frequency and given

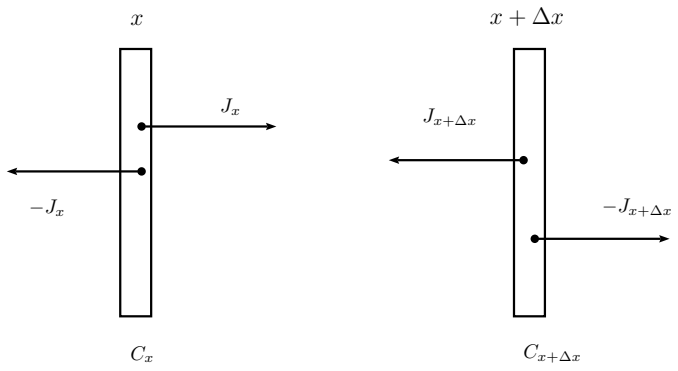

FIGURE 2.4: Diffusion

that an atom may jump in either direction the flow left to right will be

$$J = \frac{1}{2}\Gamma N_x \tag{2.1.14}$$

and from right to left

$$J_{x+\Delta x} = \frac{1}{2}\Gamma N_{x+\Delta x}. \tag{2.1.15}$$

Thus the net flow rate J left to right is

$$J = J_{x+\Delta x} - J_x = \frac{1}{2}\Gamma \left(N_{x+\Delta x} - N_x\right). \tag{2.1.16}$$

Describing J in terms of unit volume gives

$$J = \frac{1}{2}\Gamma \frac{N_{x+\Delta x} - N_x}{\Delta x} \tag{2.1.17}$$

introducing Δx for the concentration gradient gives

$$J = \frac{1}{2}\Gamma \Delta x \frac{N_{x+\Delta x} - N_x}{\Delta x}. \tag{2.1.18}$$

We may replace N/x with the number concentration C

$$J = -\frac{1}{2}\Gamma (\Delta x)^2 \frac{\partial C}{\partial x} = -D\frac{\partial C}{\partial x} \tag{2.1.19}$$

$$\text{i.e. } D_{chem} = \frac{1}{2}\Gamma (\Delta x)^2. \tag{2.1.20}$$

Δx in the limit is the inter-atomic spacing a. For a non-cubic system where a_x, a_y, a_z and the jump frequencies Γ_{xyz} along the crystallographic axes may be unequal we may write

$$J = -\frac{1}{6}\left[\Gamma_x a_x^2 \frac{\partial C}{\partial x} + \Gamma_y a_y^2 \frac{\partial C}{\partial y} + \Gamma_z a_z^2 \frac{\partial C}{\partial z}\right] \tag{2.1.21}$$

thus giving three values for D_{chem}. In the case of a cubic system such as PdH where the a and Γ values are equal we have

$$D_{chem} = \frac{1}{6}a^2\Gamma. \tag{2.1.22}$$

2.1.6 Temperature Dependence of Diffusion

The empirical Arrhenius relationship is widely applicable to chemical kinematics including diffusion:-

$$D = D_0 e^{-\frac{Q}{RT}} \tag{2.1.23}$$

Here Q is the activation energy. In this case Q will be a measure of the energy barrier that a diffusing hydrogen ion has to overcome when jumping between adjacent sites. Thus $D \to D_0$ as $T \to \infty$. Similarly for D_{chem}.

2.1.7 Tracer Diffusion

Chemical diffusion refers specifically to the diffusion of a whole population of atoms in some form of potential or concentration gradient. Tracer diffusion refers to the spontaneous movement of a single particle in the absence of such a driving force i.e. in a system at equilibrium. Taking the general case of Fick's Law $J = -D\frac{\partial C}{\partial x}$ we can factor in a concentration dependent correction.

$$\begin{aligned} J &= -\left(\frac{D}{kT}\right) C\frac{d\mu}{dx} = -\left(\frac{D}{kT}\right) C\frac{d\mu}{dC}\cdot\frac{dC}{dx} \\ &= -\left(\frac{D}{kT}\right) C\frac{kT}{C\,(1-C)}\cdot\frac{dC}{dx} = -\frac{D}{(1-C)}\cdot\frac{dC}{dx} \end{aligned} \tag{2.1.24}$$

$$\therefore J = -\frac{D_t}{1-C}\cdot\frac{dC}{dx} \tag{2.1.25}$$

where $D_{chem} = \frac{D_t}{1-C}$ i.e. at $C = 0$ $D_{chem} = D_t$

2.1.8 The Tracer Correlation Factor f_t

In tracer diffusion we are interested in how far an atom moves in given time – i.e. per Monte-Carlo cycle, it is apparent that whilst net diffusion may be zero the particles are still moving and thus some measure of their migration may be determined. Take the case of a single atom on an empty lattice which is free to jump to any of its 6 neighbours see fig 2.5. If the atom jumps from site a to site b then it has a 1:6 chance of jumping back to site a again, a *memory* effect. Now taking a much higher concentration see fig 2.6. An atom at a can jump either to p, q, r or b. If it jumps to b then it has but 2 subsequent options either jumping to c or back to a.

The extreme case of only one vacancy now becomes interesting. Rather than looking at a particular atom jumping into the vacancy we have a symmetry with the first case if we consider the vacancy moving through the lattice (much like a hole in a semiconductor. This 'tracer correlation factor' distorts the jump probabilities and thus diffusion rates. It has been extensively studied analytically and via simulation. [81]

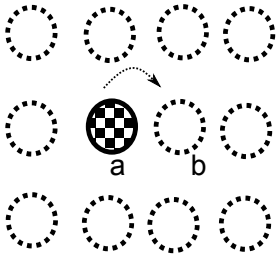

FIGURE 2.5: Tracer Correlation low C

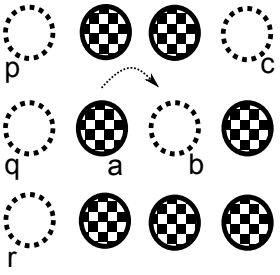

FIGURE 2.6: Tracer Correlation high C

$$D_t(C) = f_t(C)\frac{l^2}{6\tau(C)} = \frac{<\boldsymbol{r}^2>}{6\tau} \tag{2.1.26}$$

$$\tau(C) = \frac{\tau(0)}{(1-C)} \quad \text{where} \quad \tau(C) \xrightarrow{C\to 1} \infty \tag{2.1.27}$$

$(1-C)$ is the *site blocking factor* In the case of an F.C.C lattice it can be shown that [81] :-

$$f_t \xrightarrow{C\to 1} 0.7814 \tag{2.1.28}$$

2.1.9 Widom Insertion Method

The Widom 'Ghost Particle' Insertion Method [18] has been used to determine the chemical potential of the lattice gas. The potential of a species is calculated by comparing the free energy of a system containing N particles with one containing $N + 1$ by simply repeatedly temporarily inserting an extra particle at random locations and determining the mean rise in internal energy ΔU. We are obviously assuming that adding a single particle does not significantly disturb the system. This rise in interaction energy ΔU is averaged over Boltzmann factor for that temperature.

$$\mu - \mu^{\oslash} = k_B T \langle e^{-\Delta U/k_B T} \rangle \tag{2.1.29}$$

$$\mu = \mu^0 + \mu^* \tag{2.1.30}$$

where μ^0 is the chemical potential of an ideal lattice gas and μ^* the excess chemical potential. Moving from the molar to particle view as $k_B = \frac{R}{N_A}$ Hence for large N

$$\mu^* = -k_B T < \ln e^{-\Delta U/k_B T} > \tag{2.1.31}$$

Here the average is calculated from many random additions of a single particle to yield the chemical potential.

2.1.10 Measuring the degree of Ordering

The simplest metric to apply here is to monitor some mean of the number of nn and nnn sites that are occupied around each occupied interstitial. One generally accepted method is the Warren-Cowley short range order parameter.

$$\alpha_{s.r.o.} = \left[1 - \frac{p_{nn}}{C_H}\right] \tag{2.1.32}$$

Here p_{nn} or p_{nnn} is the probability of a nn or nnn site being occupied.

Chapter 3

Simulating Diffraction Patterns

3.1 Introduction

Diffraction techniques provide powerful tools to study how materials order at the atomic level. X-rays were first used to probe microscopic order. These have since been supplemented with electron and neutron diffraction methods. In the specific case of this work the ordered structures produced by Monte-Carlo molecular dynamic simulations can be compared to real world samples by calculating their virtual diffraction patterns for comparison with those from experiment

The study of diffraction patterns from 3-d structures is very well established. Thomas Young famously observed two slit interference of light in $\sim$1802 concluding that light was a wave rather than a particle as proposed by Newton. Such interference patterns are a natural consequence of Huygens construction where every point on a wavefront may be assumed to be a source of secondary *wavelets*. 2-d diffraction gratings were well developed by the mid 1800s. The possibility of diffraction from 3-d atomic structures was suggested by Ewald and Laue in 1912 with the first x-ray diffraction pattern produced shortly thereafter.

The terminology here is somewhat imprecise. A diffraction pattern is the result of the *interference* of *diffracted* waves. At a physical level the processes are the same, we tend to use interference when referring to a few scatterers and diffraction for many.

X-rays, electrons and neutrons are used in atomic diffraction studies. Relatively inexpensive and compact equipment is capable of generating x-rays the wavelength of

which is of the order of the inter-atomic spacing. X-rays scatter from electrons – thus the scattering power of an atom depends upon the number of electrons it possesses i.e. its atomic number. Palladium with 46 electrons scatters much more strongly than hydrogen with only 1. In the case of Pd-H, scattering from the palladium masks the signal from the hydrogen. Instead thermal neutrons with de-Broglie wavelengths of the order of Angstroms may be used as the neutron scattering factor does not vary simply with Z number and is highest for hydrogen. A suitably bright neutron source may be a nuclear reactor, such as the I.L.L. at Grenoble or a proton synchrotron such as ISIS at the Rutherford-Appleton Laboratory which generates neutrons by spallation from a tungsten target illuminated by GeV energy protons. This equipment is many times larger, more expensive and complex than x-ray diffractometers. As x-ray, electron and neutron scattering patterns are due to the summing of scattered waves from the target, it is straightforward to simulate this process.

A brief overview of scattering theory is first presented followed by a discussion of how a diffraction pattern may be computed from a simulated sample.

3.1.1 General Scattering Theory

The kinematic model provides a simple view of scattering. An incident wave-front may be scattered by discontinuities in its path. X-rays scatter from orbital electrons whilst neutrons scatter from atomic nuclei. These scattering centres act as sources of spherical wavefronts (*s-wave* scattering) see fig 3.1. At some distance wave-fronts from many scatterers interfere thereby creating regions of high and low intensity depending on the phase contributions from each wave. In this simple treatment the scattering is assumed

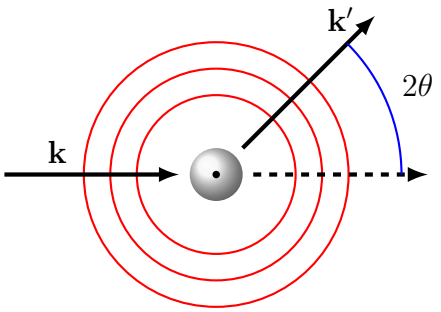

FIGURE 3.1: Simple Kinematic Scattering

to be elastic i.e. the magnitude of the scattered wave vector is equal to that of the

incident. $|\mathbf{k}'| = |\mathbf{k}|$. The scattered amplitude A_j arriving at a detector at a distance R_j from the j^{th} atom is given by

$$A_j = A_0 f e^{i\boldsymbol{K}\cdot\boldsymbol{r_j}} \tag{3.1.1}$$

Where f the *atomic scattering factor* is a measure of the scattering power of the atom. If the distance to the detector is very much greater than the atomic spacing then R_j may be approximated to a constant R see fig 3.2. In reality a scattered wave is likely to undergo further scattering. In simple models this effect is ignored as it greatly increases computing time.

3.1.2 The Scattering Vector q

Consider two atoms i and j, illuminated by a coherent beam of radiation from a source at ∞, of wavelength λ and thus wavevector $|q| = \frac{2\pi}{\lambda}$. The difference between the incident and scattered wave vector is known as the scattering vector where $\mathbf{k}' = \mathbf{k} + \mathbf{q}$ see fig 3.3.

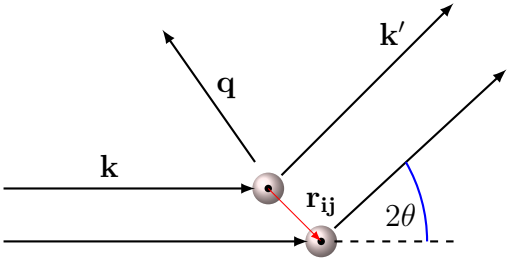

FIGURE 3.2: Wave Vectors

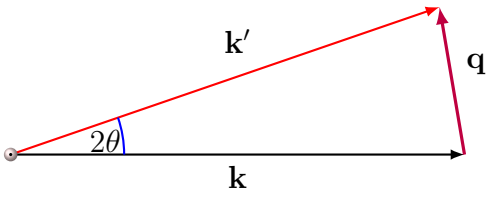

FIGURE 3.3: $\mathbf{k}$ incident, $\mathbf{k}'$ diffracted and $\mathbf{q}$ diffraction vectors

Given that $|\mathbf{k}'| = |\mathbf{k}|$ and $\angle$ the angle between them

$$|\mathbf{q}| = 2|\mathbf{k}| \sin\left(\frac{\mathbf{k}\angle\mathbf{k}'}{2}\right) \tag{3.1.2}$$

Waves incident on the detector, scattered as $\mathbf{q_i}$ and $\mathbf{q_j}$ will interfere and thus a diffraction pattern may form.

3.1.3 Formation of a Diffraction Pattern

We now imagine an ensemble of N identical atoms sitting at 3d positions $\mathbf{r_i}$ from some arbitrary origin $\mathbf{r_0}$ with a detector at a distance much greater than the size of the sample see fig 3.4. We may thus approximate the distance from all points to the detector as a constant and ignore the amplitude-distance terms. The position of each detector pixel may be described by $\mathbf{k}'$ with respect to the origin of the sample. At some point $\mathbf{k}'$ on

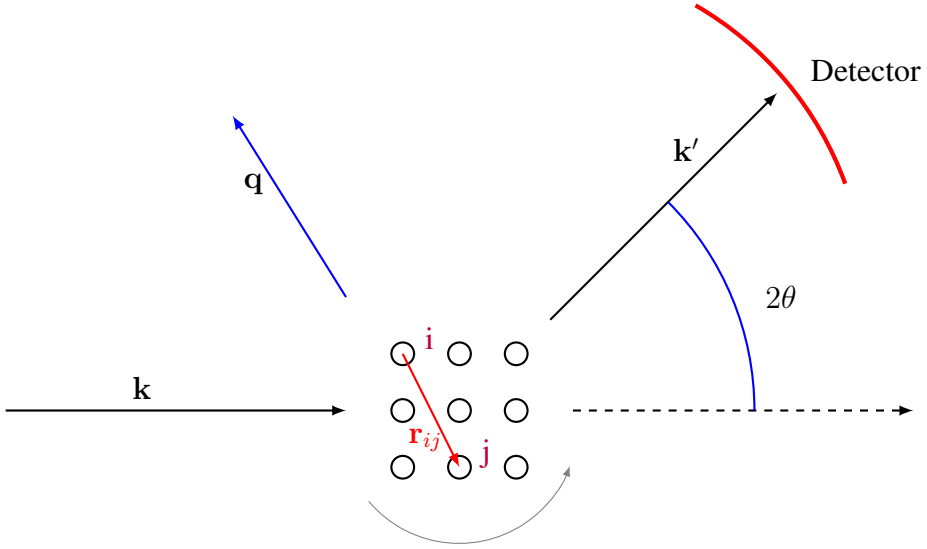

FIGURE 3.4: Diffraction pattern from many scattering points

the detector waves scattered from the atoms arrive and interfere. The amplitude of each scattered wave is given by

$$A(\mathbf{k}') = fe^{-i(\mathbf{k}-\mathbf{k}')\cdot\mathbf{r}} \tag{3.1.3}$$

As $\mathbf{q} = (\mathbf{k} - \mathbf{k}')$

$$A(\mathbf{q}) = fe^{-i(\mathbf{q}\cdot\mathbf{r})} \tag{3.1.4}$$

For N scatterers we sum the waves from each scatterer j

$$A(\mathbf{q}) = \sum_{j=1}^{N} f_j e^{-i(\mathbf{q}\cdot\mathbf{r_j})} \tag{3.1.5}$$

The detector will measure the intensity of the radiation at each pixel summed over all scatterers. This is equal to the square of the scattering amplitude A, being a complex number - strictly the product of the amplitude with its first complex conjugate.

$$I(\mathbf{q}) = |A||A^*| = \sum_{j=1}^{N}\sum_{k=1}^{N} b_j b_k e^{-i\ \mathbf{q}\cdot\mathbf{r_{jk}}} \tag{3.1.6}$$

The Bragg peaks at $n\lambda = 2d\sin\theta$ give information from any long-range ordering. These simulations are concerned with short-range order resulting from the growth of crystal domains. The size of domains may be inferred from the broadening of the Bragg peaks using the Scherrer equation [133]

$$\tau = \frac{K\lambda}{\beta\sin\theta} \tag{3.1.7}$$

where τ is the domain size, K a dimensionless shape parameter generally taken as 0.9. β is the full width - half maximum peak broadening expressed in radians and θ the Bragg angle.

3.1.4 The Role of Reciprocal Space

Reciprocal space (also known as *momentum space or k-space*) is is a convenient abstraction when considering diffraction from a periodic structure being the Fourier transform of the real space *direct* lattice. Points in reciprocal space represent families of planes in the direct lattice, see fig 3.5. A key feature is that the vector direction between any two point in the reciprocal lattice represents the direction between two planes in the direct lattice and the spacing between points in k-space is the reciprocal of the inter-planar spacing. Expressing these reciprocal lattice vector lengths as $|\mathbf{G}| = \frac{2\pi}{\lambda}$ gives the distance in radians per unit length.

If we have a set of atomic positions in real space $\mathbf{r_i} = (h\mathbf{x_i} + k\mathbf{y_i} + l\mathbf{z_i})$ then the Fourier transform is given by

$$f(\mathbf{r}) = \sum_{G} f(\mathbf{G})e^{i(\mathbf{G}\cdot\mathbf{r})} \tag{3.1.8}$$

The key point here is that this transform maps directly the diffraction pattern from the scatterers i.e.

$$S(\mathbf{q}) = \sum_{i,j,k} e^{i\mathbf{G}\cdot\mathbf{r}} \tag{3.1.9}$$

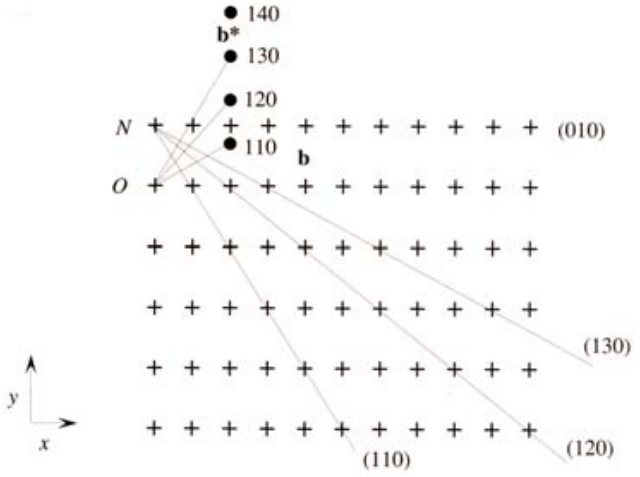

FIGURE 3.5: Construction of the Reciprocal Lattice.

Real space points are +, reciprocal points •

The reciprocal lattice axis vectors are given by

$$\mathbf{b}_1 = 2\pi\frac{\mathbf{a}_2 \times \mathbf{a}_3}{\mathbf{a}_1 \cdot \mathbf{a}_2 \times \mathbf{a}_3} \qquad \mathbf{b}_2 = 2\pi\frac{\mathbf{a}_3 \times \mathbf{a}_1}{\mathbf{a}_1 \cdot \mathbf{a}_2 \times \mathbf{a}_3} \qquad \mathbf{b}_3 = 2\pi\frac{\mathbf{a}_1 \times \mathbf{a}_2}{\mathbf{a}_1 \cdot \mathbf{a}_2 \times \mathbf{a}_3} \tag{3.1.10}$$

Note that $\mathbf{b}_1$ is orthogonal to both $\mathbf{a}_2$ and $\mathbf{a}_3$, $\mathbf{b}_2$ is to both $\mathbf{a}_1$ and $\mathbf{a}_3$ and so on. Points in the reciprocal lattice are mapped as

$$\mathbf{G} = h\mathbf{b}_1 + k\mathbf{b}_2 + l\mathbf{b}_3 \tag{3.1.11}$$

As is generally accepted, diffraction peaks occur when $\mathbf{q} = \mathbf{G}$. [84]

3.2 Simulating a Diffraction Pattern

Given a known crystal structure one may calculate the reflections from specific planes - the inverse of conventional experimental crystallography. The alternative approach, used here is to calculate the diffraction pattern from a set of atomic positions mirroring the physical processes in experimental x-ray or neutron crystallography. Such an *a priori* technique makes few of the assumptions of conventional crystallography such as 'reflection from planes' though is computationally somewhat expensive. Since we are

considering an *a priori* algorithm it may be helpful to initially limit standard crystallographic terminology and formulate the problem in general physical terms.

We wish to simulate the diffraction pattern formed when a beam of radiation is incident upon group of atoms. These scatterers interact with the incident radiation resonating and emitting a spherical wavefront. Different scatterers will have different scattering powers. Here we are only considering scattering by hydrogen so this scattering *factor* can be set to unity i.e. we can ignore the scattering from Pd. A number of methods have been developed to simulate diffraction patterns directly from atomistic data.

The most direct method takes a rather *brute force* approach. One simply determines the linear path lengths, L_i from a monochromatic coherent radiation source to each atom in the model and from there to every pixel on the detector array . Sin and cos of $2\pi\frac{L_i}{\lambda}$ for each path are summed at each pixel giving the resultant amplitude and phase. This scales directly with $N_{atoms} \times n_{pixels}$ for a sample of 10^6 atoms and a linear detector of 10^4 pixels one has of the order of 10^{10} iterations - perfectly acceptable on a modern workstation. Since each calculation does not depend on the others then this is easily optimised by parallel processing. One problem here though is the need for the path lengths to be very long compared to the size of the sample and hence the differences in atomic positions. This is to avoid distortion of the pattern by some parts of the sample being significantly closer to the detector than others. If the simulation mirrors a real diffractometer the sample $\rightarrow$ detector distance will be $> \ 10^8\times$ the inter-atomic spacing. Assuming that we need to resolve path differences of 10^{-2} of this spacing we require a precision of $\ 1 : 10^{10}$. To overcome this one needs to use high precision 'long' real numbers which significantly slows the computation.

A more sophisticated approach involves calculating

$$I(\mathbf{k}') = \sum_{i \neq j} \sum_{j} e^{i\mathbf{q}\cdot\mathbf{r}_{ij}} \tag{3.2.1}$$

to every point on the detector array see fig 3.4. If we assume that, to the incoming radiation, each atom acts as a point scatterer and that the atoms do not move their positions may be represented as a series of δ-functions. A further simplification may be introduced by assuming that the size of the region being sampled is much smaller than the distance between the sample and the detector. Thus we can assume that the scattering distance and angle from each atom to each point on the detector are approximately constant. The problem with this method is again the computational load. For a sample of

10^5 atoms and a 2d detector of 10^6 pixels one would need to perform some 10^{16} calculations before needing to rotate the sample to ensure that all possible peaks are detected. Without some optimisation of the algorithm this is impractical. This has the appearance of Fourier transform and so it should be practical to perform an F.F.T. if we assume that the scatterers are both point entities and sit on points fixed on a regular 3d lattice. If the points are permitted to displace from these regular points, via thermal vibration or during diffusion one cannot perform an FFT. This could be addressed by defining a grid whose spacing is much smaller than the lattice parameter and limiting scatters to these discrete positions. With say 10^6 atoms and 10 intermediate points between the *regular* lattice sites results in a grid of 10^9 points with only 0.1% filled at any time. This will lead to very large data-arrays which without some optimisation will again add to the computation time.

3.2.1 Pair Distribution Functions (PDF)

The diffraction pattern is a function of the degree of spatial ordering within the sample and therefore of the density distribution of scatterers. Taking into account such a pair distributions is of particular importance when considering partly ordered systems.

The reduced pair distribution function – $g(r)$ is simply the probability of finding a pair of particles at a specific distance r from one another. $g(r)$ is often expressed in the normalised form such that as $r \to \infty, g(r) \to 1$ and for $r <$ distance of closest approach $g(r) = 0$. The pair distribution function may be obtained directly from a molecular dynamics simulation where it is related to the pair density function $\rho(r)$ by $\rho(r) = \rho_0 g(r)$. As $r \to \infty$, $\rho(r)$ will tend to ρ_0, the mean number density of the sample and tend to zero as $r \to 0$

$$g(r) = 4\pi r \left(\rho(r) - \rho_0\right) = 4\pi\rho_0 r \left(g(r) - 1\right) \tag{3.2.2}$$

Within a shell at a range $r_1 \to r_2$ we may specify the number of neighbours, a site's coordination number as

$$N_c = \int_{r_1}^{r_2} R\left(r\right) dr \tag{3.2.3}$$

In the Debye-Glatter scattering method [64] rather than performing the computationally intensive *sin* calculation for every atom pair the calculation is optimised 'binning' these

coordination numbers, see fig 3.6, in advance then calculating

$$I(q) = \frac{1}{N}\sum_{i=1}^{N} f_i N_{c_i} \frac{sin(2\pi q r_i)}{2\pi q r_i} \tag{3.2.4}$$

i.e. The inter-atomic distances are calculated for every atom-atom pair then divided into a histogram where the width of each 'bin' is suitably small to give the desired resolution. The double summation over all atomic pairs is thus reduced to a single sum over N bins.

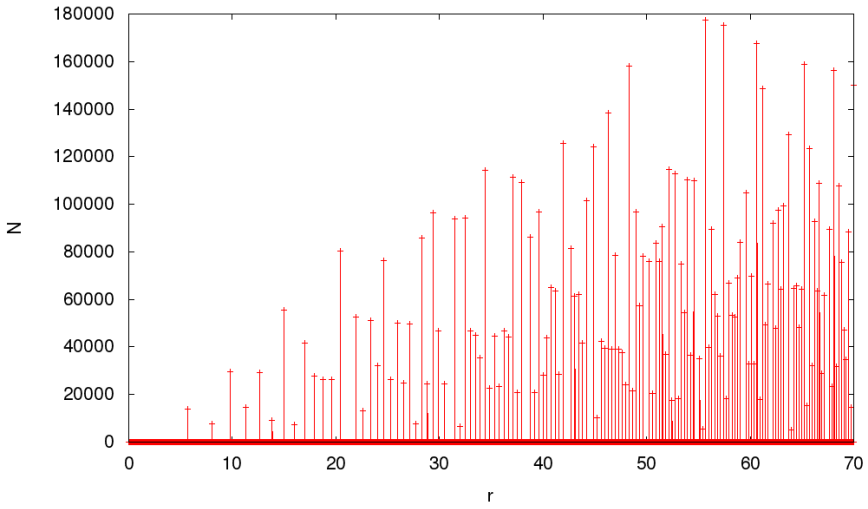

FIGURE 3.6: Example of binned interatomic distances for C=0.29 ordered f.c.c. lattice

We may now specify a radial distribution function $R(r)$ describing the number of atoms in a shell of thickness $d(r)$ at a distance r:-

$$R(r) = 4\pi r^2 \rho(r) \tag{3.2.5}$$

giving

$$g(r) = \frac{R(r)}{r} - 4\pi r \rho_0 \tag{3.2.6}$$

This may be easily determined at any point in a molecular dynamics simulation. If we assume initially that atoms sit at precise positions $\mathbf{r_i}$ without thermal or other displacements then their positions may be expressed as a series of delta functions $\delta\left(\mathbf{r_0} - \mathbf{r_i}\right)$. Setting $\mathbf{r_0} = 0$ gives

$$R(r) = \frac{1}{N}\sum_{i}\sum_{j} \delta\left(\mathbf{r_{ij}}\right) \tag{3.2.7}$$

The reduced pair distribution function $g(r)$ is the Fourier Transform of $S(q)$ the total scattering structure function – effectively the normalised diffraction intensity.

$$G(r) = \frac{2}{\pi}\int_{qmin}^{qmax} q[S(q) - 1]sin(qr)dq \tag{3.2.8}$$

The inverse transform is more useful here

$$S(q) = 1 + \frac{1}{q}\int_{0}^{\infty} r(r)sin(qr)dr \tag{3.2.9}$$

In the 1980s a simulation technique using the Debye scattering equation for powder samples was developed [64].

$$I(q) = \frac{1}{N}\sum_{i=1}^{N}\sum_{j=1}^{N} f_i f_j \frac{sin(2\pi q r_{ij})}{2\pi q r_{ij}} \tag{3.2.10}$$

where f_i, f_j are the scattering factors of the respective atoms and q, r_{ij} are equal to $|\mathbf{q}|$ and $|\mathbf{r_{ij}}|$ respectively.

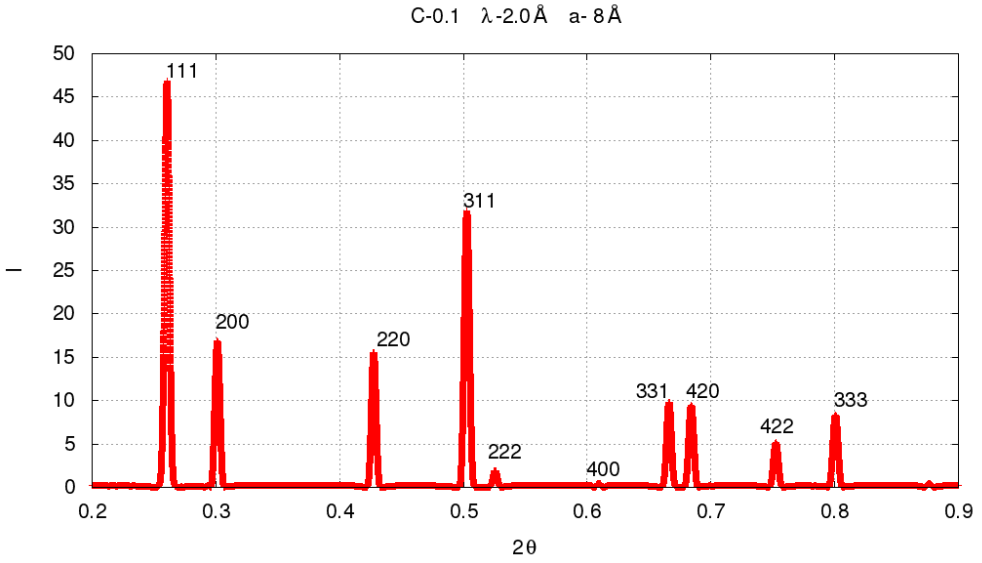

FIGURE 3.7: Virtual Debye Diffraction Pattern of H in Pd demonstrating hkl all odd or all even as expected for f.c.c. structure

The algorithm may be optimised by binning the distances r_{ij} before performing the computationally intensive sin calculations. With sufficiently narrow bins the errors

generated are minimal, see fig 3.6. In effect this technique loses the absolute spatial, i.e. directional, information in favour of a computationally faster method of generating pair distributions (the bins). The size of crystal regions may be inferred from peak broadening rather than being directly observed. This technique is very fast, on a 3 GHz workstation a pattern from 10^4 atoms, with 10^4 detector pixels and 10^5 bins computes in some 100 seconds, see fig 3.7. Scaling to a more realistic 10^6 atoms takes $\sim$ 3 hours.

The technique used here for the contour 2d plots involves summing $e^{i(\mathbf{G}\cdot\mathbf{r}_i)}$ over a range of G_x and G_y see fig 3.8.

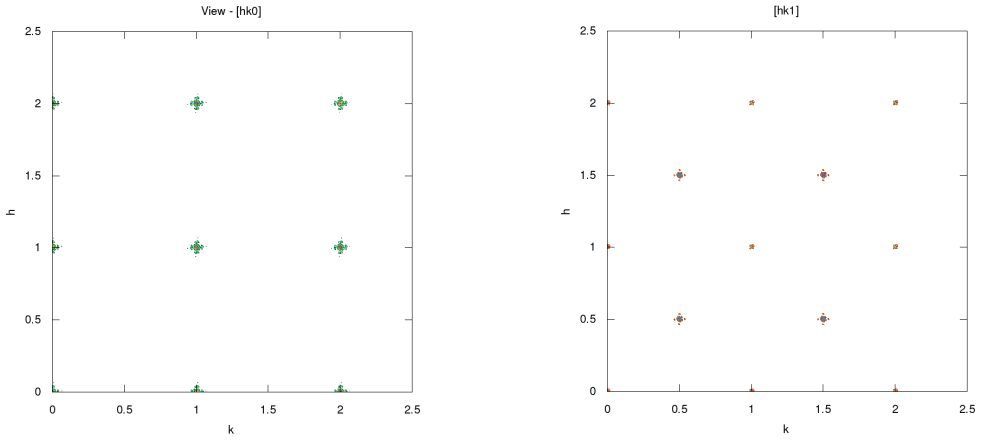

FIGURE 3.8: Sample 2d contour plots of partly filled f.c.c. *(f.c.c. real space $\rightarrow$ b.c.c reciprocal space)* lattice in hk0 and hk1

Chapter 4

Refining the Computational Model

4.1 The Code

The core simulation was written in Fortran 2003, compiled with Fortran Compiler XE 14.0 and gfortran 4.6x. Benchmarking these CPU intensive linear simulations indicates that Intel Fortran appears some 10% faster than gFortran. However the code is tested on both compilers to encourage use of standard code. The aim has been to develop simple rigorous code rather than optimisations that may be physically invalid. The program is highly modular and presently runs to some 3000 lines. Data from runs is written-out to results files which may include the variations in temperature, nn & nnn Warren-Cowely order parameters, concentration, mean potential energy, mean displacement due to diffusion and others. The same code is used for Canonical, Grand Canonical and flow-rate simulations to minimise and hopefully eliminate algorithmic differences.

The code allows for three different hydrogen isotopes. Several smaller applications have been written in vPython. The primary one aids visualisation of a snapshot of the lattice output as a datafile where the lattice appears as a rotatable, pseudo-3d model with various visualisation tools such as slicing through in differing planes specified by their Miller indices, see figs : 4.1 & 4.1 .

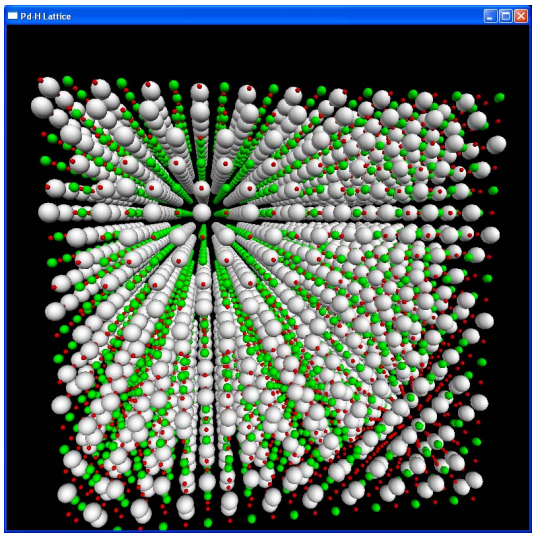

FIGURE 4.1: Rotatable view of lattice

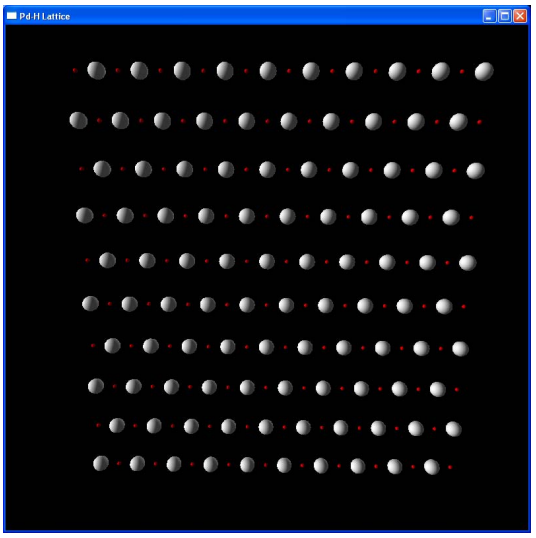

FIGURE 4.2: Slices through lattice

4.1.1 The Algorithm

The code used a simple and direct model of a Pd lattice with atoms and interstitials being represented directly by the elements of a multidimensional array i.e. the position of an atom is not determined by some vector or coordinate data appended to the atom description but rather is determined from the element's position within array. The model employed various periodic boundaries; either atoms 'wrap around' in the xyz directions, or only in the yz with the two x faces being adjacent to a heat bath. The simulation dimensions may be specified separately in the yz and x directions i.e. either a cube ($x = yz$) or rectangle($x \neq yz$). Thus diffusion into or through a thin slice may be represented.

There are four main modes of operation. Grand-Canonical Monte Carlo (GCMC), Canonical Monte Carlo (CMC) in either case employing Kawasaki dynamics where exchanges are between nearest neighbour (nn) pairs or Glauber dynamics with exchanges permitted over an arbitrary range. In the CMC case hydrogen migrates around a closed lattice whilst with the GCMC case hydrogen within the lattice may exchange with the external bath & sink. The bath and sink may be set to different potentials to model flow through a thin membrane. In either case periodic boundaries may be simulated. Wherever practical common subroutines are used regardless of whether the code is configured to simulate canonical or grand-canonical ensembles employing only nn jumps or those over arbitrary distances. Boolean flags were used to switch between the different modes.

The algorithm picks a hydrogen atom from within the lattice (or an external bath in the case of the GCMC) then seeks an empty interstitial site to jump to. This may be a nearest neighbour site or one at an arbitrary distance - in modelling diffusion only nn exchanges are performed. If an empty destination site is found the sum of the interaction potentials at each site are compared with the jump probability being determined as a function of the difference in site potential. If the potential of the destination is lower than the origin then the jump always proceeds. If it is higher the jump may proceed with a probability given by the Metropolis algorithm $p = exp(\frac{\Delta E}{k_B T})$ [111] as discussed in Chapter 2

4.2 Brief Overview of Testing

A comprehensive series of runs have been carried out with both the canonical and grand canonical configurations testing operation and optimising performance. Runs have compared the operation of the model with theory. In summary:-

- Testing with interactions turned off in the case of the GCMC configuration shows the concentration of hydrogen within the lattice tending towards 0.5 as one would expect, see fig:4.3.
- In the case of GCMC simulations of thin samples the concentration varies as $r \propto P^{0.500}$ (to better than 1:1000) as per Sievert's Law $r \propto P^{0.5}$ see fig:5.1.
- Canonical runs where the temperature kT is dropped or raised show a clear transition in mean site potential, fig 6.1 with two changes occurring in a narrow concentration range around $r_H \sim 0.65$, see fig:6.2.
- Simulations appear to have generated results very similar to Bond and Ross [23] for the variation of transition temperature with C_H in the canonical simulation see fig: 6.6.
- In the case of the Grand Canonical simulation using only short-range repulsive forces reproduce the expected phase chages but do not correctly reproduce the miscibility plateau see fig 4.5. Introducing long-range forces based on the Lacher model produces a clear plateau where the concentration changes dramatically over a very narrow pressure range, see fig: 7.6. Thus r_H varies with U_{bath} in

a similar manner to Bond & Ross . The plateau width diminishes as the temperature rises disappearing altogether by $kT \sim 0.4$ - the transition temperature seen in the canonical assemblies.

- The $I4_1/amd$ structure is seen below the transition temperature in the concentration range from ~ 0.25 to ~ 0.75.

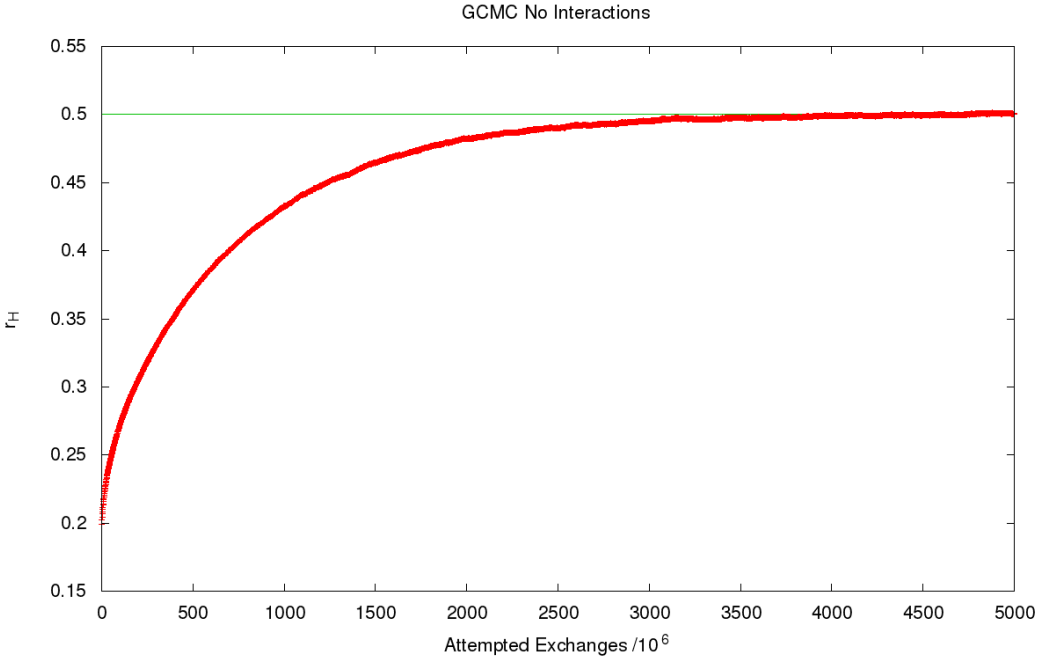

FIGURE 4.3: r_H vs. t, GCMC , Interactions Off, $T \simeq 200K$

4.3 Experimental Parameters

There exists a wealth of data on the PdH system spanning over 100 years. The review by Joubert [78] summarises this data. The computational model was calibrated against Joubert's recommended values of $T_C = 566K, \chi_C = 0.22(r = 0.282), P_C, = 20.15 \times 10^5 Pa$ and $r = 0.66$ at $T = 100K$.

4.4 The Grand-Canonical Model

Initially diffusion in from an infinite external bath was tested, i.e. one where the concentration and pressure remain constant with the external chemical potential μ at zero

in the absence of HH interactions within the lattice one would expect the concentration to tend to $r_H = 0.5$ at $\mu = 0$. The is perfectly reproduced as shown in fig: 4.3.

Now introducing a chemical potential in the external bath — still with zero interactions between atoms in the lattice we again see the lattice concentration rising to 0.5 H/Pd at $\mu_{bath} = 0$ with C asymptotically approaching 0 and ∞ as $\mu_{bath} \rightarrow = -\infty$ and $+\infty$, see fig: 4.4.

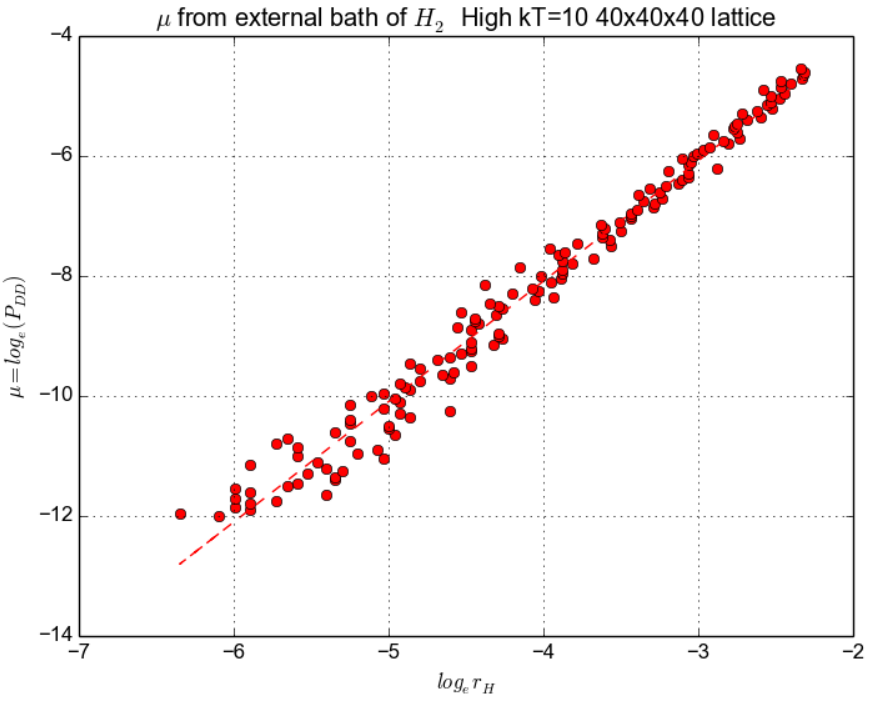

FIGURE 4.4: r_H vs μ_{bath} – CMC simulation with zero lattice interactions

4.4.1 Sieverts Law

The programs deliver an excellent fit to Sieverts Law in that the simulations generated $r = P^{0.498\mu}$ [28] under conditions when the long and short-range interactions are insignificant, see fig: 5.1.

4.4.2 The Lacher Model

Lacher proposed an attractive force via some undefined mechanism connected to the lattice expansion which could explain the adsorption /desorption curves. A number of models were investigated which are detailed in Chapter 5.

4.4.3 The Role of Short-Range Forces

As has been discussed previously the long-range attraction reproduces the general shape of the ab/desorption curves . In the presence of only this long-range attraction there is no requirement for the hydrogen to adopt any particular configuration. It is the short-range repulsion that encourages the formation of crystalline structures.

In these simulations the short-range forces are limited to nearest neighbour (nn) and next-nearest neighbour (nnn) interactions. A site's interaction potential is computed as the sum of the interaction potential of the n_{nn} and n_{nnn} neighbours. The values V_{nn} and V_{nnn} were taken from Bond and Ross [23] to test the model against their work where $V_{nn} = \frac{1}{4}V_{nnn}$. V_{nn} refers to the 12 nearest neighbour sites and V_{nnn} to the 6 next nearest neighbour sites. These were originally chosen for a number of reasons - primarily because the experimental diffuse scattering peak is roughly spherically symmetric corresponding to the calculated peak when $V_{nn} = 0.25V_{nnn}$ for $T > T_{critical}$. The lack of the Ni_4Mo structure at high concentrations suggests that additional near neighbour, or triplet, interactions will need to be included.

The problem then arises of determining an effective ratio for the short-range repulsive to long-range attractive forces.

As one expects simulations show that increasing the strength of the short-range repulsion pushes the high concentration end of the miscibility gap towards greater concentrations whilst too low a value suppresses ordering.

It would be reasonable to expect that a suitable ratio is one in which the two forces cancel at a concentration of $r = 0.50$. However runs demonstrate that this is far too high. More realistic P-r curves are obtained setting the short range repulsion such that the net attractive force is a maximum at $r = 0.5$, see fig: 5.7.

4.4.4 GCMC- Ab/desorption Curves

The code can simulate a Grand Canonical Ensemble with a rectangular block of palladium (strictly a block of interstitial sites) situated between two external baths of hydrogen. The isotopic composition and chemical potential of the two baths may be varied independently as can the temperature and initial composition of the lattice. The code

may alter the temperature and/or external chemical potential (pressure) and the evolution of the system monitored. The chemical potential within the lattice can be determined using the Widom insertion method and the state of ordering determined via short and long range ordering parameters and mean site potentials. So far the two external baths have been set to the same state. However these may be varied to simulate a bath and sink arrangement with diffusion monitored through the lattice.

Firstly shown is a low temperature run with D adsorbing into an initially empty lattice. Superimposed onto this plot is its inverse demonstrating that the system is symmetrical, see fig 4.5.

Then a series of runs are plotted at lower concentrations. From an initially empty state the chemical potential (pressure) of the external bath is raised in steps, see fig: 4.6.

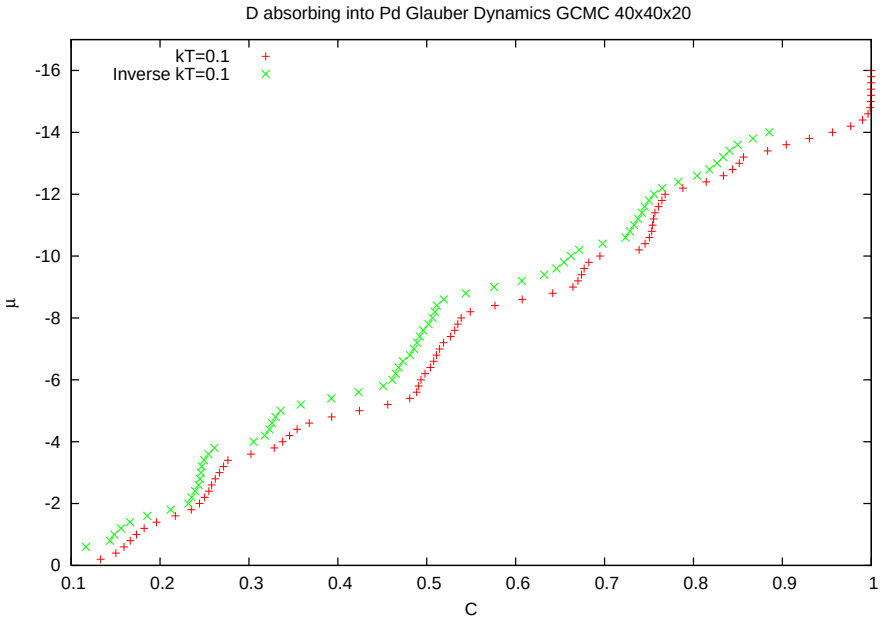

FIGURE 4.5: r_H vs μ_{bath} GCMC ensemble with short-range repulsion only- red plot is absorption green is desorption. Ordered structures appear at 0.15, 0.25, 0.33, 0.5, 0.67, 0.75 and 0.85 H/Pd, limited evidence that model reproduces hysteresis cf. fig 4.7.

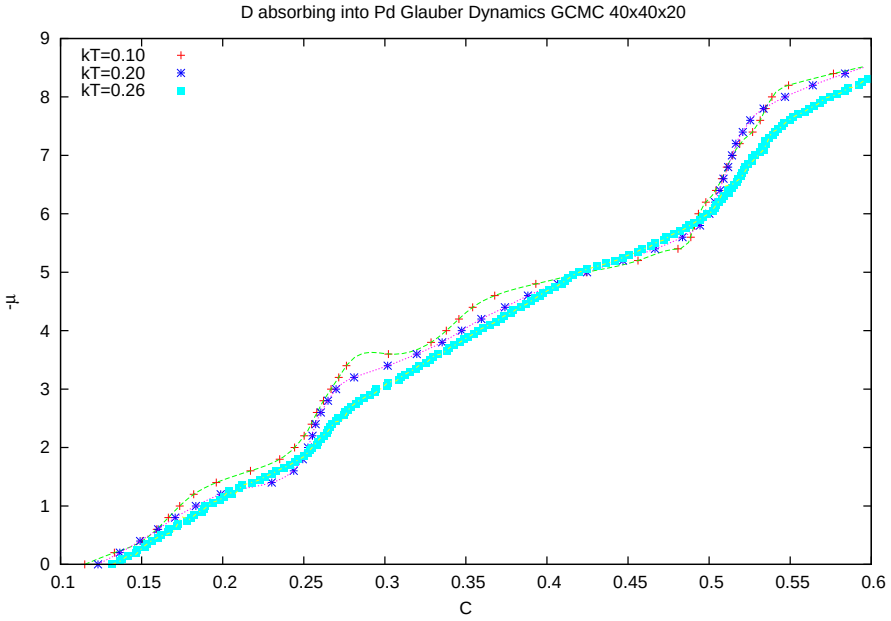

FIGURE 4.6: r_H vs μ_{bath} — GCMC ensemble with short-range repulsion only - runs at various temperatures

4.4.5 Tracer Correlation Factor f_t

In the simuations f_t tends to 0.78 as r_H tends to 1 as generally expected for a f.c.c. structure [81], fig: 4.9.

4.4.6 Zero Point Energy

Hydrogen isotopes possess differing zero point energies ZPE which affect their diffusion within the lattice and between the metal and the external gaseous baths. Firstly when moving an atom within the lattice the isotope's ZPE is ignored as it would make the same contribution at both the starting and destination site and thus not affect the energetics. If a atom is exchanging between the lattice and external baths the differing ZPEs will affect the probability of jump success. The model permits differing chemical potentials for the H_2, HD, D_2 molecules in the gas phase. Within the lattice H,D and T may be assigned differing ZPEs.

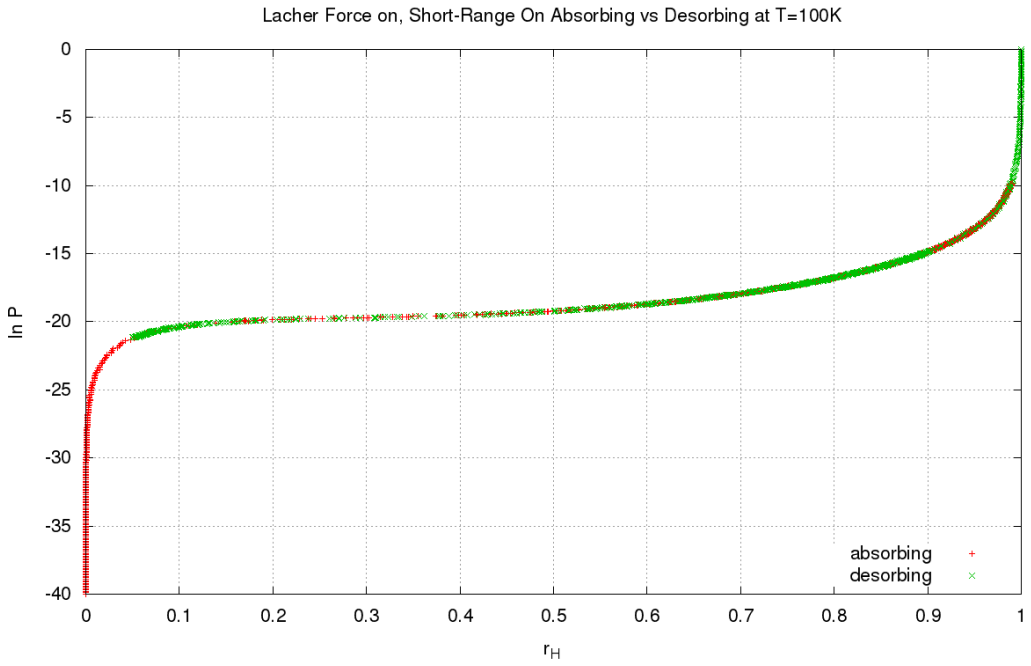

FIGURE 4.7: r_H vs μ_{bath}GCMC ensemble with both long & short range forces – absorption/desorption curves demonstrating no hysteresis cf. fig 4.5.

4.5 How Random is Intel Random?

A computer can generate a single number at random. One could set up a loop to cycle through digits stopping at a keypress. Since a person cannot reduce the time between strokes to much less than 0.1 seconds and given the speed at which the machine can cycle through a set of digits we can safely assume that a digit has been chosen at random. However digital computers are deterministic devices and as such are incapable of generating strings of genuinely random numbers without the use of some external device such as one that monitors junction noise in a semiconductor.

Monte Carlo simulations of the type described here necessitate the serial generation of large quantities of random numbers. Such routines typically develop an initial seed number from the system time. Subsequent pseudo random numbers are developed from an algorithm such as the power residue method where the n^{th} number

$$x_n = cx_{n-1} \bmod N$$

where N and c are constants and the algorithm is initialised with a seed number x_0 . The randomness is a result of rounding errors in the calculation.

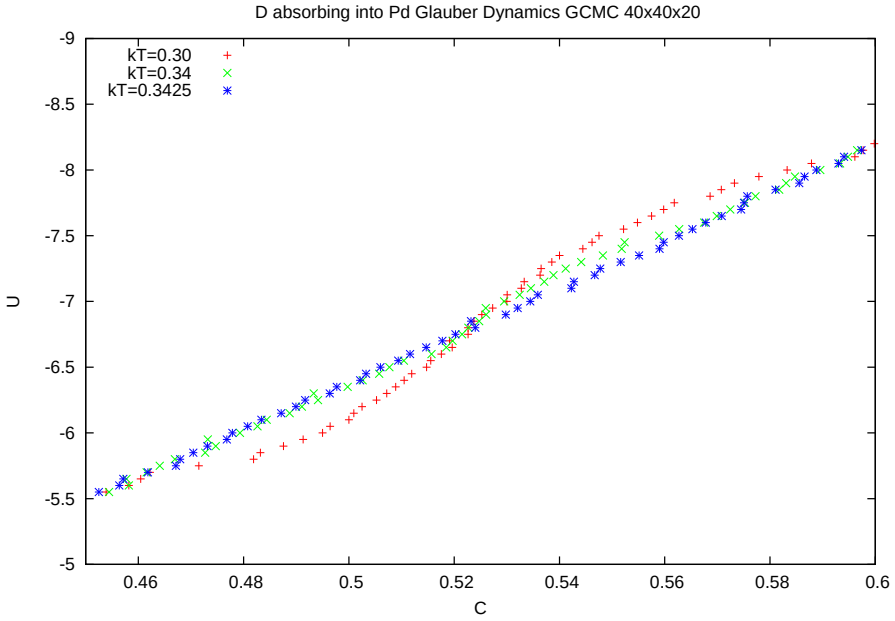

FIGURE 4.8: r_H vs μ_{bath} — indicating kT=0.3425 where r_H 0.5 transition vanishes

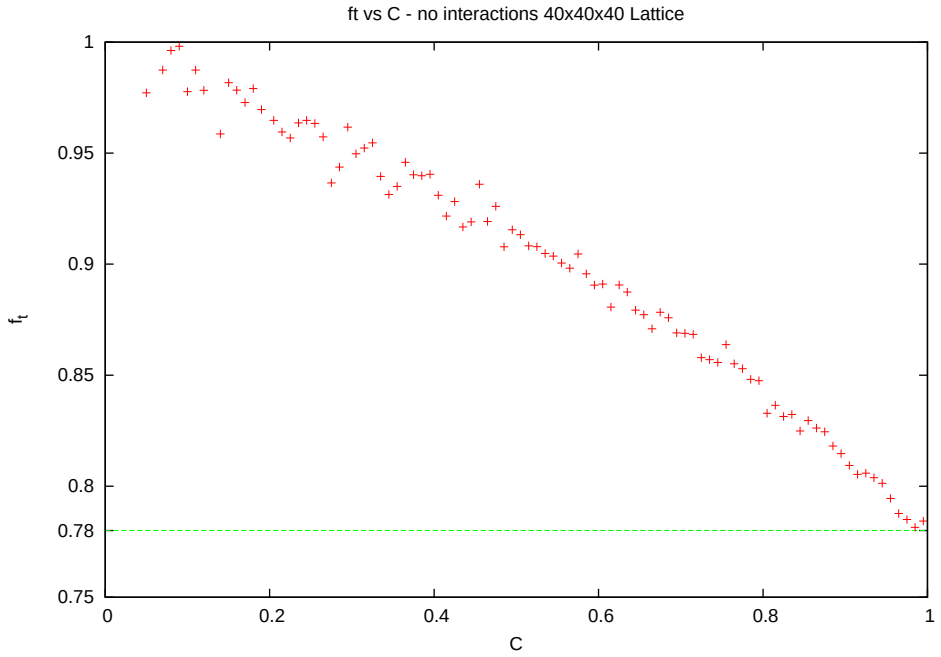

FIGURE 4.9: Tracer Correlation factor f_t vs r_H

Computers are deterministic devices and the algorithm used for such sequences can only be described as pseudo-random, it is clear that the sequence will repeat after some interval.

There would seem to be no general theoretical technique for predicting the performance of most pseudo-random number generating algorithms particularly with regard to the statistical properties of the numbers generated. The sequence length is generally less problematic. For the algorithm above this is maximised when

$c = 8n : \pm 3$ where n is any positive integer and x_0 is any odd integer.

Two comparatively simple tests of the Intel Fortran routine were performed to detect any gross deviation from a random sequence. Firstly the distribution of numbers generated, secondly looking for repeated sequences and partial-repetition.

4.5.1 Frequency Distribution

If one generates M numbers in the range $1 \rightarrow N$ and tally those which lie in each of the equal intervals l/N one would expect a uniform distribution across the intervals. One would require that the individual deviations from the mean tally in each interval should obey the appropriate statistical laws. The probability of finding x numbers within any given subinterval is given by

$$e^{-\left(\frac{(x-\bar{x})^2}{2\sigma^2}\right)} \tag{4.5.1}$$

where $\bar{x}$ is the mean number in all intervals, and σ is the standard deviation given by $\sigma = \sqrt{\bar{x}}$

$$d_{rms} = \sqrt{\frac{1}{M}\sum^{M} d_i^2} = \sqrt{\frac{1}{M}\sum^{M} (x_i - \bar{x})^2} \tag{4.5.2}$$

Given that we expect a Gaussian distribution one would expect to find 68% of the tallies to be within one standard deviation unit of the mean. Additionally we would expect the rms deviation for all subintervals to approach 0 as $M \rightarrow \infty$.

To investigate the frequency distribution a program was written to generate 10^9 numbers in the range $0 \rightarrow 1000$. These were tallied into 1000 equal intervals and the standard deviation calculated. No significant statistical deviations were noted.

4.5.2 Partial-Repetition

The second series of tests attempted to identify any tendency towards repetition of the random sequence. Intel's random number generators should have extremely long periods and it was not expected to cycle within the limit of computation time available, a comprehensive series of tests would be unfeasible. Checks for more subtle signs of partial repetition and the tendency towards serial correlation were chosen. One could look for series of numbers consistently above or below the mean, series which increment in a particular fashion, series which tend to lie within a sub-range of those required and so on. The tests monitored two aspects of the random series. The first simply measured the maximum length of any repeated series. The second test was more subtle and looked for a generalised tendency towards repetition. The program generated 10^9 integers in the range 1 to 1000. The first 1000 of which were systematically compared with the rest and the length of the maximum repeated string was measured.

For any number x_i in a string of n random integers on the range $0 \rightarrow m$ one would expect the probability of it equalling $x_{i+\delta i}$ to be given by

$$p\left(x_i\right) = p\left(x_{i+\delta i}\right) = \frac{1}{m} \tag{4.5.3}$$

and the probability of any series of length s beginning with x_i to be equal to that at an arbitary distance along the sequence to be

$$p = \frac{1}{m^s} \tag{4.5.4}$$

Therefore in any series of n numbers we would expect to find a maximum repeated string length of

$$n = m^s \tag{4.5.5}$$

On runs of 10^9 numbers tests found a maximum repetition length of 4, in line with predictions.

The second test was devised to look for a tendency towards correlation. It generated a large sample of random real numbers converting them to integers in the range $1 \rightarrow 1000$. Then it scanned for complete or *partial* repetitions.

x_i	x_{x+1}	x_{x+2}	x_{x+3}	x_{x+4}	x_{x+5}	x_{x+6}	x_{x+7}	.....	.....
$x_{i+\delta i}$	$x_{i+\delta i+1}$	$x_{i+\delta i+2}$	$x_{i+\delta i+3}$	$x_{i+\delta i+4}$	$x_{i+\delta i+5}$	$x_{i+\delta i+6}$	$x_{i+\delta i+7}$	.....	.....

TABLE 4.1: Coincidences in random number sequences

The algorithm stores a large sample of random integers in an array. Each value is compared with that at an interval d_i further on in the sequence and the number of *coincidences* - matching values is noted. The array is arranged as a loop so comparisons beyond the end of the range return to the beginning. This is then repeated for intervals d_i from 1 to the sample size. The author is unaware of this being a standard form of correlation test. It was based upon a technique used in cryptoanalysis developed by the American cryptographer William Freedman in about 1920 [56]. [1]

The probability of any integer x being equal to another x_i is given by

$$p(x) = p(x_i) = \frac{1}{m} \tag{4.5.6}$$

assuming m degrees of freedom and a uniform distribution. So for the case of m = 100, one expects to see 10 number pairs per 1000 number series compared. The program records a histogram of the number of correlations. Additionally if the number of correlations exceeds an arbitrary threshold this is recorded against the offset d_i, to help detect any periodicity in correlation peaks.

This delightfully simple yet powerful technique detects not only the repetition of complete but also partial or interrupted repetition whereby for example a repetition occurs where only some numbers in a given sample repeat. A key feature being that the computational time scales as only N^2 with the actual integer comparisons being highly efficient.

Fig 4.10 shows the correlation histogram produced. It appears to be of a normal distribution peaking at 10^3, the expected value. The mean correlation is within $< 1 : 10^4$ of the expected value implying no general tendency of partial or complete repeated sequences in the 10^6 random numbers generated.

[1] It is notable that the worlds first electronic computers applied this technique during the W.W.2 to help break the German *Enigma* and Japanese *Purple* ciphers.

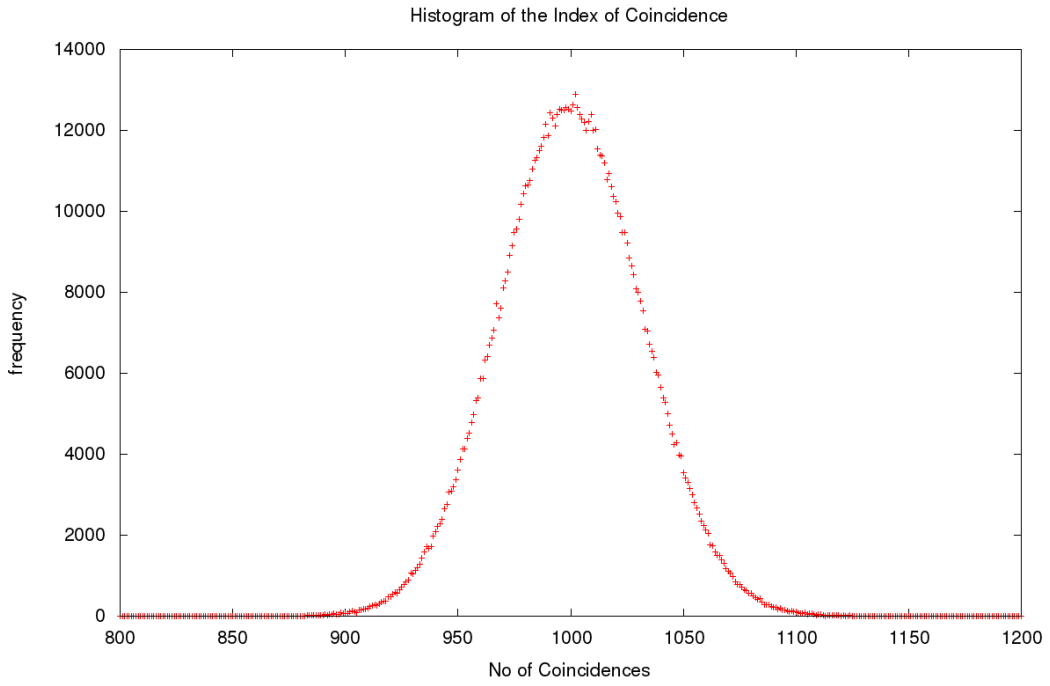

FIGURE 4.10: Coincidences of Repetition seen in a sample of 10^6 random numbers generated by IFort

In summary, runs found no marked deviation for the gross statistical properties which one would expect to see with a random sequence. thus the Intel Fortran random number routines were felt to be adequate for these MC simulations.

4.6 Configuration Options

As stated earlier all these simulations used the same core code modules. Many configuration options were built-in mostly controlled by simple flags to maximise efficiency. The most salient of these include:-

- CMC vs. GCMC with hydrogen exchanging with an external bath.
- GCMC case. Two external baths on opposite sides of the Pd lattice which can be set to differing chemical potentials to model diffusion through a thin membrane.
- Diffusion in and out may be atomic or molecular, via one or two adjacent surface sites.
- Short and long-range interactions may be disabled with flags.

- Kawasaki vs. Glauber dynamics are controlled by a flag.
- Separate interaction potentials may be specified for the 3 hydrogen isotopes.
- The composition of the external baths may be specified.
- The chemical potentials of the three hydrogen isotopes in the baths may be separately set.
- The size of the lattice may be easily reconfigured. From a cube to a thin or thick slice.

4.6.1 Output

Output is written to two or more data files. The primary file is a multi-column data file recording values periodically determined during the run. Other data files record snapshots of the atomic positions in 'standard' crystallographic XYZ format permitting reading by software such as Materials Studio and CrystalMaker. The primary data file typically records:-

- The atomic concentration of hydrogen isotopes within the lattice.
- The mean distance moved by hydrogen atoms migrating through the lattice by isotope.
- The Warren-Cowley short range order parameter for both nn and nnn atoms by isotope.
- The Separation Factor by isotope.
- the mean potential of hydrogen atoms within the lattice by isotope.
- The mean potential of the interstitials sites within the lattice.
- The mean flow rate across a slice of the lattice i.e. when modeling flow through a thin membrane from a heat bath to a sink by isotope.
- Tracer and chemical diffusion coefficients by isotope.
- Chemical Potential within the lattice via the Widom Insertion Method.
- Chemical Potential within the external gas bath calculated by isotope from the partial pressures of the isotopes.

Chapter 5

Investigating the Role of Short and Long Range Forces

This modelling exercise looked at a number of models of the interaction energies between hydrogen atoms in the lattice. Interaction between the palladium and hydrogen atoms was limited to assuming that hydrogen sat at fixed octahedral positions between palladium atoms as has been generally reported. Three scenarios were investigated in detail

1. Short-range, concentration independent, nearest and next-nearest neighbour repulsion, 'Bond-Ross' model.
2. Long-range 'Lacher-Alefeld model', with a concentration dependent attraction.
3. The addition of a concentration dependent scaling to nn and nnn repulsion.

5.1 Testing Sieverts' Law

Sieverts' Law predicts the solubility of diatomic gases in various metals. It is easy to show in the absence of conflicting effects that the solubility at equilibrium is proportional to the square root of the partial pressure in the gas phase. In the case of the Pd-H system at low temperatures and pressures this law breaks down with rising concentration as the system enters the mixed phase region. Presumably due to interactions between the H atoms as they order into stable configurations resisting concentration changes. It

may thus be better to regard Sieverts' law as an empirical relationship broadly applicable to a range of metal-gas systems.

Take the case of hydrogen. The gas must dissociate at the metal surface and we only need be concerned with the mono-atomic hydrogen which enters the metal.

$$H_2 \rightleftharpoons 2\,H$$

$$\text{The equilibrium constant } K^2 = \frac{r_H^2}{P_{H_2}} \tag{5.1.1}$$

where r_H is the concentration of H in Pd and P_{H_2} the partial pressure of H in the gas phase. Thus

$$r_H = K\sqrt{P_{H_2}} \tag{5.1.2}$$

Clearly the PdH system does not conform to this across the composition range. At low concentrations in the α phase, however, it does [28]. Simulations here generated $r_H \propto P^{0.498\mu}$ (figs 5.1) This held for long-range 'Lacher' forces only, short-range repulsion only and a combination of the two. This was to be expected as at low concentrations or high temperatures, the long and short-range forces may be neglected and the system approaches ideality.

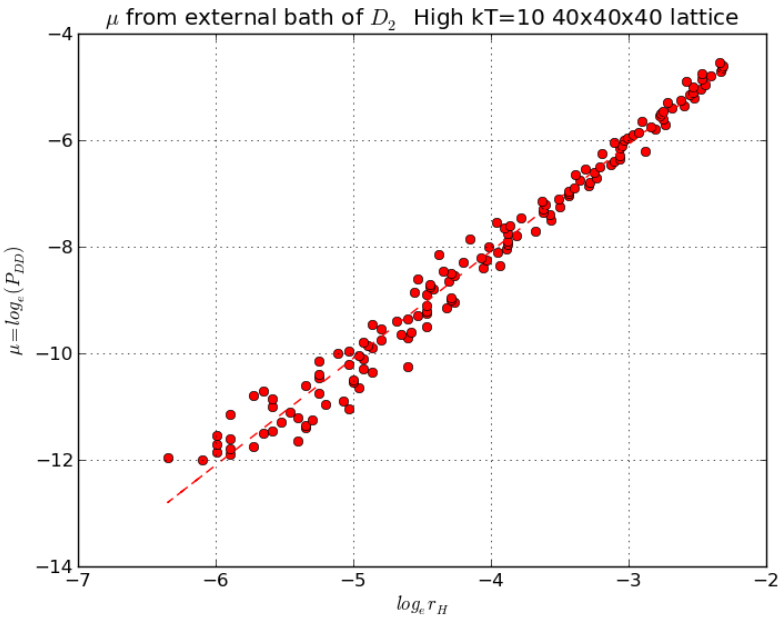

FIGURE 5.1: $Log_e r_D$ vs. μ_{bath} GCMC ensemble

5.2 The Lacher-Alefeld Model

Initially simulations were performed with a long-range attractive force of $V = kr(1-r)$ and without short-range repulsion. The assumptions being a) that the lattice expansion is a zero at zero concentration, the first hydrogen added being free to expand the 'unstressed' lattice, b) as the concentration rises expansion due to subsequent hydrogen atoms decreases.

This correctly simulated a two phase region through to the pure β phase beginning at $r \leq 0.5$ rather than $r \simeq 0.6$ (fig 5.2). Increasing temperature showed the miscibility gap shrinking towards a critical temperature at $r \simeq 0.25$ rather than the expected value of 0.29. Increasing the value of the long-range force only slightly extended the two phase region. Introducing a much smaller n.n and n.n.n attractive force correctly reproduced the I_4/amd structure around $C = 0.5$.

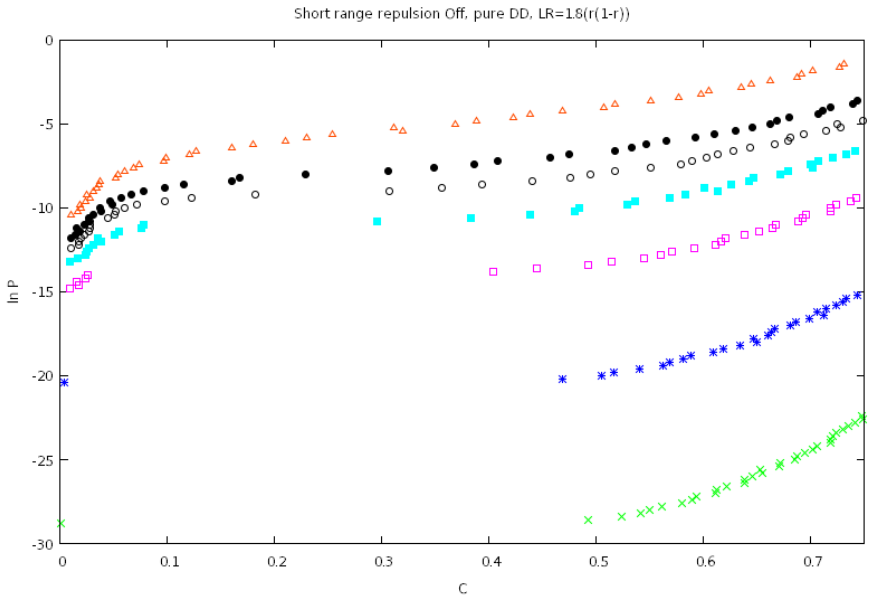

FIGURE 5.2: lnP vs. r, long-range force only, ascending temperature bottom to top

Lacher proposed an empirical fit to the data in that the heat of absorption varied as $-\Delta H = 8535n_H + 9443n_H^2$ Joules per mol [90]. This could be taken to imply that the long-range potential of a hydrogen atom at a site varies as

$$V_{LR} = -k_1 r - k_2 r^2. \tag{5.2.1}$$

This is as as opposed to the later Alefeld [3] model which suggested a variation of

$$V_{LR} = -kr - kr^2. \tag{5.2.2}$$

see fig: 5.3

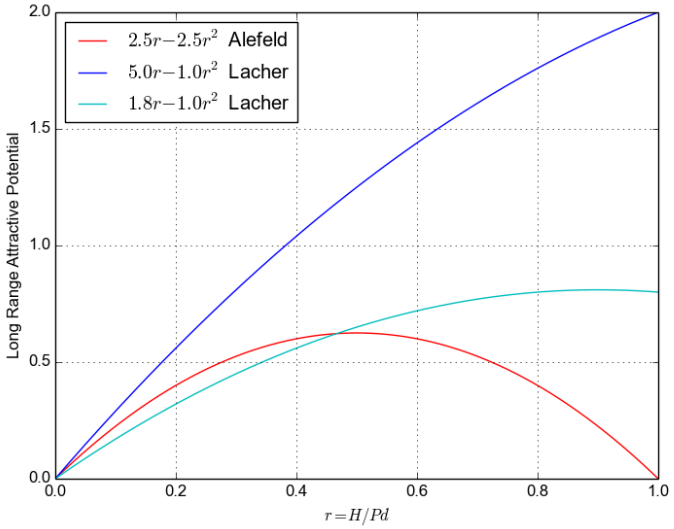

FIGURE 5.3: A simplified Lacher-Alefeld model.

The question then becomes finding suitable values for k_1 and k_2. Simulations were performed around the ratio of $\frac{k_2}{k_1} = \frac{9443}{8535}$ suggested by Lacher. The k_2 reduces the long range attraction at higher concentration and thus extends the two phase plateau region in line with experimental results (fig 5.4). Runs were also performed at a wide range of values for k_2. The ratio given by Lacher appeared to be the optimum of those tested.

The plateau pressure varies as $1/T$ suggesting that the model is in line with expectations. (fig 5.5)

This was a rather simplistic interpretation of Lacher's work. In full form he proposed a curve fitting of

$$log_e p^{\frac{1}{2}} = log\left(\frac{\theta}{1-\theta}\right) - \frac{k_1\theta}{RT} + k_2 \tag{5.2.3}$$

Here $\theta = n/s$ is the number of hydrogen atoms to s - the number of absorption sites fig 5.6. Lacher took this to be 0.59. His reasoning being that Pd as a transition metal possess overlapping s and d electron orbitals, further that studies of Pd-Au alloys and the magnetic susceptibility of Pd-H suggested that the extra electrons provided by the hydrogen completely filled the d orbital at between 0.55 and 0.6 electrons per palladium

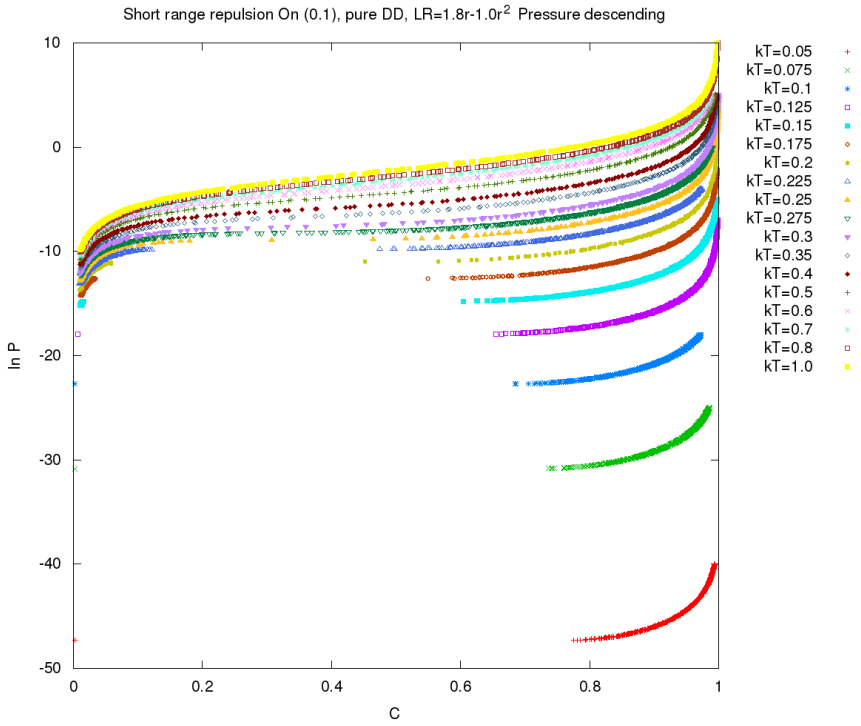

FIGURE 5.4: lnP vs. r, long-range force only, ascending temperature bottom to top

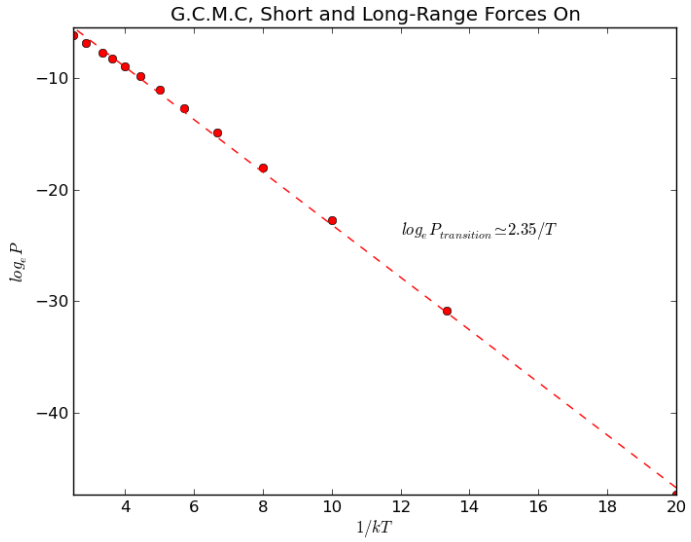

FIGURE 5.5: GCMC Long and short-range forces on.

and that *'a definite process of hydrogen absorption will reach completion when* $r = 0.6$. However, whilst this provides good fitting to experimental data concentrations above $0.59H/Pd$ are seen experimentally.

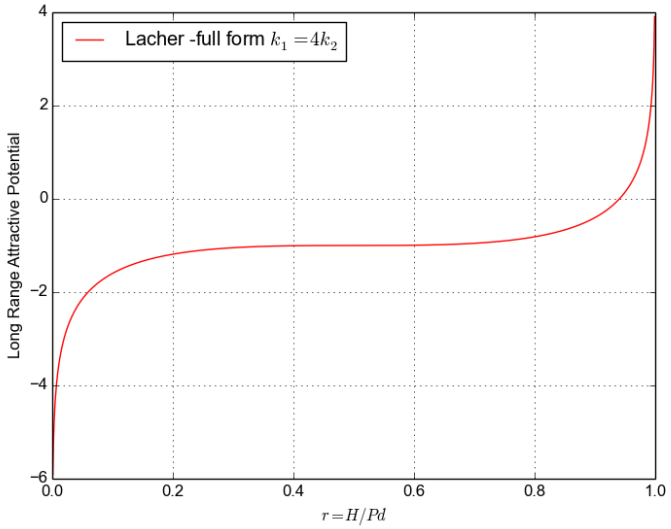

FIGURE 5.6: The full fit as proposed by Lacher $V_{LR} = -k_1 r - k_2 r^2$

5.2.1 Lacher-Alefeld - the Role of Short-Range Forces

As has been discussed previously the long-range attraction reproduces the general shape of the ab/desorption curves . In the presence of only this long-range attraction there is no requirement for the hydrogen to adopt any particular configuration. It is the short-range repulsion that encourages the formation of crystalline structures.

In those simulations the short-range forces are limited to nearest neighbour and next-nearest neighbour interactions. A site's interaction potential is computed as the sum of the interaction potential of the n_{nn} and n_{nnn} neighbours.

As expected, simulations show that increasing strength of the short-range repulsion pushes the high concentration end of the miscibility gap towards greater concentrations whilst too low a value suppresses ordering. It would be reasonable to expect that a suitable ratio is one in which the two forces cancel at a concentration of $r = 0.50$. However runs demonstrate that this is far too high. More realistic P-r curves are obtained by setting the short range interactions such that the net attractive force is a maximum at $C = 0.5$ (fig 5.7).

Wang *et al.* [165] presented a total energy study of various structures in Pd-H (fig 5.8) indicating that the interaction energy is a minimum at $r = 0.5$. The scaling was adjusted on the long vs. short-range forces to produce a mean site energy minimum at $r = 0.5$. An extensive range of runs indicated that this did not affect the shape of the

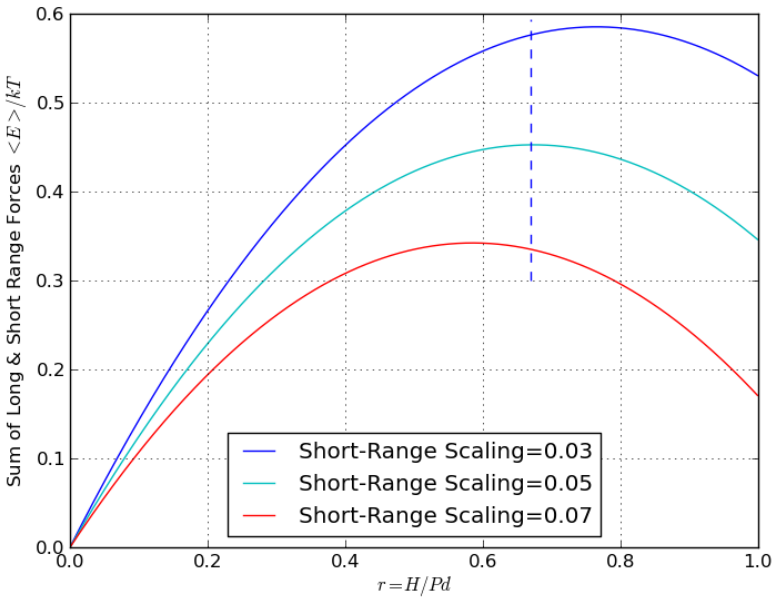

FIGURE 5.7: Various short range scaling factors, dashed line at r=0.67. These are summed with a long-range force scaled at 1.0

phase diagram. However it did cause interesting additional structures to appear above $r = 0.76$.

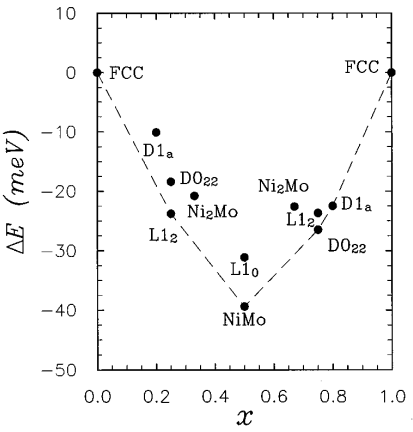

TABLE I. Symmetry of various ordered phases considered in the calculation and their lattice constants.

	Structure	Symmetry		Lattice constant (Å)
PdH_0	fcc	O_h^5	$Fm3m$	3.94
$PdH_{0.2}$	$D1_a$ (Ni_4Mo)	C_{4h}^5	$I4/m$	3.98
$PdH_{0.25}$	$L1_2$	O_h^1	$Pm3m$	3.99
	$D0_{22}$ (Ni_3Mo)	D_{4h}^{17}	$I4/mmm$	3.99
$PdH_{0.33}$	Ni_2Mo	D_{2h}^{25}	$Immm$	4.01
$PdH_{0.50}$	$L1_0$	D_{4h}^1	$P4/mmm$	4.04
	NiMo	D_{4h}^{19}	$I4_1/amd$	4.04
$PdH_{0.66}$	Ni_2Mo	D_{2h}^{25}	$Immm$	4.06
$PdH_{0.75}$	$D0_{22}$ (Ni_3Mo)	D_{4h}^{17}	$I4/mmm$	4.07
	$L1_2$	O_h^1	$Pm3m$	4.07
$PdH_{0.80}$	$D1_a$ (Ni_4Mo)	C_{4h}^5	$I4/m$	4.08
PdH_1	fcc	O_h^5	$Fm3m$	4.11

FIGURE 5.8: Formation energies for various Pd_AH_B structures. The dashed line represents the lowest-energy states. Wang *et al.* [165]

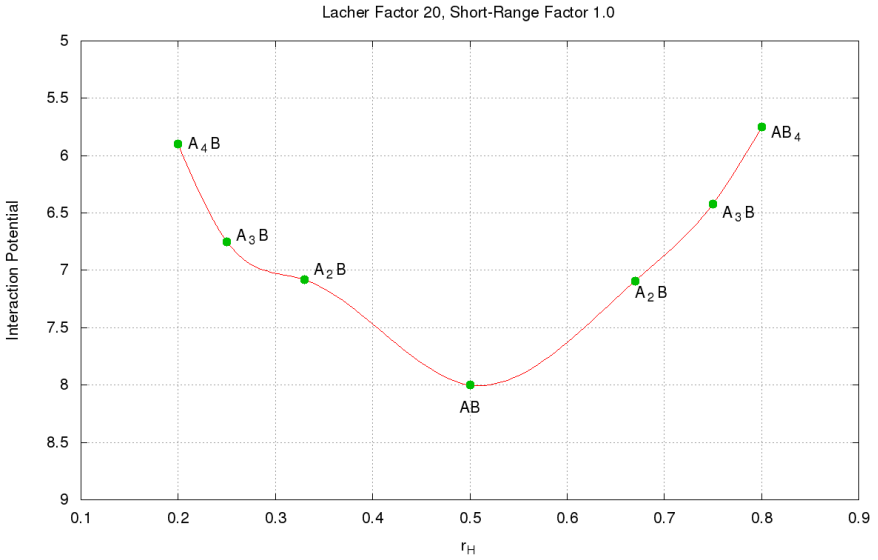

FIGURE 5.9: Formation energies for various Pd_AH_B structures - CMC simulations employing both long and short-range forces. The similar fit to fig: 5.8 may imply that these models are valid.

5.3 Combining Long and Short-Range Forces (Bond-Ross-Lacher-Alefeld)

Many simulations were performed to test the effects of combining the long and short-range forces. As expected the introduction of the long-range attraction did not change the form of the phase diagram nor temperatures of the phase changes (fig:5.10). Further simulations were performed to investigate the short-range structures which formed when both long and short-range forces were involved as compared to short-range only.

5.3.1 Force Parameters

Simulations indicate that the following combination of long and short range interactions correctly reproduced many features of the phase diagram in both canonical and grand-canonical scenarios.

- Long-range attraction $= L.R.ScalingFactor * (1.8r - 1.0r^2)$

- Short-range repulsion $= S.R.ScalingFactor * (1.0n_{nn} + 0.25n_{nnn})$

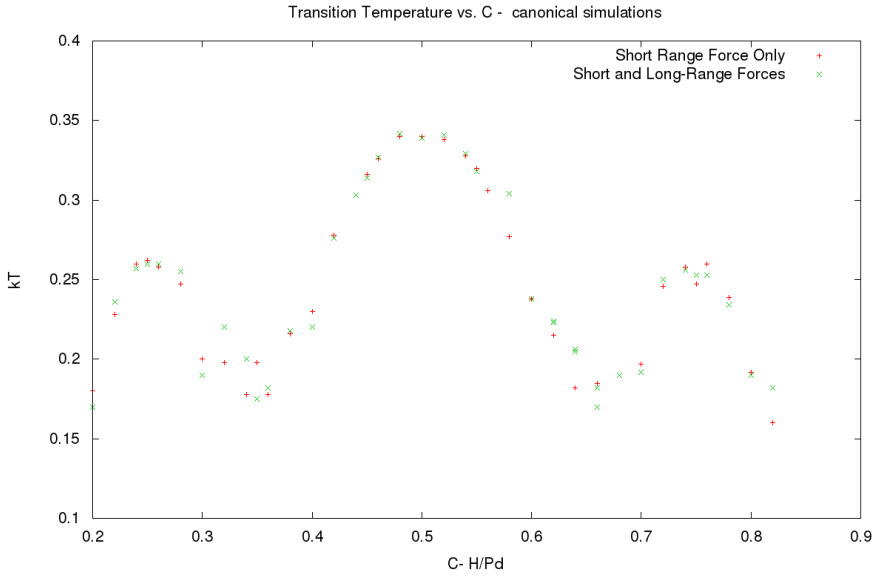

FIGURE 5.10: Phase Diagram for various fixed concentrations - (red points:- short-range forces only, green points:- short and long-range forces)

where n_{nn}, n_{nnn} = numbers of nearest and next nearest neighbour hydrogens to a site and L.R. ScalingFactor = 1.0 and S.R. ScalingFactor =0.02-0.10.

5.4 Summary

The use of a long-range concentration dependent attraction of the form $V_{LR} = (1.8r - 1.0r^2)$ reproduces the 2-phase region over the expected concentration range with the plateau pressure varying as $1/T$.

To this may be added a short-range repulsion of the form $V_{SR} = (1.0n_{nn} + 0.25n_{nnn})$. With suitable scaling between the two, both the plateau and phases changes appear to conform to experimental data.

However there is a trade-off in this simplistic model in that if too low a ratio of LR:SR is chosen then steps occur in the pressure composition isotherms at lower temperatures.

Chapter 6

Phase Structures

As the primary focus of these studies was to investigate short-range ordering. routines were written to calculate virtual diffraction patterns as discussed earlier. These generated either conventional 1d diffractographs or 2d contour plots from selected crystal planes as defined by their Miller indices.

6.1 Previous Studies

Wang *et al.* [165] report the results of a total energy study of Pd-H in which they looked specifically at ordering in the (420) planes. The I_4/amd structure was apparent as two fully filled planes in (420) followed by two empty stoichiometric at C=0.5. As the concentration rose to C=0.75 one of the empty planes fills to 3 filled and 1 empty at c=0.75. In the range to C=0.8 they report that development of the Ni_4Mo structure - I_4/m (spacegroup 87) should be energetically favourable. This structure should be apparent as four filled followed by one empty plane in (420).

6.2 Order-Disorder vs. Temperature

Ordering takes place as the temperature of a canonical or G.C ensemble is reduced. Plots at $r_H = 0.05$ and $r_H = 0.65$ are shown in fig 6.1 & fig 6.2. These are canonical runs with mean site potential vs T. The temperature of the phase transitions are unaffected by the long-range Lacher attraction.

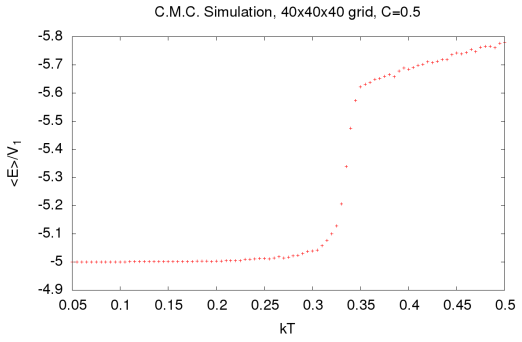

FIGURE 6.1: mean site potential vs T, r=0.50, single phase transition

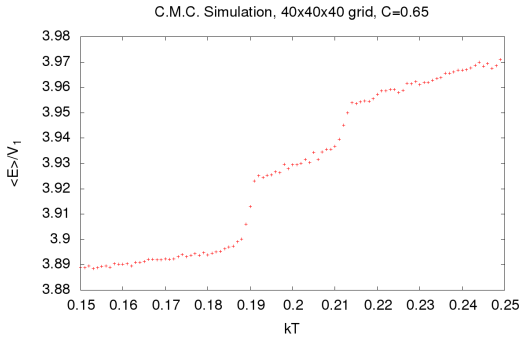

FIGURE 6.2: r=0.65, two phase transitions appear

Phase transitions may be observed via a range of metrics. The mean site potential will change abruptly as atoms undergo a dramatic reordering. One may also observe changes in the fraction of neighbouring atoms. Whilst the number of nearest neighbours are a poor indicator of transitions the fraction of next-nearest neighbours shows useful and interesting detail. Fig 6.3 & Fig 6.4 show the n.n.neighbour plots corresponding to fig 6.1 & fig 6.2 . Routines to monitor the size of grain boundaries via localised changes in interaction potential also proved useful.

Code was written in Visual-Python to generate pseudo-3d representations of the lattice which could be viewed using stereo glasses. Specific planes could be selected and one could move through the lattice viewing neighbouring planes in sequence (figs 4.1 & 6.7 & 6.9).

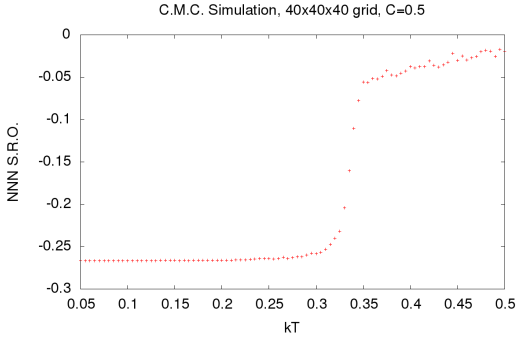

FIGURE 6.3: n.n.n. Short-Range Order, r=0.50, single phase transition

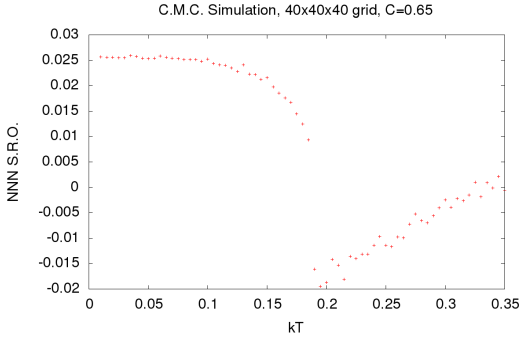

FIGURE 6.4: r=0.65, two phase transitions appear

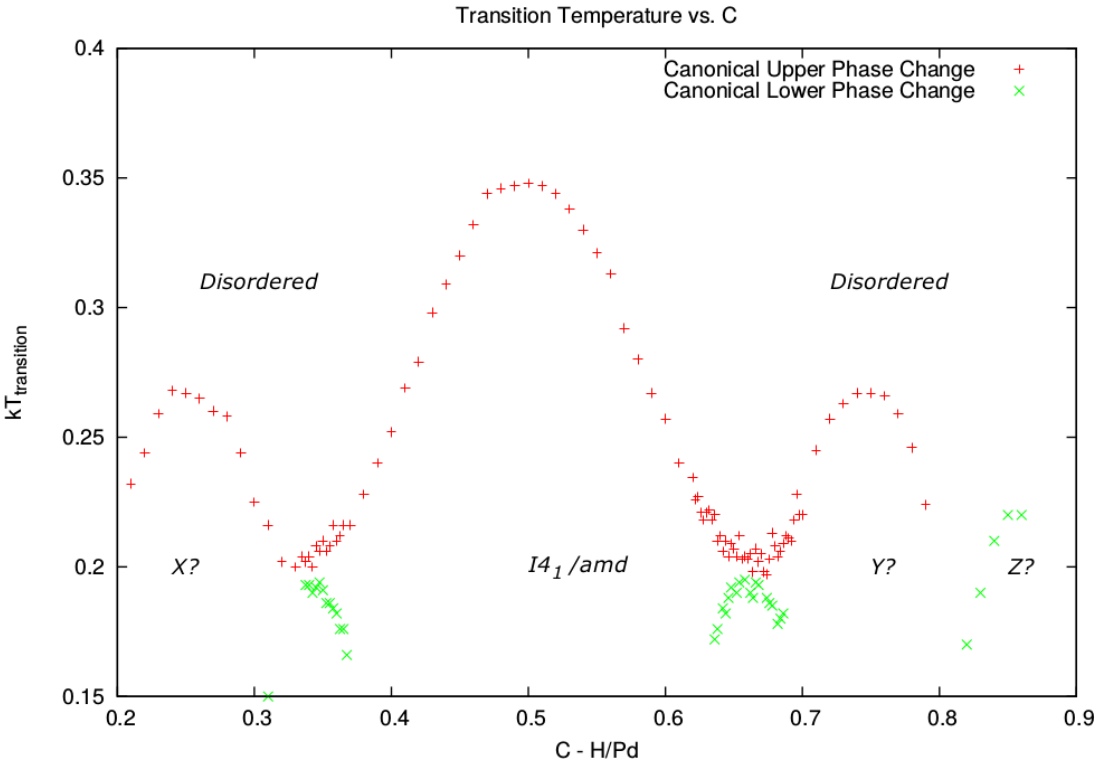

FIGURE 6.5: Variation of Transition temperature with r_H - canonical ensemble

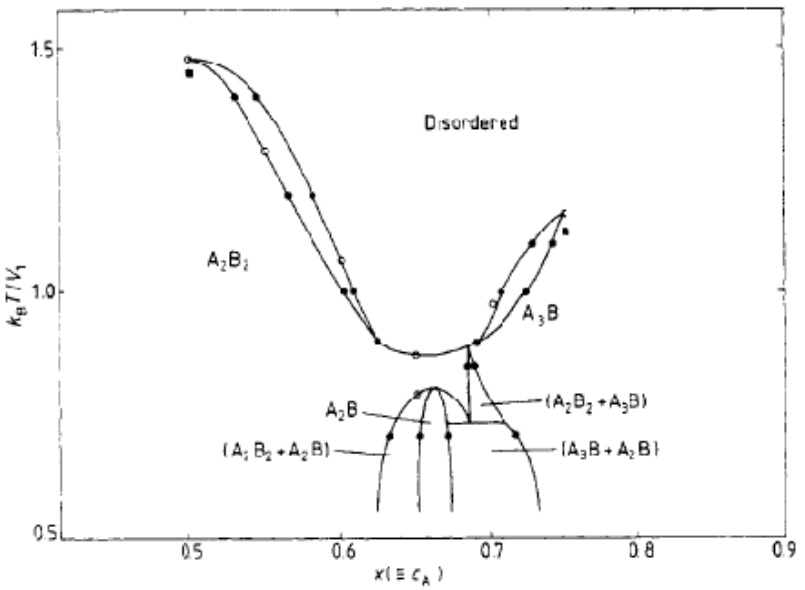

FIGURE 6.6: Corresponding plot from Bond & Ross [23]

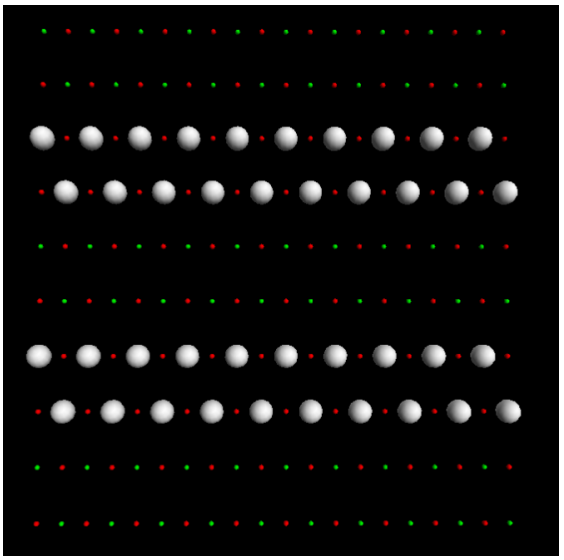

FIGURE 6.7: View in 420 plane, r=0.5, H-white, Pd-red, Vacancy-green

Concentration	Symmetry	Structure	(4,2,0) plane fill	Superlattice Reflections
0.20	$I4/m$	$D1_a$ Ni_4Mo	F-F-F-F-E	$\left(\frac{4}{5}, \frac{2}{5}, 0\right)$
0.25	$I4/mmm$	Ni_3Mo	F-E-E-E	$\left(1, \frac{1}{2}, 0\right)$
0.33	$Immm$		F-E-E	$\left(\frac{4}{3}, \frac{2}{3}, 0\right)$
0.50	$I4_1/amd$		F-F-E-E	$\left(1, \frac{1}{2}, 0\right)$
0.50	$P4/mmm$	$L1_0$	F-F-E-E	$(1, 0, 0)$
0.67	$Immm$		F-F-E	$\left(\frac{4}{3}, \frac{2}{3}, 0\right)$
0.75	$Pm3m$	$L1_2$ Ni_3Mo	F-F-F-E	$(1, 0, 0)$
0.75	$I4/mmm$	DO_{22} Ni_3Mo	F-F-F-E	$\left(1, \frac{1}{2}, 0\right)$ $(1, 0, 0)$
0.80	$I4/m$	$D1_a$ Ni_4Mo	F-F-F-F-E	$\left(\frac{4}{5}, \frac{2}{5}, 0\right)$

TABLE 6.1: Predicted superlattice reflections Blaschko:1991 [21]

6.3 Reference plots in 1 and 2d

As a starting point, plots were generated for a series of the expected structures. Lattices were generated with ideal phases which were checked using a 3d visualiser which allowed one to 'move' through the lattice along the (420) planes to visually confirm structure [Appendix B figs B.1 to B.5].

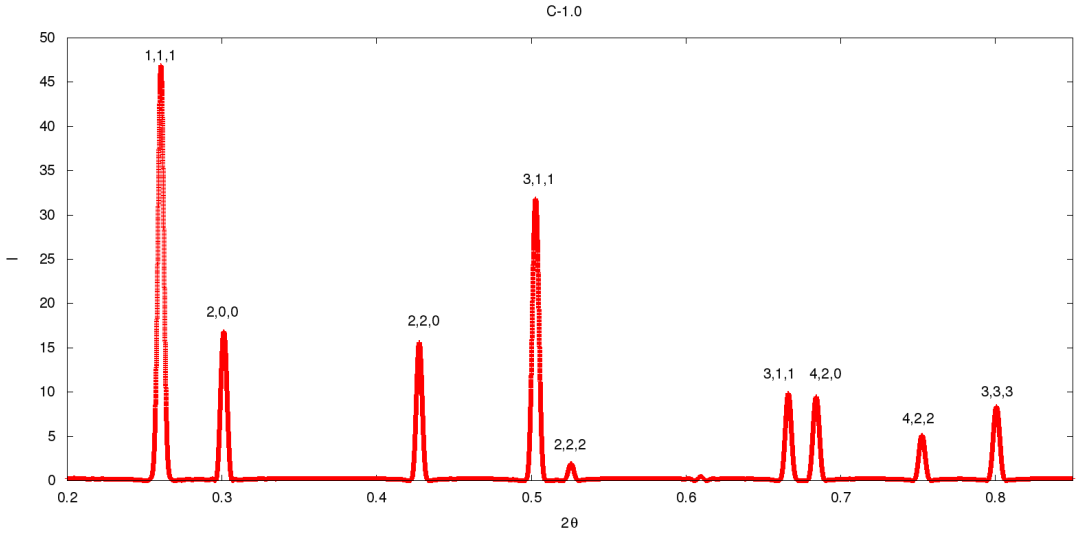

FIGURE 6.8: Fully filled lattice showing reflections expected from an F.C.C. structure *(the small size of the (2,2,2) peak is puzzling).*

This becomes interesting when recalling that phases transitions occurred at the same temperatures with and without the long-range 'Lacher' Force active. This confirms the expectation that the long-range attraction has little effect upon short-range ordering. The 1d diffractograms appeared identical across concentrations from 0.1 to 1.0 for both short-range force only and both long plus short range.

6.4 Observed Structures

A great many simulations were performed at differing concentrations and ratios of short to long-range forces. The most salient features are described, particularly comparing ordering with only short-range active with both long and short-range active.

6.4.1 Concentrations below 50%

As the stable structures of these structures of the form A_xB_y the diffraction patterns at 25% and 33% mirror those at 67% and 75%.

6.4.2 Concentrations above 50%

As predicted the I_4/amd structure is apparent with two filled followed by two empty planes in [420]. This happens whether the long-range forces are active or not.

With the long-range forces scaled as stated previously as the concentration increases one of the empty planes progressively fills to 3 empty and one filled (420) at $r = 0.75 H/Pd$. This appears to be the $I4/mmm$ - Ni_3Mo structure.

The situation above this concentration becomes interesting though problematic to interpret.

6.4.3 Concentrations 75% to 80%

With long-range forces active this region becomes rich in features. As one would expect the empty fourth plane in (420) begins to fill. Notably this is partly at the expense of two of the three filled planes i.e. vacancies start to appear in the two planes either side of the empty one as that fills more quickly than just from the increased overall concentration. At $r = 0.76$ visual observation of four adjacent planes in (420) appears to indicate that micro-domains are growing into the filled planes fig 6.9. This appears to corroborate the paper by Blaschko, Fratzl and Klemencic [21]. In this they proposed that for Pd-D in the concentration range $0.7 < C \leq 0.78$ microdomains of various composition ratios Ni_xD would form.

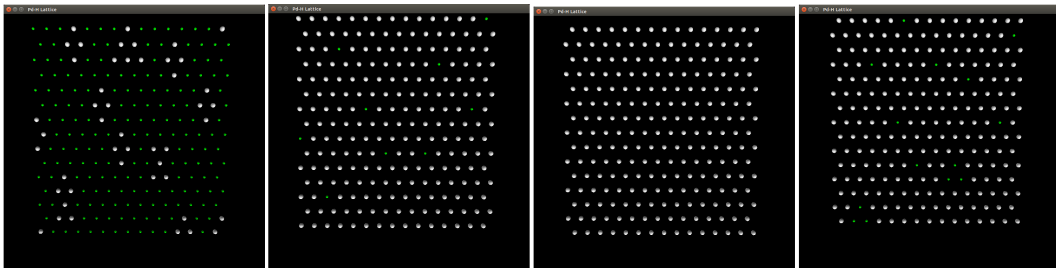

FIGURE 6.9: r=0.76, progressive filling of fourth plane (left) in (420) partly due to vacancies (green) appearing in adjacent planes

The 2d diffraction pattern in (hk0) has now radically changed from that at $r = 0.75$ fig 6.10 & table: 6.1.

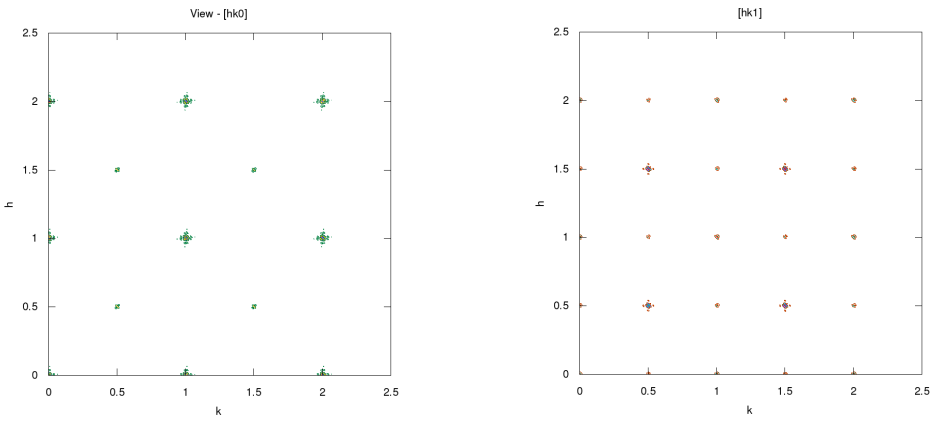

FIGURE 6.10: r=0.76 , possible superlattice reflections at (0.5,0.5,0) – same at 0.78

At 80% full the structure once again changes giving fig 6.11. Visual inspection of the lattice indicates that it is forming a degraded Ni_3Mo structure i.e small fairly well ordered regions with 'clumps' of interstitials within the ordered regions.

Further work may be required here to be confident that these models can reproduce the Ni_4Mo structure.

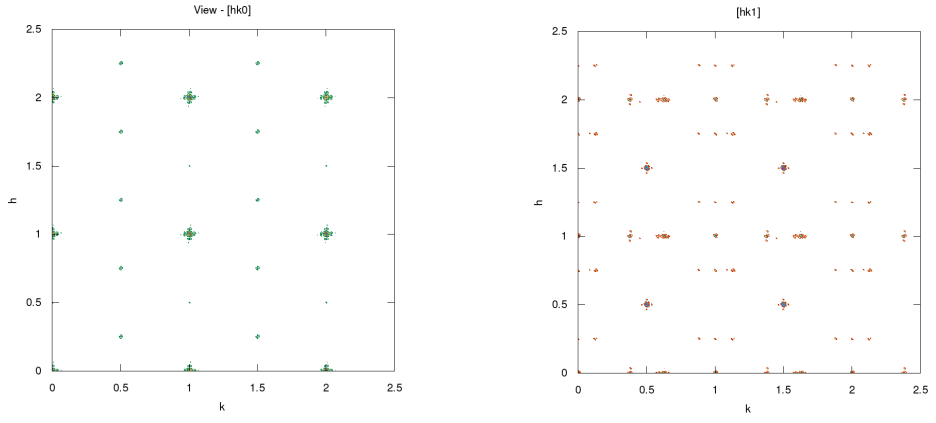

FIGURE 6.11: r=0.80, *Long-range scaling factor=20*

6.5 Seeking I4/m

Neutron diffraction studies have reported the emergence of the Ni_4Mo (I4/m) structure at $C = 0.76$ & 0.78 [45, 21] illustrated by superlattice reflections at $\frac{4}{5}, \frac{2}{5}, 0$ (see fig: B.3). Two body pairwise interactions such as the Bond-Ross model do not generate this structure and this was confirmed here by simulation. Kanamori and Kakehashi [79] concluded that one would need to extend interaction beyond the 9th nearest neighbour to replicate these structure.

It was hoped that introducing reasonable values for a 'Lacher' long-range interaction would cause Ni_4Mo to appear. This does not seem to be the case. Many simulations were performed at fixed concentrations where the temperature was gradually lowered to a simulated temperature of approx 10K. These were repeated for various values of the long range Lacher interaction where

$$\text{Long-range attraction = L.R. ScalingFactor } * \left(1.8r - 1.0r^2\right)$$

$$\text{Short-range repulsive potential } = \left(N_{nn}V_{nn} + \frac{1}{4}N_{nnn}V_{nnn}\right)$$

with values for the LR:SR scaling factor of between 0 and 500. At no point was there strong evidence for Ni_4Mo. It would be reasonable to conclude that more sophisticated interactions are required to model this phase.

Given that the introduction of the Lacher interaction reproduced the miscibility gap simulations modelling the stability of the Ni_4Mo structure were performed.

Reversing the above process simulated lattices of ideal Ni_4Mo structure had their temperatures raised from approx 10K to observe stability and transitions, again for concentrations between 0.70 and 0.85 and long-range scaling from 0 to 500. The temperature at which Ni_4Mo disappeared, $\sim 359K$, was independent of the long-range force. As expected the subsequent phases which formed did differ with temperature. This was to be expected as such local ordering one would predict would be due to short-range forces.

6.6 Summary

At concentrations below $r \simeq 0.5$ the long-range Lacher attraction appears to have little effect upon the structures observed i.e. the short-range forces dominate. As above $r \simeq 0.7$ the Lacher attraction would appear to add more complex structures than the short-range forces alone. Simulations over a wide ratio of forces did not reproduce the Ni_4Mo structure, however there were faint hints from visual inspection that it may have started to form.

Interestingly, C.M.C. runs in which the temperature of lattices populated with Ni_4Mo was raised indicate that the temperatures at which this structure disappeared were unaffected by the strength of the Lacher attractive force. This may imply that more localised short-range forces need to be invoked to explain the formation of this phase. Possibly a combination of localised attractive as well as repulsive effects or triplet rather than simple pairwise interactions are required.

Chapter 7

Ab/Desorption Studies

A primary aim of these studies was to produce accurate simulations of the ad/desorption of hydrogen into bulk Palladium particularly reproducing the mixed phase region where concentration rises and falls over a very narrow pressure range. Should this be successful one could then model differences in diffusion between the three hydrogen isotopes.

Initially attempts were made to model the fine details of transfer at the surface. A hydrogen molecule was assumed to dissociate at the surface if there were two closely spaced vacancies and if the process was energetically favourable. Similarly for diffusion out from the metal. This approach was abandoned as it was felt to be excessively complex and computationally expensive. It was felt that the dominant factors on diffusion, saturation of surface sites aside, would be within the bulk of the Pd i.e. that $H_2 \longrightarrow 2\,H$ occurs very quickly.

Thus after much simulation the model was simplified to a Pd lattice where hydrogen could move either between adjacent sites within the lattice or occasionally 'jump' to one of two external 'baths'. The probability of *attempting* an exchange with the external baths was equal to that of an atom attempting to jump in. This probability was of the order of 10^{-4} of the probability that an atom would attempt simply to exchange to a neighbouring site to ensure that the lattice was able to stabilise to a preferred structure.

The Pd lattice was modelled as a rectangular slab situated between two external baths on opposing faces. This was to permit studies of diffusion as through a membrane with differing pressures and/or isotope concentrations in either bath. Periodic boundaries were applied on the four faces not in contact with the external reservoirs.

Typical lattice sizes used were a cube of 40x40x40 palladium atoms with octahedral interstitial sites half-way between the Palladium atoms. 10^8 attempted site exchanges were attempted for each data point, i.e. for each temperature or bath pressure increment.

The main focus of these studies was to investigate the role of long-range attraction in reproducing the miscibility region.

7.1 Absorption with only Short-Range Repulsive Forces

Initial simulations were performed employing only the Bond-Ross neighbour and next nearest neighbour repulsions e.g. fig: 7.1. The short-range repulsion alone does not

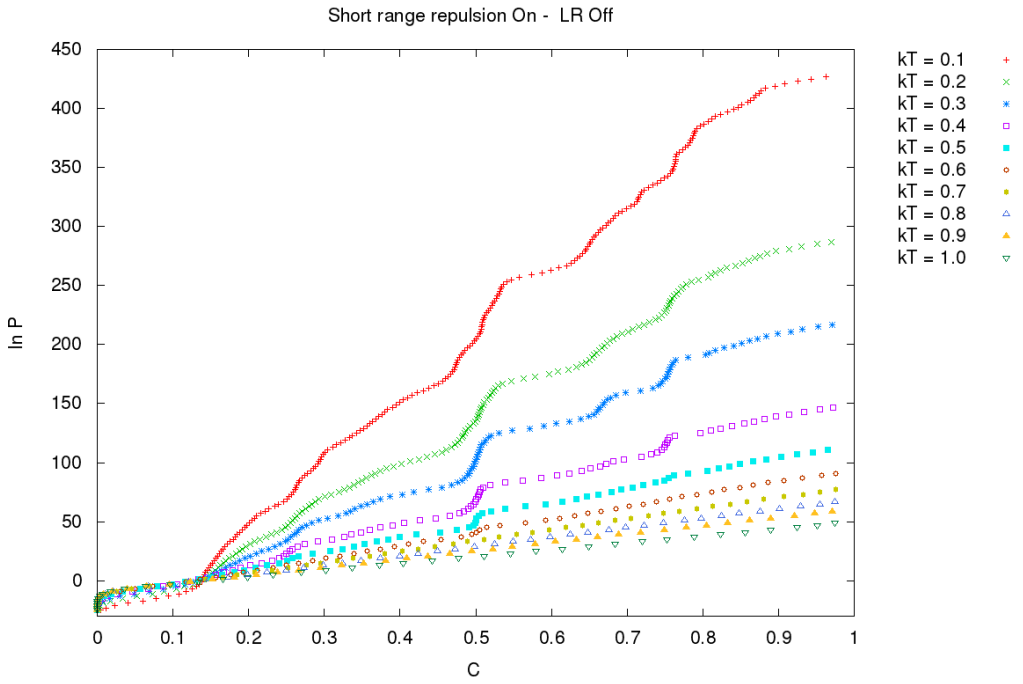

FIGURE 7.1: Short range repulsion On, Long-Range Off, DD absorbing from bath

seem able to reproduce the level pressure plateau in the two-phase region at although one could clearly discern steps due to phase ordering processes.

7.2 Absorption with only Long-Range Attractive Forces

The first studies looked at reproducing the miscibility region using a simple long-range attraction where $V_{L.R.} = z(r - r^2)$ fig: 7.2. Tests were performed with short-range repulsion switched off then on.

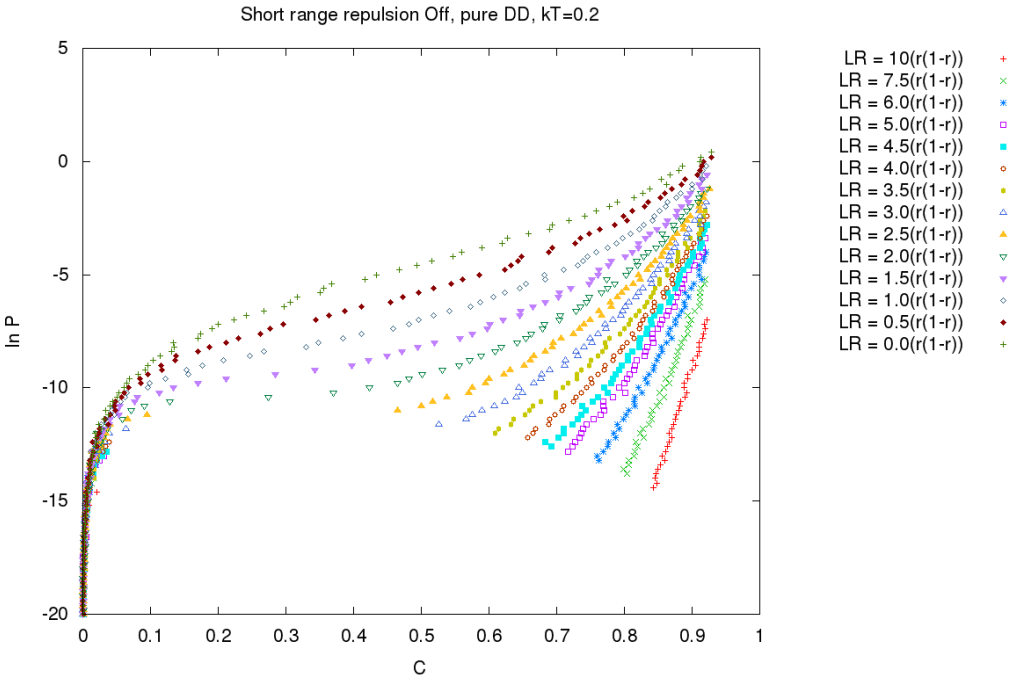

FIGURE 7.2: Short range repulsion off, Long range $V_{L.R.} = k(r - r^2)$

Runs at various temperatures confirmed that as the temperature rose the miscibility plateau shrank for a given value of $V_{L.R.}$. Matching a suitable miscibility concentration range to temperature allowed a reasonable value to be estimated for $V_{L.R.}$. A problem became apparent in that this model did not match the experimentally observed concentration range well, tending to centre at too low a value of c=0.25 rather than 0.29. Furthermore, when the short-range repulsive forces were activated ordering processes became apparent fig 7.3. A variety of models of long-range concentration dependent force were carefully investigated: $V_{L.R.} = k(r)$, $V_{L.R.} = k(1 - r)$, $V_{L.R.} = k(r(1 - r))$ and $V_{L.R.} = k_1 r - k_2 r^2$. Of these the last best reproduced miscibility plateau over the desired concentration range.

As discussed previously Lacher's study [90] was taken to imply that a more realistic model would have $V_{L.R.} = -k_1 r - k_2 r^2$ where $k_1 = 1.8k_2$. This reproduced the plateau centred on $r = 0.29\frac{H}{Pd}$with $log_e p \propto \frac{1}{T}$ (fig:5.5). The problem now comes in finding a ratio of short to long-range potentials that reproduces both the miscibility plateau and

the short-range ordering esp. for $r \leq 0.5$. Too low a ratio will cause ordering process to dominate, too high and the ordering is suppressed. The width of the miscibility region was taken from a number of sources, esp. Bond & Ross [23] and Wilkinson [173]. The fact that the upper limit of the 2 phase region is generally accepted to be $\simeq 566K$ allows a temperature scale to be set on plot of mean site interaction potential kT. Looking at fig:7.2, $kT = 0.2$ corresponds to $T \simeq 330K$ giving an expected concentration range of $r \simeq 0.05- \simeq 0.55$.

7.3 Adsorption in the Presence of Short and Long-Range Forces

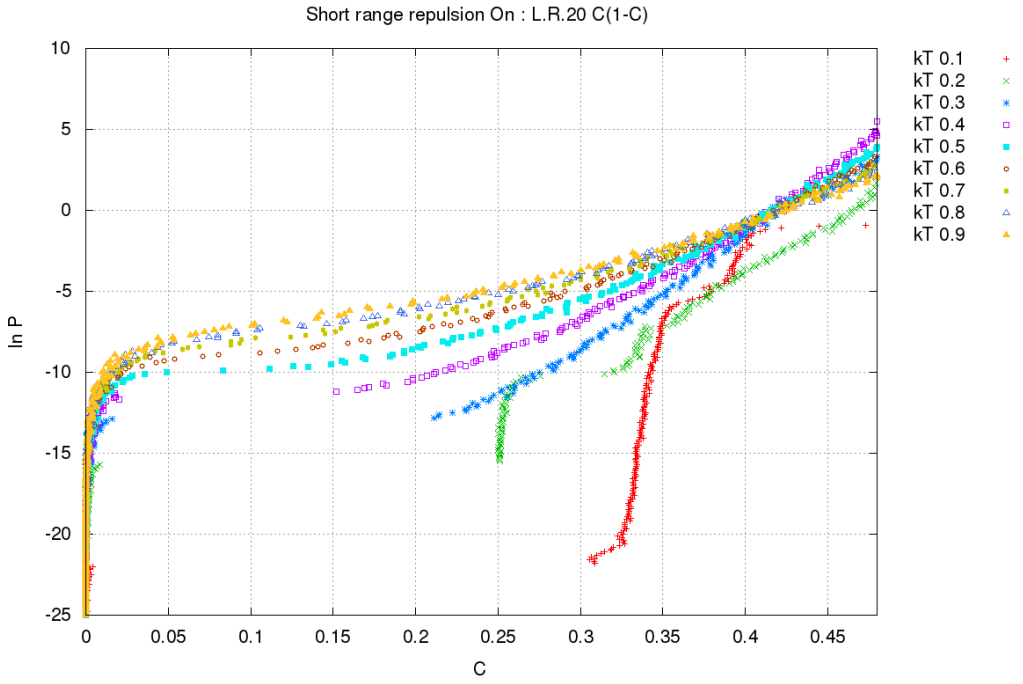

FIGURE 7.3: Short range repulsion on. Long range $V_{L.R.} = k(r - r^2)$. Ordering process become apparent at too high a ratio of S.R. to L.R. force.

The problem becomes one of finding a suitable ratio of short to long-range force which accurately reproduces the miscibility plateau whilst permitting short-range ordering to occur. This was at least partial successful in this simplistic model.

Increasing the ratio of S.R. repulsion to a concentration dependent L.R attraction has four main effects.

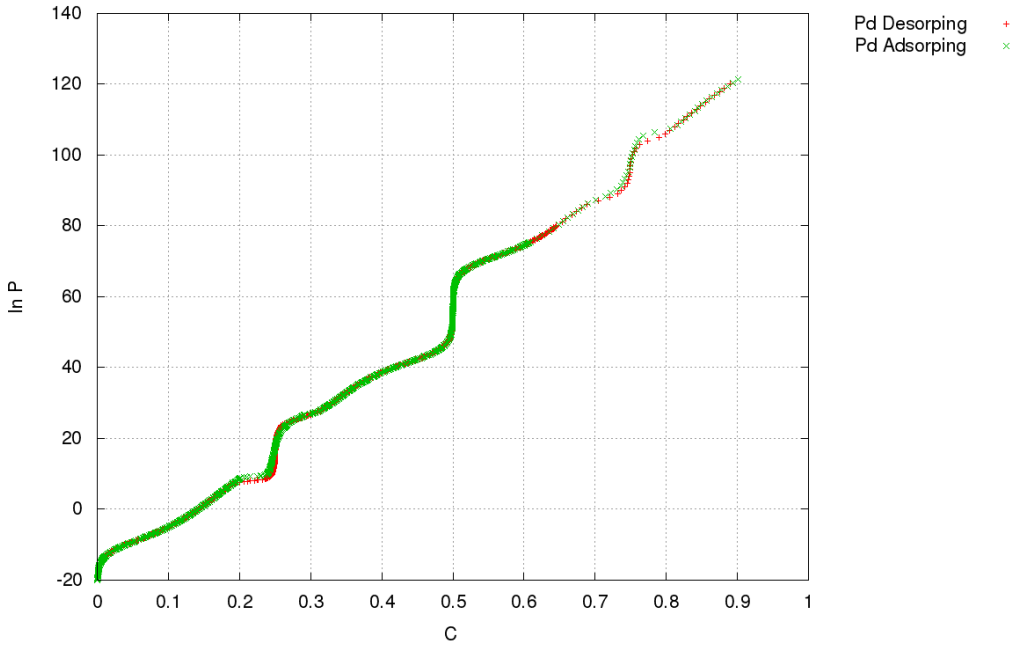

FIGURE 7.4: Moderate ratio L.R:S.R - ad/desorption pressure very similar with short-range ordering apparent though no clear phase separation

- The width of the two-phase region decreases particularly from the high concentration side.
- The pressure range of the plateau increases i.e. it develops a slope.
- Short-range ordering introduces steps in plots of chemical potential vs. concentration.
- Short-range ordering effects become more clearly defined. i.e. in plots of mean site potential vs. temperature.

However even at low S.R.:L.R. ratio ordering can still be clearly seen in plots of short-range order parameter vs. temperature or virtual diffraction patterns.

7.4 Summary

In summary this simplistic model does appear to reproduce ad/desorption curves well whilst reproducing phases changes across the concentration range. However the long-range attraction does inhibit short-range ordering leading to very long anneal times. As expected it did not reproduce hysteresis seen in experiment.

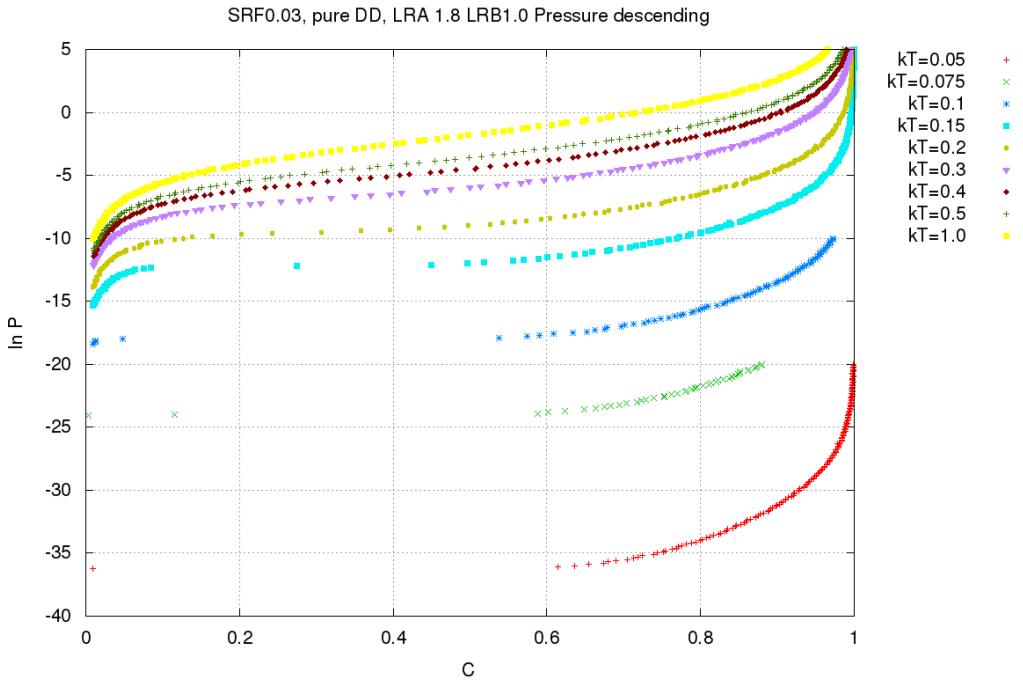

FIGURE 7.5: High ratio L.R:S.R - effect of short-range ordering is masked. As the relative strength of the short-range repulsion is increased then steps appear in the β phase as seen in fig 7.3

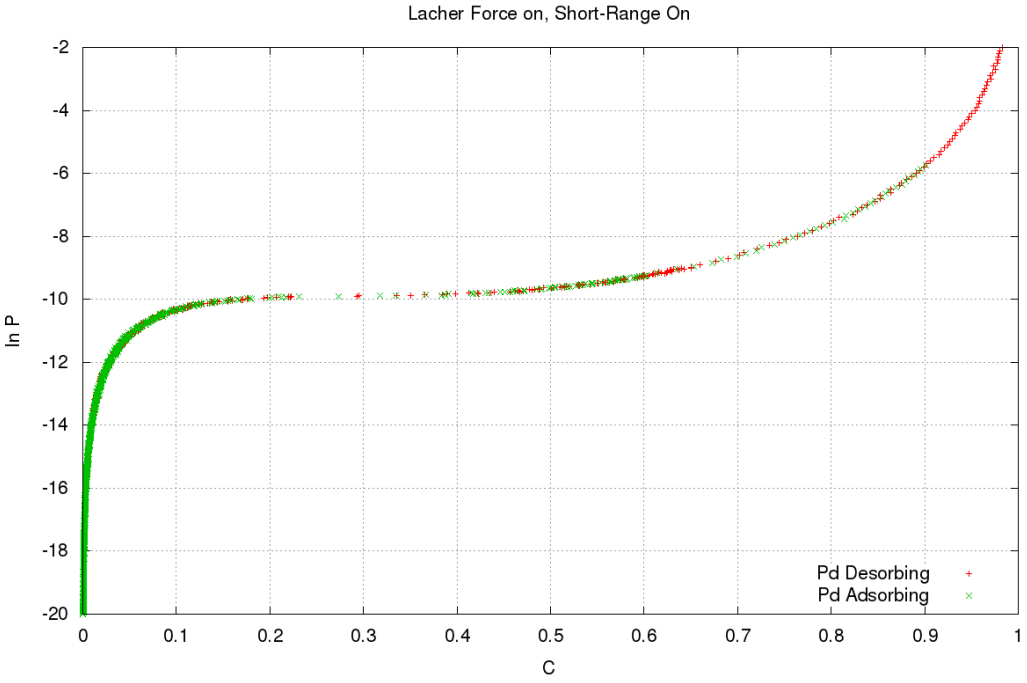

FIGURE 7.6: High ratio L.R:S.R - ad/desorption pressures very similar.

Chapter 8

Diffusion within the Palladium Lattice

8.1 Theoretical Background

In section 2.1.5 it was shown that the chemical diffusion coefficient was defined as

$$D_{chem} = \frac{1}{6} l^2 \Gamma = \frac{-J}{\frac{\partial r}{\partial x}} = \frac{D_t}{(1-r)} \tag{8.1.1}$$

Where

$$D_t = f_t(C) \frac{l^2}{6\tau(r)} = \frac{< r^2 >}{6\tau} \tag{8.1.2}$$

Setting $D_0 = D_t(r=0) = \frac{l^2}{6\tau(r=0)}$

$$D_{chem} = D_0 \frac{d\mu}{dr} = \frac{< r^2 >}{6\tau} \frac{d\mu}{dr} \tag{8.1.3}$$

It is thus easy in a simulation to determine both D_t and thereby D_{chem}. The ordering at any point may be determined by generating a virtual diffraction pattern from a snapshot of the lattice.

Two broad scenarios were investigated, canonical and grand-canonical assemblies looking at ordering.

8.2 Canonical Assembly

Simulations were performed to investigate how the tracer diffusion coefficient relates to ordering processes both with and without long-range forces. D_t and the NNN short-range order parameter clearly illustrate when the lattice reorders fig: 8.1. Fundamentally short-range ordering is better simulated without a strong long-range attraction. When this is present the simulation will still order as without but the anneal times are increased very significantly indeed to the point where they became impractical.

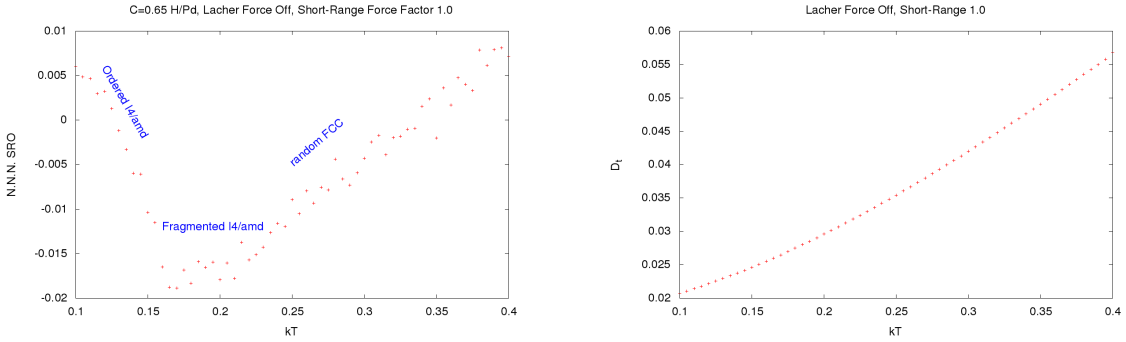

FIGURE 8.1: NNN SRO & D_t around the transition temperatures, Long-Range Force Off, r=0.65 *(scale 600K ∼ kT 0.35)*

In the above run D_t varied smoothly without abrupt change, this was unexpected but consistently reproducible. At lower concentrations the NNN SRO plot failed to rise at low temperature as the system, being only partly filled was unable to form a consistently stable structure fig: 8.2. This was discussed by Blaschko et al [21] in which they postulated that at low temperature microdomains of various Pd_nH would form. The virtual diffraction patterns did indicate a *smearing* of the superlattice points as the temperature fell though no definitive new reflections appeared.

Introducing the long-range attraction dramatically changes the shapes of these plots presumably as the attractive force, being much larger than the repulsive at high concentrations inhibits movement of hydrogen until larger *stresses* have built up at which point dramatic reordering occurs fig: 8.3.

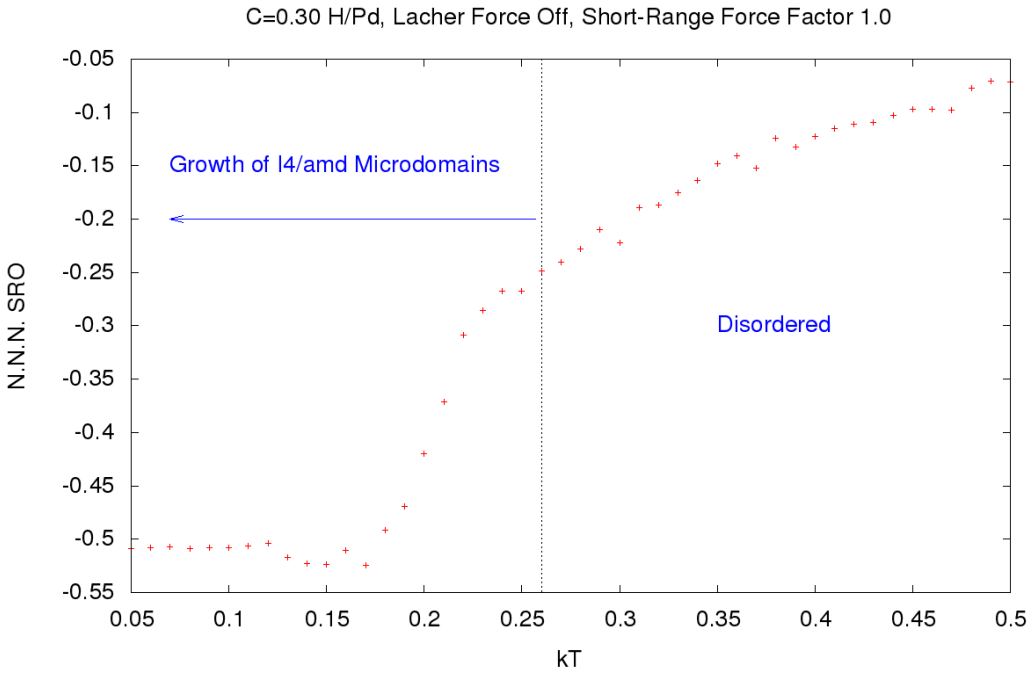

FIGURE 8.2: NNN SRO around the transition temperatures r=0.30. Scale 600K $\sim$ 0.35

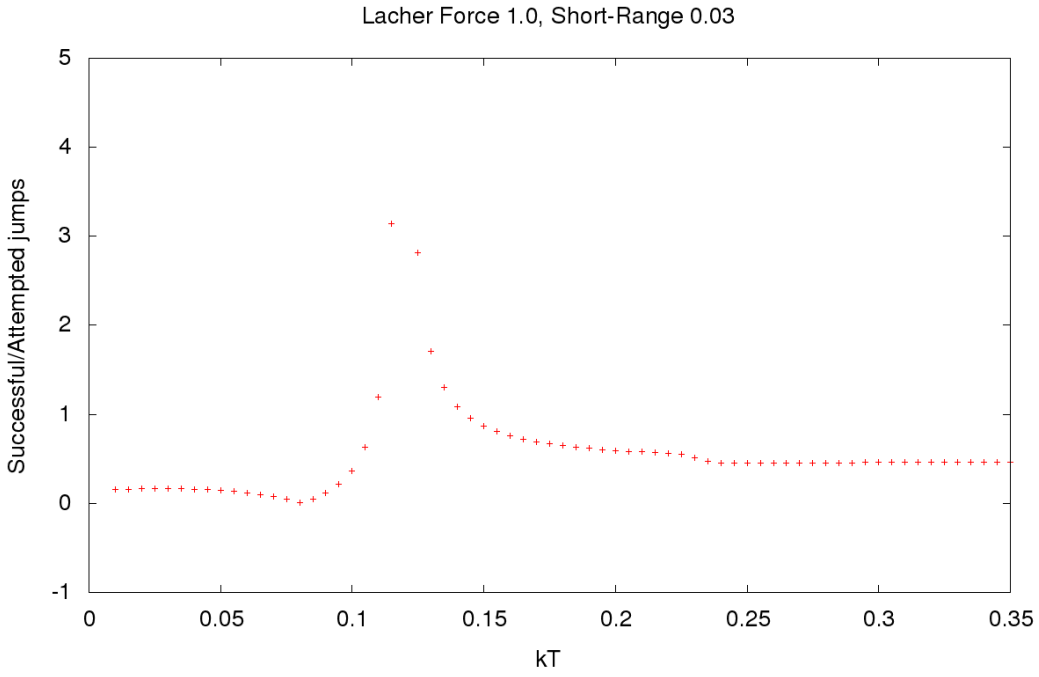

FIGURE 8.3: Successful jump probability around the transition temperatures r=0.65. Scale 600K $\sim$ 0.35- arbitrary vertical scale

Chapter 9

Isotopic Effects

9.1 Ab/Desorption Studies

9.1.1 Composition of the External Gases

The manner in which the proportions and energies of the H,D,T external gas mixtures were represented evolved during this work. The code was developed from the outset to permit differing chemical potentials to be applied to H_2, HD, D_2 and so on. It may be presumed that the chemical potential of a gas phase of a H_2, HD and D_2 mixture depends only on P_{H_2}..

$$\mu_H = \frac{1}{2}(\mu^0_{H_2} + RT\ln(P_{H_2}) \tag{9.1.1}$$

and

$$\mu_D = \frac{1}{2}\left[\mu^0_{D_2} + RT\ln\left(P_{D_2}\right)\right] \tag{9.1.2}$$

Given that

$$\mathrm{H_2} + \mathrm{D_2} \rightleftharpoons 2\mathrm{HD} \tag{9.1.3}$$

thus

$$2\mu_{\mathrm{HD}} - \mu_{\mathrm{H_2}} - \mu_{\mathrm{D_2}} = 0 \tag{9.1.4}$$

Therefore

$$2\mu^0_{\mathrm{HD}} + 2RT\ln\left(P_{\mathrm{HD}}\right) - \left[\mu^0_{\mathrm{H_2}} + RT\ln\left(P_{\mathrm{H_2}}\right)\right] - \left[\mu^0_{\mathrm{D_2}} + RT\ln\left(P_{\mathrm{D_2}}\right)\right] = 0 \tag{9.1.5}$$

thus

$$2\mu^0_{\mathrm{HD}} - \mu^2_{\mathrm{H}_2} - \mu_{\mathrm{D}_2{}^2} = -RT\left(\frac{P^2_{\mathrm{HD}}}{P_{\mathrm{HD}}P_{\mathrm{D}_2}}\right) \tag{9.1.6}$$

therefore

$$\Delta\mu_{\mathrm{H}_2} = RTln\left(P_{\mathrm{H}_2}\right) \tag{9.1.7}$$

Similarly

$$\Delta\mu_{\mathrm{D}_2} = RTln\left(P_{\mathrm{D}_2}\right) \tag{9.1.8}$$

Thus we can neglect the proportion of HD which will form in equilibrium in the gas phase.

9.2 Modelling Isotope Differences

Two effects need to be taken into consideration. The differing chemical potentials of molecules in the external baths and their differing zero point energies in the Pd lattice.

Taking the lattice first. The interaction potential scaling was determined by comparing the mean site potentials from the phase diagram with the transition temperature of 566K allowing them to be converted to meV. To an atom's interaction potential was simply added the zpe from fig:1.8.

In the gas phase a similar process was followed though its validity is more debatable. The program scaled the chemical potentials of HH, DD and TT, which were pressure and temperature dependent to a potential scaled against V_{nn}. Very extensive testing as reported earlier showed that this reproduced the form of the pressure isotherms tolerably well. To these chemical potentials were added isotope specific zpe again taken from fig:1.8. The zpe were fixed i.e. were independent of temperature. This simplification may well not be valid.

Referring to fig: 1.8 the differences in ZPE for a H,D,T atom migrating into or out of the lattice are -32.5 meV, -23 meV and -18.5 meV respectively. This should energetically favour the ingress of $H > D > T$. For movement within the lattice the variation of ZPE $H > D > T$ should lead to higher diffusion rates for the lighter isotopes.

9.3 Canonical Simulations

Introducing zpe appears to have two clear consequences. Whilst phase formation appears unaffected i.e. $I4_1/amd$ at r ~ 0.5 it appears that D and T tend to cluster as in fig: 9.1 . This does not appear to have been reported in the published literature.

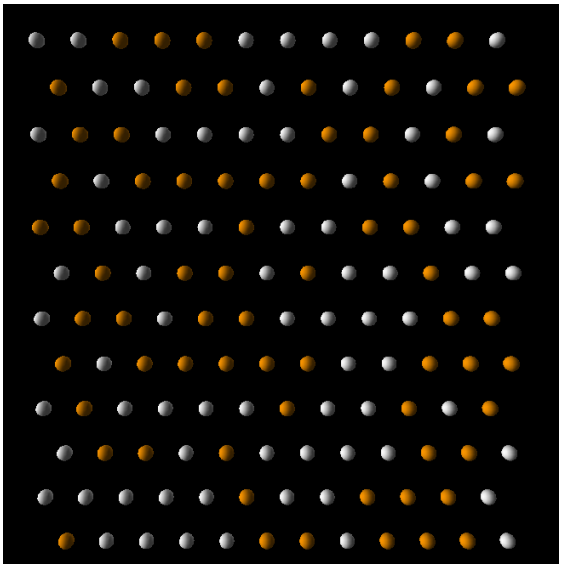

FIGURE 9.1: Clustering of isotopes due to differing ZPE. [420] plane $I4_1/amd$, *protium orange, deuterium white*

Secondly a measure of mean mobility vs concentration plots show the same form with clear signs of dramatic re-ordering at similar temperatures for the three isotopes

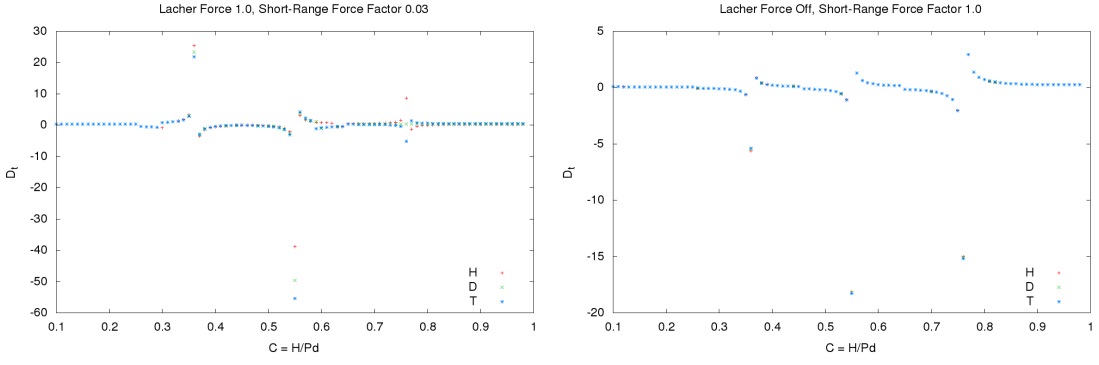

FIGURE 9.2: Canonical simulations, mean mobility vs concentration at T $\sim$ 150K. D_t differs little between the isotopes for differing interaction models.

9.4 Grand Canonical Simulations

Firstly, in the absence of the long-range attractive force which does not reproduce the pressure-composition isotherms well the separation factor α_{HD} varies unusually fig: 9.3-left. With the long-range force active α appears more in line with experiment fig: 9.3-right. This would appear to be further evidence to support the use of a long-range attraction in the modelling.

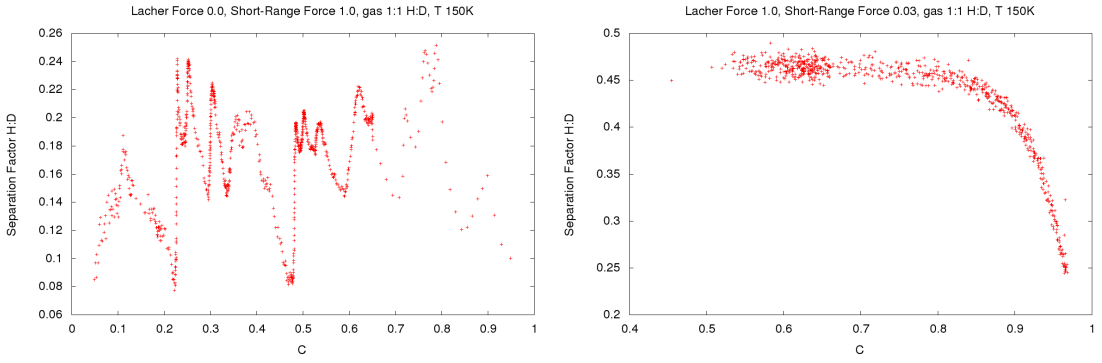

FIGURE 9.3: GCMC α_{HD} vs concentration absorbed from a gas mixture of 1:1 H_2:D_2at T $\sim$ 150K. Without Lacher force - left, with Lacher - right.

9.4.1 Variation of Plateau Pressure with Isotope

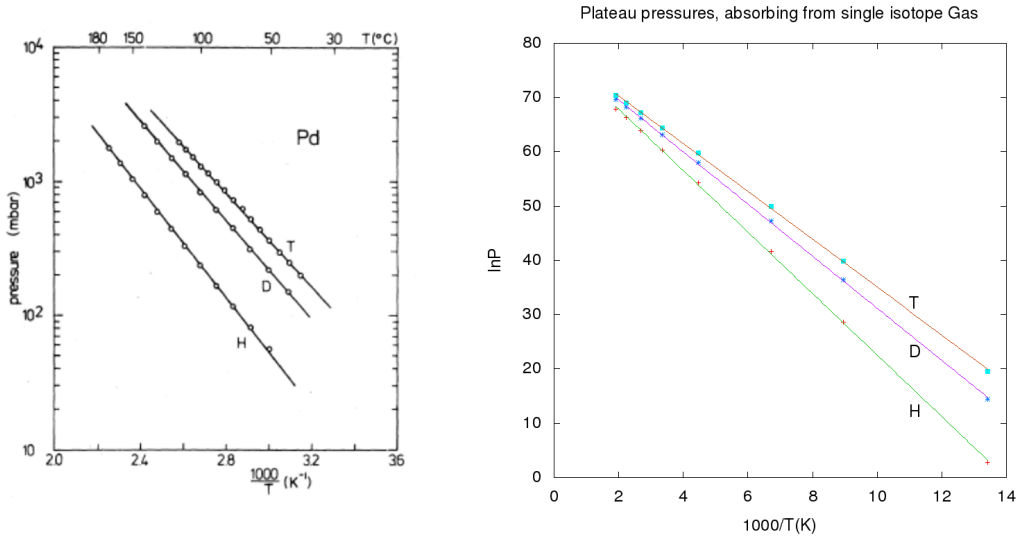

FIGURE 9.4: *Left*- Experimental results Lasser [92] : *Right*- GCMC Simulation: Variation of Plateau Pressure for H,D and T

The model would appear to reproduce experimental results of the variation in plateau pressure in the $\alpha - \beta$ region tolerably well fig:9.4.

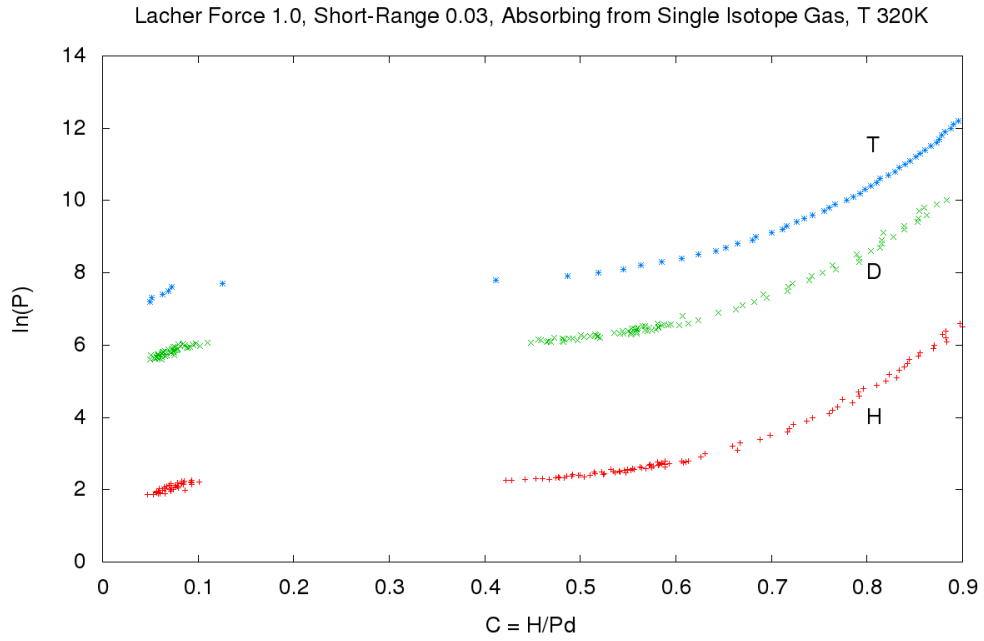

FIGURE 9.5: GCMC Simulation: Variation of Plateau Pressure with H,D,T at 320K.

9.4.2 Variation of Separation Factor with Temperature

The separation factors were measured with a GCMC simulation where the pressure was lowered such that the lattice concentration dropped from a 100% fill of the two isotopes in a 1:1 ratio. The external gas was also at a 1:1 composition. α varied approximately linearly over a temperature range of $\sim$ 100K to 400K though diverged outside this range. This may be compared to the results of Andreev [5] where the figures are obtained over a similarly narrow range fig: 9.7.

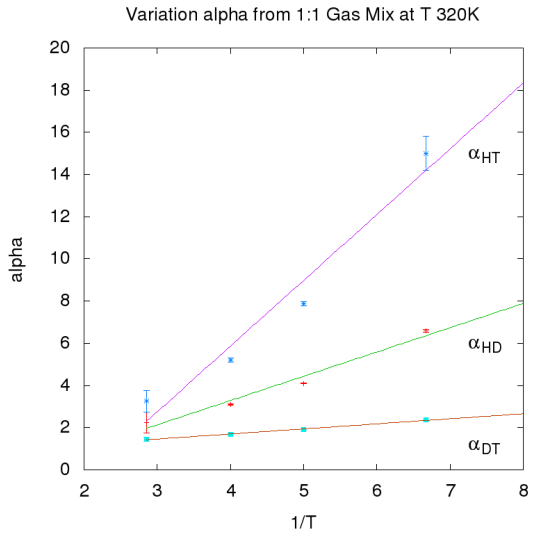

FIGURE 9.6: GCMC Simulation: $\alpha_{x,y}$ with T, reading taken at r=0.7. Absorbing from a gas mixture of 1:1 composition

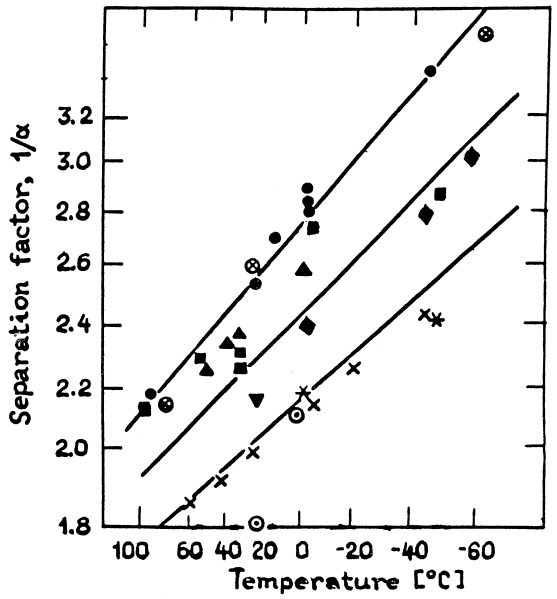

FIGURE 9.7: Experimental variation of α [5]

Chapter 10

Conclusions and Outlook

These studies have developed a simple model of the Pd-H system employing a combination of long-range concentration dependent attractive forces and pairwise repulsive forces out to the fourth nearest neighbour. These has been extensively tested with over 2000 runs at relatively high resolution and lattice size - typically $10^4 \rightarrow 10^5$ atoms. The code from the outset was monolithic; in the sense that the same *engine* was used for all simulations to minimise difference between the differing classes of runs such as GCMC vs CMC. It finally ran to over 4000 lines of Fortran though could be rendered down to about half of that if error checking and test routines were removed.

Programs have also been developed to produce virtual diffraction patterns in 1 and 2d as well as interactive programs to examine the lattice structure in pseudo 3d.

It has been found that a combination of attractive force rather stronger than the repulsive force reproduces the pressure composition isotherms whilst still permitting short-range ordering to occur. It appeared unecessary to extend the short-range repulsion beyond the second nearest neighbour. Most of the expected phase structures appeared but there was no conclusive sign of the Ni_4Mo. However simulated diffraction studies showed signs of an unusual structure faintly forming at $C \sim 0.8H/Pd$. The model did not generate signs of hysteresis in the pressure decomposition curves, this was the be expected. However this is further indication that a more complex model needs to be considered.

Incorporating differing zero point energies for the three isotopes in both the gas and solid phases produced variation in separation factor in-line with experiment. The simulations however produced tracer diffusion coefficients for pure D systems higher than expected.

More generally – what is the purpose of such a model? If the aim is to model pressure-composition the lack of discontinuity in the isotherms implies that short-range ordering may be neglected. In this case one would use the simple long-range attractive forces scaling the model against experimental data. In this modelling at least it has been shown that the long-range attraction has little effect upon short-range ordering aside from dramatically increasing the anneal times. Investigation of ordering therefore may best be performed using short-range forces only. Or a model of long-range attraction more complex than the simple concentration dependent one here. It is reasonable to propose that if the attraction is indeed due to lattice distortion then it should be greater in localised regions of high concentration i.e. have a short-range component.

Appendix A

Some Definitions

A.1 Notes & Definitions

A.1.1 Acoustic vs. optical Phonons:

Acoustic phonons are coherent movements of atoms. Optical phonons occur in solids with more than one type of atom and are characterised by out of phase displacements due to differences in charge or mass. Here two atoms move in opposite directions about a stationary centre of mass.

Chemical Potential of a Gas

$$\mu_H = \frac{1}{2}(\mu^0_{H_2} + RT\ln(P_{H_2}) \tag{A.1.1}$$

ref [53] . Here the approximation $\mu_H = \ln(P_{H_2})$ was used.

Enthalpy

$$H = U + PV \tag{A.1.2}$$

Fick's First Law

for an isotropic medium

$$J = -\left(D_{xx}\frac{\delta C}{\delta x} + D_{yy}\frac{\delta C}{\delta y} + D_{zz}\frac{\delta C}{\delta z}\right) = -D_{ii}\nabla C_i \tag{A.1.3}$$

Fick's Second Law

again for an isotropic medium

$$\frac{\delta C}{\delta t} = D_{xx}\frac{\delta^2 C}{\delta x^2} + D_{yy}\frac{\delta^2 C}{\delta y^2} + D_{zz}\frac{\delta^2 C}{\delta z^2} = D_{ii}\nabla^2 C_i \tag{A.1.4}$$

Fugacity

term for non-ideality of a gas

$$\mu = \mu^0 + RTln\frac{f(P)}{P^0} \tag{A.1.5}$$

where f(P) is the fugacity, the deviation from ideality.

Gibbs Free Energy

$$G = G^0 + RTln\frac{P}{P_0} \tag{A.1.6}$$

where G^0 is the value of G at P_0.

Hamiltonian

The value of the Hamiltonian $\hat{\mathbf{H}}$ in the case of a closed system is the sum of potential and kinetic energies of the system.

Metropolis Algorithm

Transitions down a potential gradient always proceed, only those ascending a potential gradient are probabilistic.

$$p(E_i \rightarrow E_j) = 1 \text{ if } \Delta E \leq 0 \tag{A.1.7}$$

$$p(E_i \rightarrow E_j) = e^{\Delta E_{ij}/k_B T} \text{ if } \Delta E > 0 \tag{A.1.8}$$

Whether a jump occurs is determined here by generating a random number r in the range $0 \rightarrow 1$. If $r < e^{\Delta E_{ij}/k_B T}$ then the jump proceeds.

A.1.2 Molarity

The mole-fraction is defined as

$$\chi_H = \frac{\text{moles of H}}{\text{total no of moles present}} \tag{A.1.9}$$

in this case of an fcc lattice of interstititials equal to the number of palladium atom

$$\chi_H = \frac{N_H}{N_H + N_{Pd}} \tag{A.1.10}$$

Sievert's Law

$C = sP^{1/2}$ where s is the Sievert's Parameter and P the pressure [129] . hence

$$C = se^{1/2\mu} \tag{A.1.11}$$

Separation Factor

defined by Flanagan & Oates [53] as

$$\alpha_{DH} = \frac{(C_g/C_s)_D}{(C_g/C_s)_H} \tag{A.1.12}$$

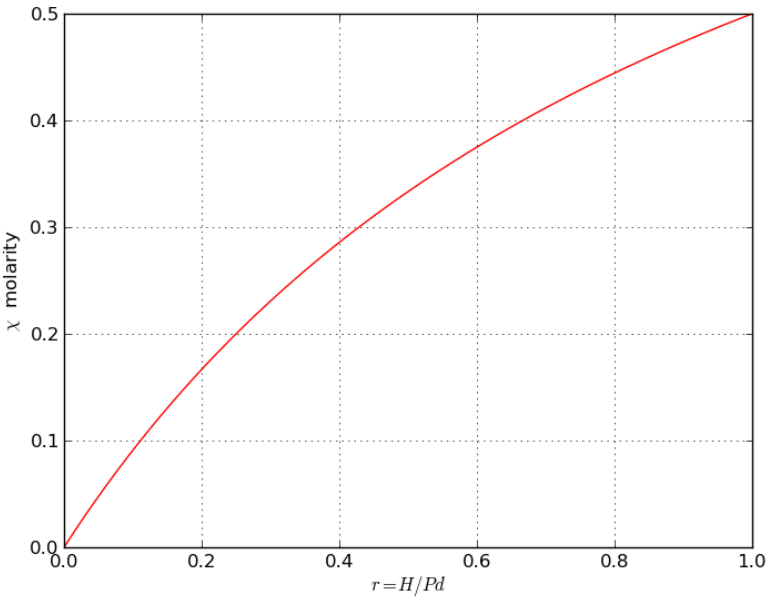

FIGURE A.1: Molarity vs number concentration

where g and s denote the gaseous and solid phases

Tracer Correlation Factor

$$f_t(C) = \frac{< r^2 >}{t_{mcc}} \tag{A.1.13}$$

where t_{mcc} refers to the time elapsed in a Monte Carlo Simulation.

Tracer Diffusion Coefficient

The tracer diffusion coefficient may be determined simply from the ratio of jump attempts to successful jumps [24] $D_t = \frac{nr^2}{2t}$ where n = no of jumps, r= step length (assume=1) and t is the time elapsed. Since t_{mcc} =jump attempts per atom, one may determine

$$D_t = \frac{n_{actual} r^2}{2n_{attempted}} \tag{A.1.14}$$

A.1.3 van't Hoff Equation

The van't Hoff equation relates the equilibrium constant K of a reaction to the temperature and (standard) enthalpy change ΔH^0. Working in moles:-

$$\frac{d \ln K}{dT} = \frac{\Delta H^0}{RT^2} \tag{A.1.15}$$

Warren-Cowley short range order parameter

$$\alpha_{W.C.} = \left[1 - \frac{P_{nn}}{r_H}\right] \tag{A.1.16}$$

where P_{nn} is the mean number of nearest neighbour pairs. This may be extended to P_{nnn} and so on.

Appendix B

Reference Diffractographs

The following virtual diffraction patterns were generated from ideal lattices. Their structure was checked by the use of a 3d viewer, written in Visual Python which enabled one to view either a rotatable 3d image or step though along specified crystal planes such as (4,2,0) to check that they were filled as expected.

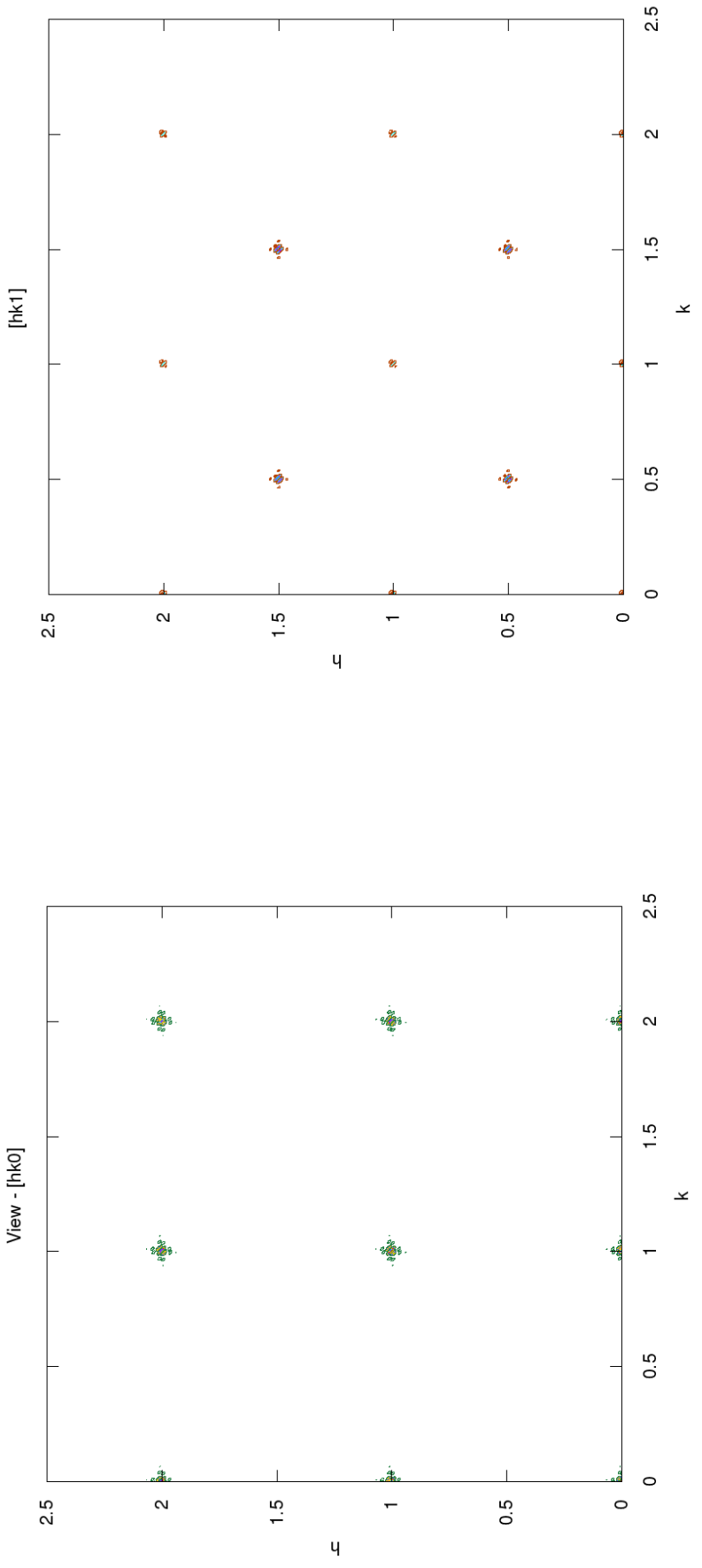

FIGURE B.1: r = 1.0 H/Pd, reference plots in hk0 and hk1

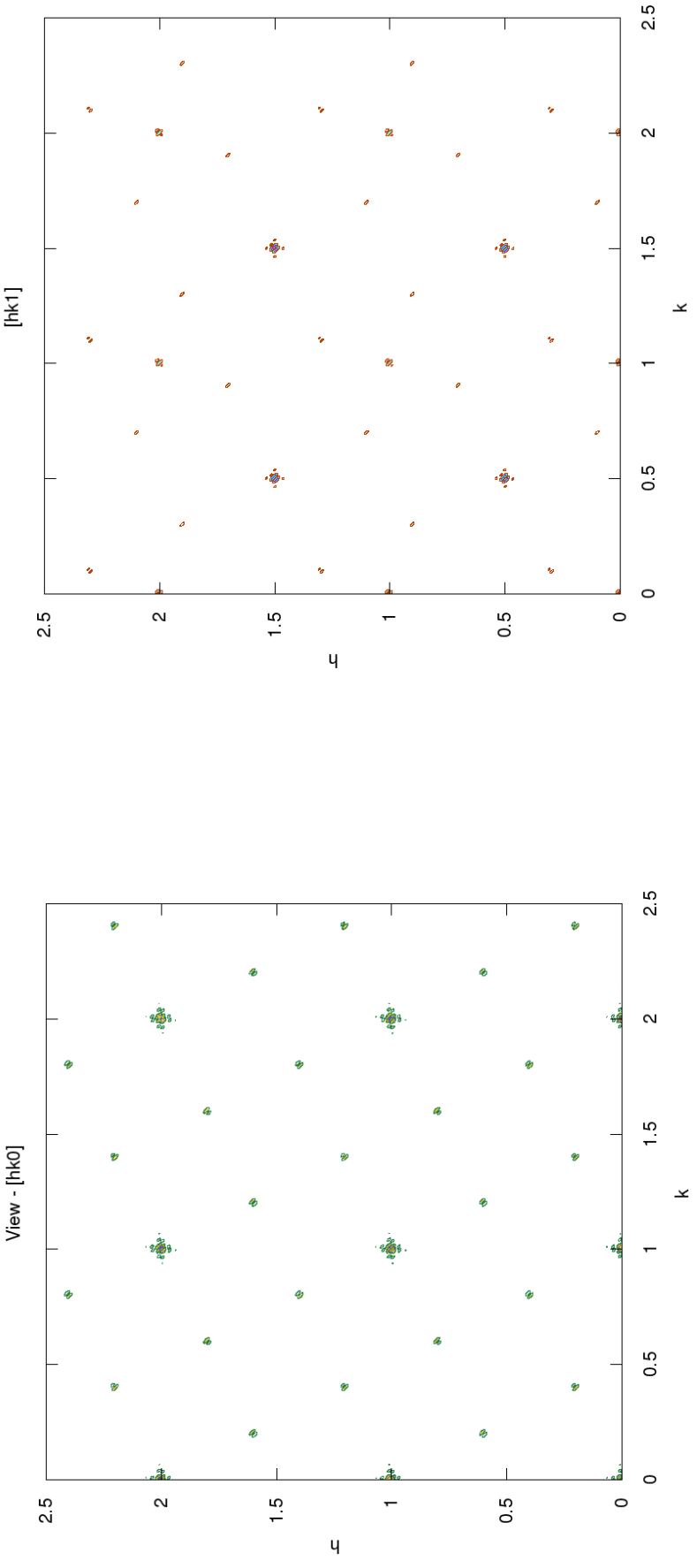

FIGURE B.2: r = 0.80, reference plots $I4/m$– Ni_4Mo

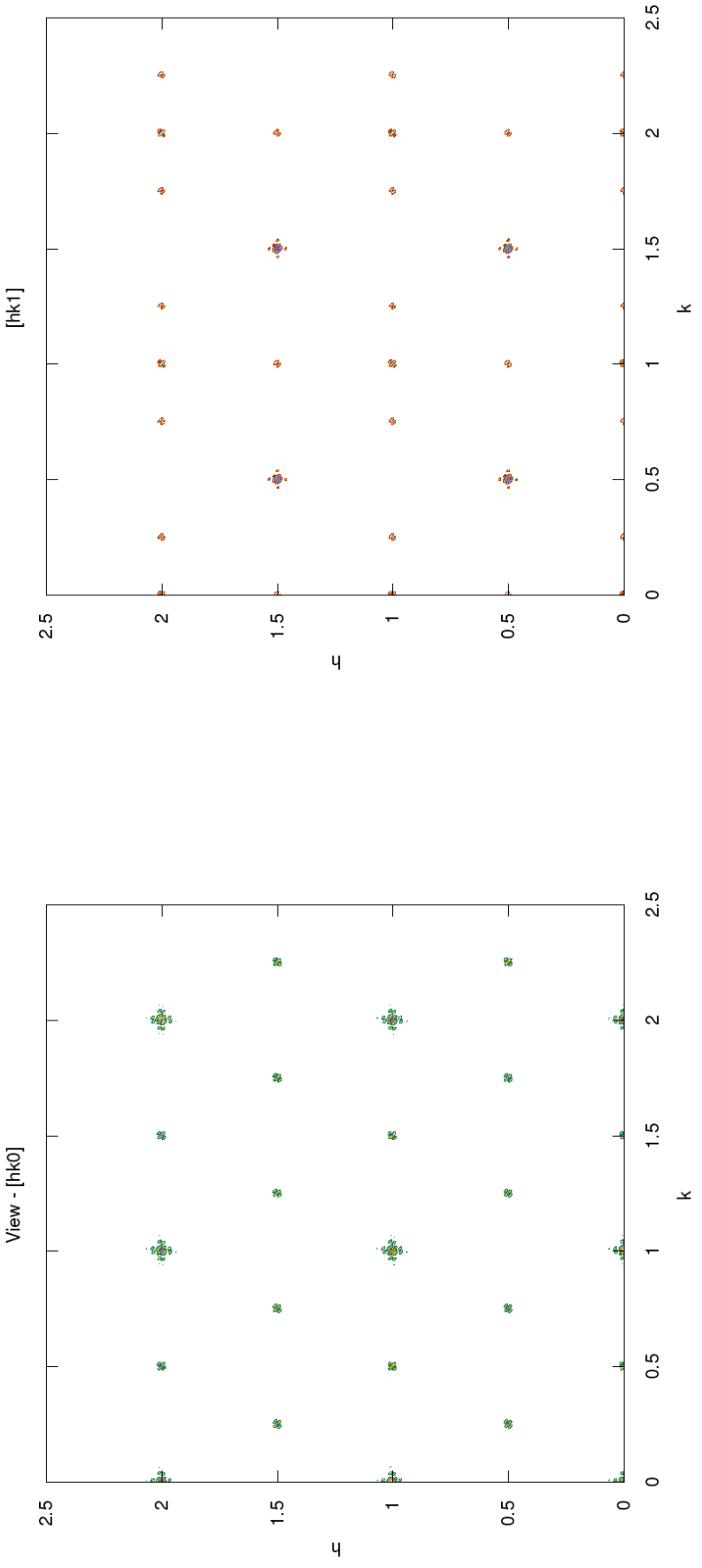

FIGURE B.3: r = 0.75, reference plots $I4/mmm$– Ni_3Mo $D0_{22}$ superlattice reflection at $\left(1, \frac{1}{2}, 0\right)$

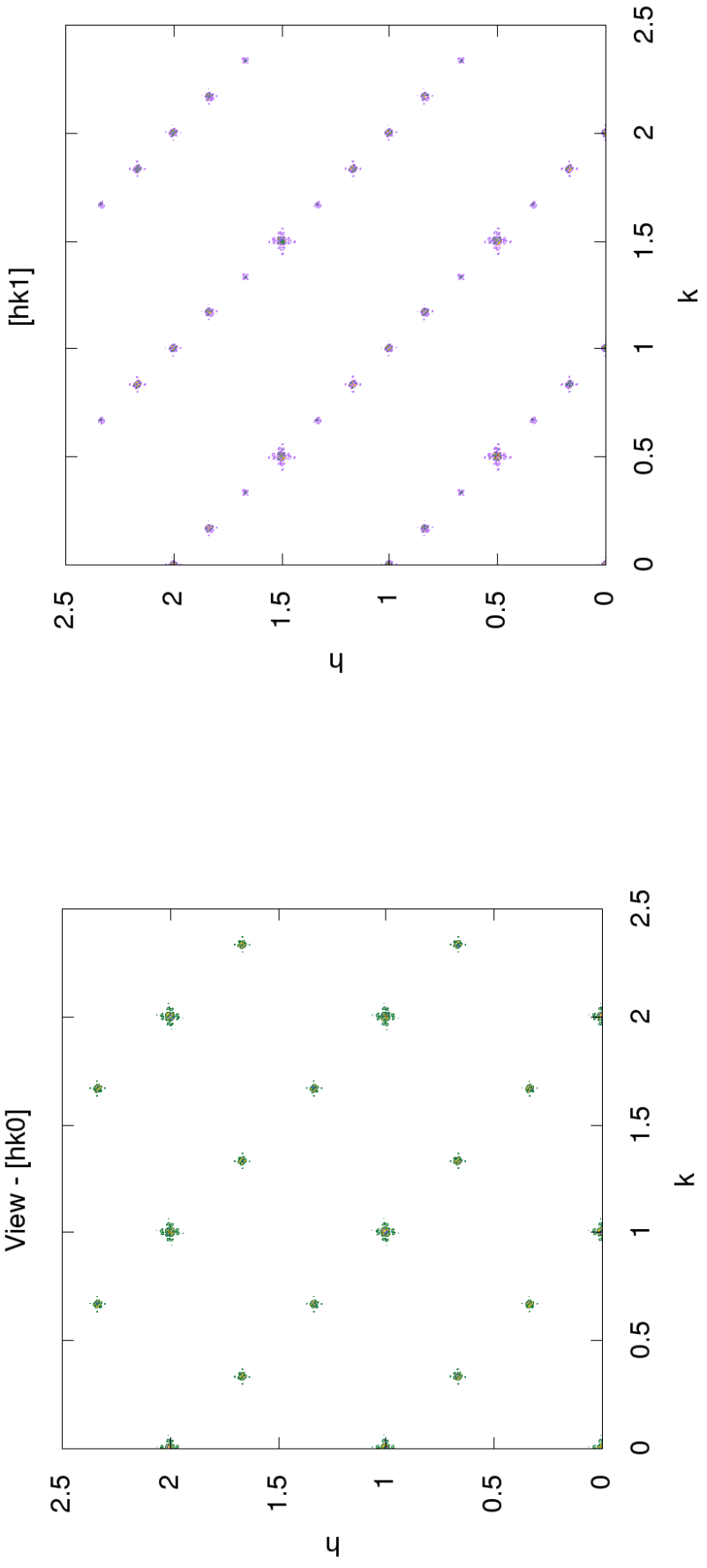

FIGURE B.4: r = 0.67, reference plots, superlattice reflection at $\left(\frac{4}{3}, \frac{2}{3}, 0\right)$

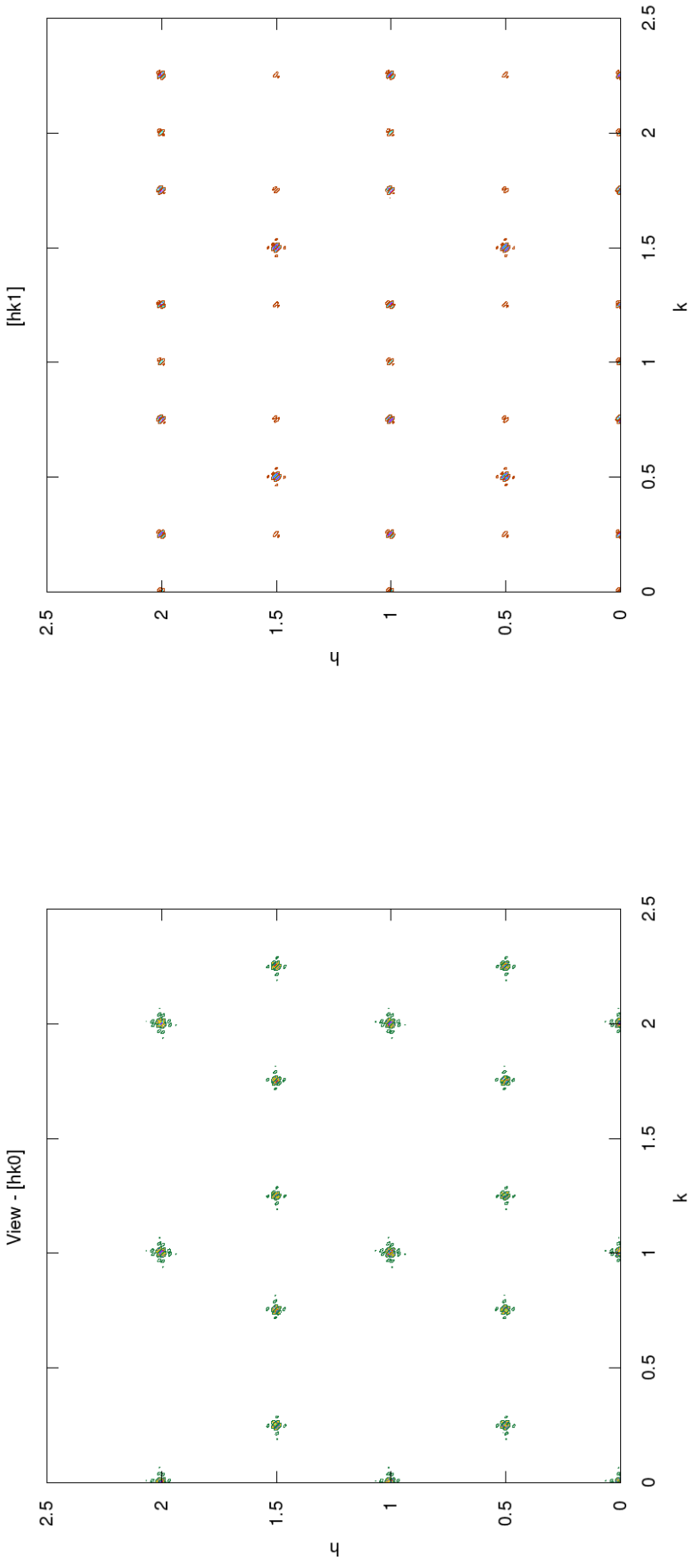

FIGURE B.5: Reference Plot r=0.50, $I4_1/amd$

Appendix C

Program Structure

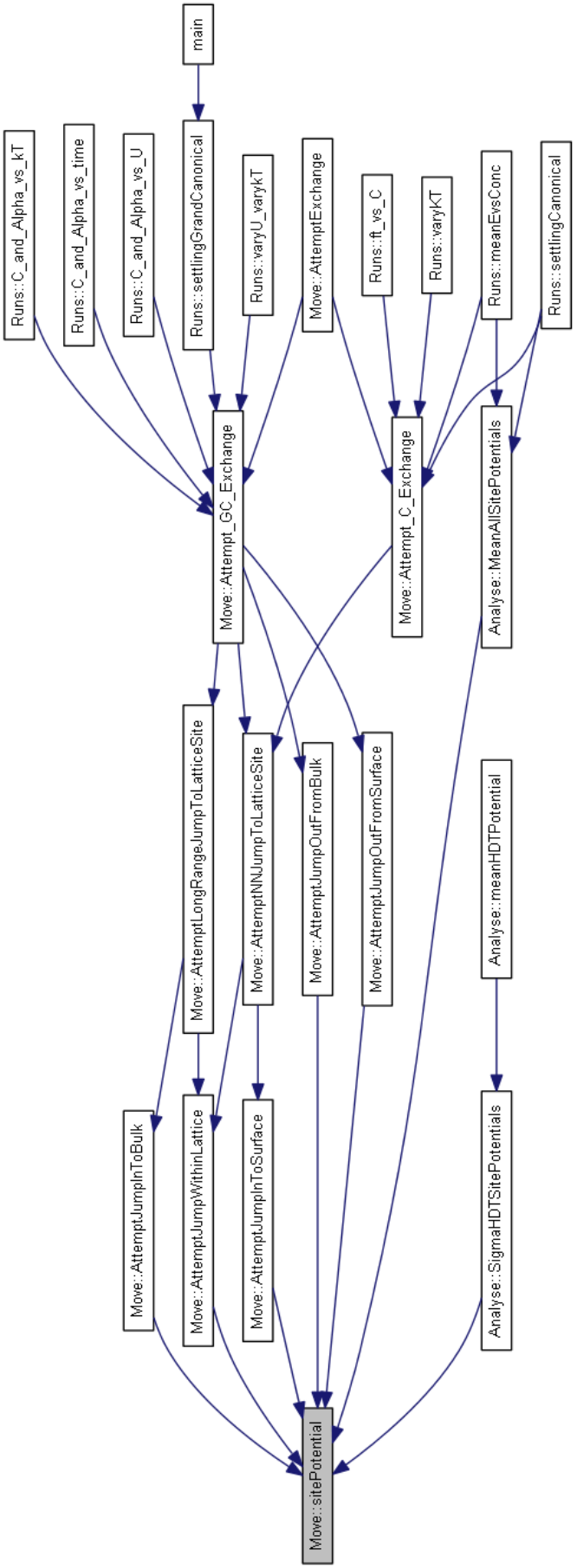

FIGURE C.1: Program Structure

Two lists of publications are presented. The first it the actual bibliography of papers quoted in the thesis. The second is the Further Reading. Both lists are presented numbered and in alphabetic order. The FR is a full data base of publications about the Pd-H system but with the papers quoted in the actual bibliography removed. In the text, the number of the paper is quoted as it appears in the bibliography. Those in the Further Reading do not appear in the text.

Bibliography

[3] G Alefeld. “Phase transitions of hydrogen in metals due to elastic interaction”. In: *Berichte der Bunsengesellschaft fr physikalische Chemie* 76.8 (1972), pp. 746–755.

[4] I S Anderson, D K Ross, and C J Carlile. “The 50K transition in Beta-phase palladium deuteride observed by neutron scattering”. In: *Journal of Physics C: Solid State Physics* 11.9 (1978), p. L381. URL: http://stacks.iop.org/0022-3719/11/i=9/a=005.

[5] B. Andreev. “Separation of Hydrogen Isotopes by Chemical Isotope Exchange in Systems Involving Metal and Intermetallic Compound Hydrides”. In: *Separation Science and Technology* (2001).

[18] K Binder. “Applications of Monte Carlo methods to statistical physics”. In: *Reports on Progress in Physics* 60.5 (1997), p. 487. URL: http://stacks.iop.org/0034-4885/60/i=5/a=001.

[21] O. Blaschko, P. Fratzl, and R. Klemencic. “Model for the structural changes occurring at low temperatures in PdDx”. In: *Phys. Rev. B* 24 (1 1981), pp. 277–282. DOI: 10.1103/PhysRevB.24.277. URL: http://link.aps.org/doi/10.1103/PhysRevB.24.277.

[23] R A Bond and D K Ross. “The use of Monte Carlo simulations in the study of a real lattice gas and its application to the alpha′ Pd-D system”. In: *Journal of Physics F: Metal Physics* 12.4 (1982), p. 597. URL: http://stacks.iop.org/0305-4608/12/i=4/a=003.

[24] R Borg and J Dienes G. *An Introduction to Solid State Diffusion*. Academic Press, Boston, 1988. DOI: 10.1002/bbpc.19900940432.

[28] A Caravella et al. “Sieverts Law Empirical Exponent for Pd-Based Membranes: Critical Analysis in Pure H2 Permeation”. In: *The Journal of Physical Chemistry B* 114.18 (2010), pp. 6033–6047. DOI: 10.1021/jp1006582. eprint: http://pubs.acs.org/doi/pdf/10.1021/jp1006582. URL: http://pubs.acs.org/doi/abs/10.1021/jp1006582.

[45] TE Ellis et al. “Evidence for H (D) Ordering in PDH_x (PDD_x)”. In: *Physical Review Letters* 42.7 (1979), 456–458. ISSN: 0031-9007. DOI: {10.1103/PhysRevLett.42.456}.

[46] C Elsasser et al. “Ab initio pseudopotential calculations of total energies and forces for hydrogen in palladium”. In: *Physica B: Condensed Matter* 172.12 (1991), pp. 217 –224. ISSN: 0921-4526. DOI: 10.1016/0921-4526(91)90434-G. URL: http://www.sciencedirect.com/science/article/pii/092145269190434G.

[53] T B Flanagan and W. A. Oates. “The Palladium-Hydrogen System”. In: *Annual Review of Materials Science* 21.1 (1991), pp. 269–304. DOI: 10.1146/annurev.ms.21.080191.001413. eprint: http://www.annualreviews.org/doi/pdf/10.1146/annurev.ms.21.080191.001413. URL: http://www.annualreviews.org/doi/abs/10.1146/annurev.ms.21.080191.001413.

[55] M Fleischmann and S Pons. “Electrochemically induced nuclear fusion of deuterium”. In: *Journal of Electroanalytical Chemistry and Interfacial Electrochemistry* 261.2, Part 1 (1989), pp. 301 –308. ISSN: 0022-0728. DOI: http://dx.doi.org/10.1016/0022-0728(89)80006-3. URL: http://www.sciencedirect.com/science/article/pii/0022072889800063.

[56] W Friedman. “The Riverbank Publications, Vol 3 (C-25), The Index of Coincidence and its applications in Cryptography”. In: (1998). URL: http://www.amazon.com/The-Riverbank-Publications-Vol-C-25/dp/0894120344.

[61] Josiah Willard Gibbs. *Scientific Papers of J. Willard Gibbs p418*. Longmans, Green and Co., 1906, p. 418.

[64] O Glatter and O Kratky. *Small angle X-ray scattering*. London: Academic Press Inc, 1982.

[73] J K Jacobs and F D Manchester. "Thermal and motional aspects of the 50 K transition in PdH and PdD". In: *Journal of the Less Common Metals* 49.0 (1976), pp. 67 –73. ISSN: 0022-5088. DOI: 10.1016/0022-5088(76)90026-6. URL: http://www.sciencedirect.com/science/article/pii/0022508876900266.

[78] J.M. Joubert and S. Thiebaut. "Thermodynamic description of the Pd-H/D/T System". In: *J of Nuclear Materials* 59.4 (2009), pp. 1680 –1691. ISSN: 1359-6454. DOI: 10.1016/j.actamat.2010.11.035. URL: http://www.sciencedirect.com/science/article/pii/S1359645410007901.

[79] J. Kanamori and Y. Kakehashi. "Conditions for the existence of ordered structure in binary alloy systems". In: *Journal de Physique Colloques 38* (1977).

[81] S W Kelly and C A Sholl. "Theory and Monte Carlo calculation of the tracer correlation factor". In: *Journal of Physics C: Solid State Physics* 20.32 (1987), p. 5293. URL: http://stacks.iop.org/0022-3719/20/i=32/a=015.

[84] C Kittel. *Introduction to Solid State Physic 8th Edition*. Wiley, 2005.

[87] T Kuji et al. "The partial excess thermodynamic properties of hydrogen in palladium". In: *Journal of Physics F: Metal Physics* 13.9 (1983), p. 1785. URL: http://stacks.iop.org/0305-4608/13/i=9/a=007.

[90] J. R. Lacher. "A Theoretical Formula for the Solubility of Hydrogen in Palladium". In: *Proc. R. Soc. Lond* (1937).

[92] R. Lasser. "Palladium-tritium system". In: *Phys. Rev. B* 26 (6 1982), pp. 3517–3519. DOI: 10.1103/PhysRevB.26.3517. URL: http://link.aps.org/doi/10.1103/PhysRevB.26.3517.

[95] R. Lasser and G. L. Powell. "Solubility of H, D, and T in Pd at low concentrations". In: *Phys. Rev. B* 34 (2 1986), pp. 578–586. DOI: 10.1103/PhysRevB.34.578. URL: http://link.aps.org/doi/10.1103/PhysRevB.34.578.

[99] W Luo, D Cowgill, and T Flanagan. "Separation Factors for Hydrogen Isotopes in Palladium Hydride". In: *The Journal of Physical Chemistry C* 117.27 (2013), pp. 13861–13871. DOI: 10.1021/jp4032332. eprint: http://dx.doi.org/10.1021/jp4032332. URL: http://dx.doi.org/10.1021/jp4032332.

[100] S. Majorowski and B. Baranowski. “Diffusion coefficients of hydrogen and deuterium in highly concentrated palladium hydride and deuteride phases”. In: *Journal of Physics and Chemistry of Solids* 43.12 (1982), pp. 1119 –1127. ISSN: 0022-3697. DOI: 10.1016/0022-3697(82)90140-8. URL: http://www.sciencedirect.com/science/article/pii/0022369782901408.

[102] F.D. Manchester, A. San-Martin, and J.M. Pitre. “The H-Pd (hydrogen-palladium) System”. English. In: *Journal of Phase Equilibria* 15.1 (1994), pp. 62–83. ISSN: 1054-9714. DOI: 10.1007/BF02667685. URL: http://dx.doi.org/10.1007/BF02667685.

[107] K. G. McLennan, E. MacA. Gray, and J. F. Dobson. “Deuterium occupation of tetrahedral sites in palladium”. In: *Physical Review B* 78.1 (2008). ISSN: 1098-0121. DOI: {10.1103/PhysRevB.78.014104}.

[111] N. Metropolis et al. “Equations of State Calculations by Fast Computing Machines”. In: *Journal of Chemical Physics* (1953).

[122] M Nishikawa, T Shiraishi, and K Murakami. “Solubility and Separation Factor of Protium-Deuterium Binary Component System in Palladium”. In: *Journal of Nuclear Science and Technology* 33.6 (1996), pp. 504–510. DOI: 10.1080/18811248.1996.9731943. eprint: http://www.tandfonline.com/doi/pdf/10.1080/18811248.1996.9731943. URL: http://www.tandfonline.com/doi/abs/10.1080/18811248.1996.9731943.

[129] R. A. Oriani. “The physical and metallurgical aspects of hydrogen in metals”. In: *in ICCF4, Fourth International Conference on Cold Fusion*. 1993.

[133] A. L. Patterson. “The Scherrer Formula for X-Ray Particle Size Determination”. In: *Phys. Rev.* 56 (10 1939), pp. 978–982. DOI: 10.1103/PhysRev.56.978. URL: http://link.aps.org/doi/10.1103/PhysRev.56.978.

[137] MP Pitt and EM Gray. “Tetrahedral occupancy in the Pd-D system observed by in situ neutron powder diffraction”. English. In: *Europhysics Letters* 64.3 (2003), 344–350. ISSN: 0295-5075. DOI: {10.1209/epl/i2003-00187-x}.

[146] C San Marchi et al. “Solubility of hydrogen and its isotopes in metals from mixed gases”. In: *Journal of Nuclear Materials 372* (2008).

[151] J. E. Schirber and B. Morosin. "Lattice constants of β-PdHx and β-PdDx with x near 1.0". In: *Phys. Rev. B* 12 (1 1975), pp. 117–118. DOI: 10.1103/PhysRevB.12.117. URL: http://link.aps.org/doi/10.1103/PhysRevB.12.117.

[163] G.H. Vineyard. "Frequency factors and isotope effects in solid state rate processes". In: *J. Phys. Chem. Solids.* (1957).

[165] Y Wang, S Sun, and M. Y. Chou. "Total-energy study of hydrogen ordering in PdHx". In: *Phys. Rev. B* 53 (1 1996), pp. 1–4. DOI: 10.1103/PhysRevB.53.1. URL: http://link.aps.org/doi/10.1103/PhysRevB.53.1.

[167] E Wicke and J Blaurock. "New experiments on and interpretations of hysteresis effects of Pd-D2 and Pd-H2". In: *Journal of the Less-Common Metals* (1986).

[168] E Wicke and J Blaurock. "New experiments on and interpretations of hysteresis effects of Pd-D2 and Pd-H2". In: *Journal of the Less Common Metals* 130.0 (1987), pp. 351 –363. ISSN: 0022-5088. DOI: 10.1016/0022-5088(87)90129-9. URL: http://www.sciencedirect.com/science/article/pii/0022508887901299.

[170] B. Widom. "Some Topics in the Theory of Fluids". In: *J. Chem. Phys* (1963). DOI: http://dx.doi.org/10.1063/1.1734110.

[173] D Wilkinson. "Hydrogen-Hydrogen Interactions". PhD thesis. Salford University, 2013.

Further Reading

[1] T Abbas et al. “Calculation of Short Range Order in NiRh, NiPd and CuRh Alloys”. In: *Materials Science-Poland, Vol. 25, No. 4* (2007).

[2] G J Ackland. “Calculation of free energies from ab initio calculation”. In: *Journal of Physics: Condensed Matter* 14.11 (2002), p. 2975. URL: http://stacks.iop.org/0953-8984/14/i=11/a=311.

[6] B. Andreyev et al. “Isotopic effects in hydrogen-intermetallic compound systems”. In: *Journal of the Less Common Metals* 90.2 (1983), pp. 161 –168. ISSN: 0022-5088. DOI: 10.1016/0022-5088(83)90066-8. URL: http://www.sciencedirect.com/science/article/pii/0022508883900668.

[7] V. E. Antonov et al. “Neutron spectroscopy of H impurities in PdD: Covibrations of the H and D atoms”. In: *Phys. Rev. B* 80 (13 2009), p. 134302. DOI: 10.1103/PhysRevB.80.134302. URL: http://link.aps.org/doi/10.1103/PhysRevB.80.134302.

[8] R Baierlein. “The elusive chemical potential”. In: *American Journal of Physics* 69.4 (2001), pp. 423–434. DOI: 10.1119/1.1336839. URL: http://link.aip.org/link/?AJP/69/423/1.

[9] I S Balbaa and F D Manchester. “Superconductivity of PdH_x in relation to its phase diagram. I. Magnetic measurements”. In: *Journal of Physics F: Metal Physics* 13.2 (1983), p. 395. URL: http://stacks.iop.org/0305-4608/13/i=2/a=016.

[10] I S Balbaa, A J Pindor, and F D Manchester. “Superconductivity of PdH_x in relation to its phase diagram. II. Specific heat measurements and the form of the $T_c(X)$ relaxation”. In: *Journal of Physics F: Metal Physics* 14.11 (1984), p. 2637. URL: http://stacks.iop.org/0305-4608/14/i=11/a=019.

[11] B Baranowski, S Majchrzak, and T Flanagan. "The volume increase of fcc metals and alloys due to interstitial hydrogen over a wide range of hydrogen contents". In: *Journal of Physics F: Metal Physics* 1.3 (1971), p. 258. URL: http://stacks.iop.org/0305-4608/1/i=3/a=307.

[12] J Barber. "Simulation of X-ray Diffraction Patterns". In: *Los Alamos National Laboratory* (2010). URL: www.lanl.gov/orgs/adtsc/publications.php.

[13] R Bass et al. "Configuration-independent elastic interactions in metal-hydrogen solutions". In: *Journal of Physics F: Metal Physics* 14.12 (1984), p. 2869. URL: http://stacks.iop.org/0305-4608/14/i=12/a=010.

[14] S.Z. Baykara. "Theoretical evaluation of diffusivity of hydrogen in palladium and rhodium". In: *International Journal of Hydrogen Energy* 29.15 (2004), pp. 1631 –1636. ISSN: 0360-3199. DOI: 10.1016/j.ijhydene.2004.02.015. URL: http://www.sciencedirect.com/science/article/pii/S036031990400093X.

[15] W Betteridge and J Hope. "The Separation of Hydrogen from Gas Mixtures". In: *Platinum Metals Review* 19 (1975), pp. 50–59.

[16] K Beyerlein. "Simulation of the Powder Diffraction pattern from Nanoparticles - Studying the Influence of Surface Strain". PhD thesis. Georgia Institute of Technology, 2011.

[17] S Billinge. "Nanoscale structural order from the atomic pair distribution function: There's plenty of room in the middle". In: *Journal of Solid State Chemistry* 181.7 (2008), pp. 1695 –1700. ISSN: 0022-4596. DOI: http://dx.doi.org/10.1016/j.jssc.2008.06.046. URL: http://www.sciencedirect.com/science/article/pii/S0022459608003460.

[19] K. Binder. "Monte Carlo study of entropy for face-centered cubic Ising antiferromagnets". English. In: *Zeitschrift fr Physik B Condensed Matter* 45.1 (1981), pp. 61–69. ISSN: 0722-3277. DOI: 10.1007/BF01294277. URL: http://dx.doi.org/10.1007/BF01294277.

[20] K. Binder. "Ordering of the Face-Centered-Cubic Lattice with Nearest-Neighbor Interaction". In: *Phys. Rev. Lett.* 45 (10 1980), pp. 811–814. DOI: 10.1103/PhysRevLett.45.811. URL: http://link.aps.org/doi/10.1103/PhysRevLett.45.811.

[22] A Blomqvist et al. “Significance of Self-Trapping on Hydrogen Diffusion”. In: *Phys. Rev. Lett.* 105 (18 2010), p. 185901. DOI: 10.1103/PhysRevLett.105.185901. URL: http://link.aps.org/doi/10.1103/PhysRevLett.105.185901.

[25] F. M. Bulnes, V. D. Pereyra, and J. L. Riccardo. “Collective surface diffusion: n-fold way kinetic Monte Carlo simulation”. In: *Phys. Rev. E* 58.1 (1998), pp. 86–92. DOI: 10.1103/PhysRevE.58.86.

[26] Burch. “The Form of the Interaction between Hydrogen and Palladium”. In: *Platinum Metals Rev., 1971* (1971).

[27] R Caputo and A Alavi. “Where do the H atoms reside in PdH_x systems?” In: *Molecular Physics* 101.11 (2003), pp. 1781–1787. URL: http://dx.doi.org/10.1080/0026897031000094489.

[29] S. Chen et al. “A lattice gas model with temperature”. In: *Physica D: Nonlinear Phenomena* 37.13 (1989), pp. 42 –59. ISSN: 0167-2789. DOI: 10.1016/0167-2789(89)90116-4. URL: http://www.sciencedirect.com/science/article/pii/0167278989901164.

[30] O. B. Christensen et al. “H-H interactions in Pd”. In: *Phys. Rev. B* 40 (3 1989), pp. 1993–1996. DOI: 10.1103/PhysRevB.40.1993. URL: http://link.aps.org/doi/10.1103/PhysRevB.40.1993.

[31] P Clapp and S Moss. “Correlation Functions of Disordered Binary Alloys. I”. In: *Phys. Rev.* 142 (2 1966), pp. 418–427. DOI: 10.1103/PhysRev.142.418. URL: http://link.aps.org/doi/10.1103/PhysRev.142.418.

[32] P Clapp and S. C. Moss. “Correlation Functions of Disordered Binary Alloys. II”. In: *Phys. Rev.* 171 (3 1968), pp. 754–763. DOI: 10.1103/PhysRev.171.754. URL: http://link.aps.org/doi/10.1103/PhysRev.171.754.

[33] S P Coleman, D E Spearot, and L Capolungo. “Virtual diffraction analysis of Ni [010] symmetric tilt grain boundaries”. In: *Modelling and Simulation in Materials Science and Engineering* 21.5 (2013), p. 055020. URL: http://stacks.iop.org/0965-0393/21/i=5/a=055020.

[34] J. M. Cowley and A. P. Pogany. “Diffuse scattering in electron diffraction patterns. I. General theory and computational methods”. In: *Acta Crystallographica Section A* 24.1 (1968), pp. 109–116. DOI: 10.1107/S0567739468000148. URL: http://dx.doi.org/10.1107/S0567739468000148.

[35] M. Cyrott et al. “Effect of Short Range Order On the Electronic Structure of Disordered Transition Alloys”. In: *J. Phys. Colloques* 38.C7 (1977), pp. C7–285–C7–288. DOI: 10.1051/jphyscol:1977757. URL: http://dx.doi.org/10.1051/jphyscol:1977757.

[36] G Czarnecki et al. “Tracer diffusion of particles with soft-core interactions studied by Monte Carlo simulations”. In: *Journal of Physics A: Mathematical and General* 29.13 (1996), p. 3367. URL: http://stacks.iop.org/0305-4470/29/i=13/a=012.

[37] D De Fontaine. “Cluster Approach to Order-Disorder Transformations in Alloys”. In: ed. by H Ehrenreich and D Turnbull. Vol. 47. Solid State Physics. Academic Press, 1994, pp. 33 –176. DOI: 10.1016/S0081-1947(08)60639-6. URL: http://www.sciencedirect.com/science/article/pii/S0081194708606396.

[38] D De Fontaine. “Configurational Thermodynamics of Solid Solutions”. In: ed. by Frederick Seitz Henry Ehrenreich and David Turnbull. Vol. 34. Solid State Physics. Academic Press, 1979, pp. 73 –274. DOI: 10.1016/S0081-1947(08)60360-4. URL: http://www.sciencedirect.com/science/article/pii/S0081194708603604.

[39] N Deveau, Yi Hua Ma, and R Datta. “Beyond Sieverts’ law: A comprehensive microkinetic model of hydrogen permeation in dense metal membranes”. In: *Journal of Membrane Science* 437.0 (2013), pp. 298 –311. ISSN: 0376-7388. DOI: http://dx.doi.org/10.1016/j.memsci.2013.02.047. URL: http://www.sciencedirect.com/science/article/pii/S0376738813001749.

[40] H. T. Diep et al. “Phase Diagrams in f.c.c. Binary Alloys: Frustration Effects”. In: *European Physics Letters* 2.8 (1986), p. 603. URL: http://stacks.iop.org/0295-5075/2/i=8/a=006.

[41] S. Dietrich and H. Wagner. “Model calculation for the incoherent phase-transition in the palladium-hydrogen system”. English. In: *Zeitschrift fr Physik B Condensed Matter* 36.2 (1979), pp. 121–126. ISSN: 0722-3277. DOI: 10.1007/BF01320212. URL: http://dx.doi.org/10.1007/BF01320212.

[42] M. L. Doyle and I. R. Harris. “Palladium rare Earth Alloys, their order disorder transformations and behaviour with Hydrogen”. In: *Platinum Metals Review* 32 (1988), pp. 130–1404.

[43] B Dunlap et al. “Linear Combination of Gaussian-Type Orbitals Local-Density-Functional Cluster Studies of D-D Interactions in Titanium and Palladium”. In: *Physical Review B* (1990).

[44] Y Ebisuzaki, W Kass, and M O’Keeffe. “Solubility and Diffusion of Hydrogen and Deuterium in Platinum”. In: *Journal of Chemical Physics* (1968).

[47] C. Elsasser et al. “Range of forces on host-metal atoms around interstitial hydrogen in Pd and Nb”. In: *Phys. Rev. B* 50 (8 1994), pp. 5155–5159. DOI: 10.1103/PhysRevB.50.5155. URL: http://link.aps.org/doi/10.1103/PhysRevB.50.5155.

[48] C Elsasser et al. “Vibrational states for hydrogen in palladium”. In: *Physical Review B* 44.18 (1991), 10377–10380. ISSN: 0163-1829. DOI: {10.1103/PhysRevB.44.10377}.

[49] I Errea, M Calandra, and F Mauri. “First-Principles Theory of Anharmonicity and the Inverse Isotope Effect in Superconducting Palladium-Hydride Compounds”. In: *Phys. Rev. Lett.* 111 (17 2013), p. 177002. DOI: 10.1103/PhysRevLett.111.177002. URL: http://link.aps.org/doi/10.1103/PhysRevLett.111.177002.

[50] J. Evans, I.R. Harris, and D.K. Ross. “A proposed method of hydrogen isotope separation using palladium alloy membranes”. In: *Journal of the Less Common Metals* 89.2 (1983), pp. 407 –414. ISSN: 0022-5088. DOI: 10.1016/0022-5088(83)90350-8. URL: http://www.sciencedirect.com/science/article/pii/0022508883903508.

[51] Fernandes et al. “Monte Carlo simulations of two-dimensional hard core lattice gases”. In: *The Journal of Chemical Physics* (2006).

[52] T Flanagan, W. Luo, and J.D. Clewley. “Calorimetric enthalpies of absorption and desorption of protium and deuterium by palladium”. In: *Journal of the Less Common Metals* 172174, Part A.0 (1991), pp. 42 –55. ISSN: 0022-5088. DOI: 10.1016/0022-5088(91)90431-3. URL: http://www.sciencedirect.com/science/article/pii/0022508891904313.

[54] T.B. Flanagan and Y. Sakamoto. “Hydrogen in disordered and ordered palladium alloys”. In: *International Journal of Hydrogen Energy* 19.2 (1994), pp. 151 –159. ISSN: 0360-3199. DOI: 10.1016/0360-3199(94)90120-1. URL: http://www.sciencedirect.com/science/article/pii/0360319994901201.

[57] S Fukada, K Fuchinoue, and M Nishikawa. “Isotope separation factor and isotopic exchange rate between hydrogen and deuterium of palladium”. In: *Journal of nuclear materials* 226.3 (1995), pp. 311–318.

[58] Y Fukai and K Nobuyuki. “Evidence of Copious Vacancy Formation in Ni and Pd under a High Hydrogen Pressure”. In: *Japanese Journal of Applied Physics* 32.9A (1993), p. L1256. URL: http://stacks.iop.org/1347-4065/32/i=9A/a=L1256.

[59] Y Fukai et al. “Formation of superabundant vacancies in PdH alloys”. In: *Journal of Alloys and Compounds* 313.12 (2000), pp. 121 –132. ISSN: 0925-8388. DOI: http://dx.doi.org/10.1016/S0925-8388(00)01195-6. URL: http://www.sciencedirect.com/science/article/pii/S0925838800011956.

[60] B. Fultz. “Vibrational thermodynamics of materials”. In: *Progress in Materials Science* 55.4 (2010), pp. 247 –352. ISSN: 0079-6425. DOI: http://dx.doi.org/10.1016/j.pmatsci.2009.05.002. URL: http://www.sciencedirect.com/science/article/pii/S0079642509000577.

[62] M J Gillan. “A simulation model for hydrogen in palladium. I. Single-particle dynamics”. In: *Journal of Physics C: Solid State Physics* 19.31 (1986), p. 6169. URL: http://stacks.iop.org/0022-3719/19/i=31/a=012.

[63] M J Gillan. “A simulation model for hydrogen in palladium. II. Mobility and thermotransport”. In: *Journal of Physics C: Solid State Physics* 20.4 (1987), p. 521. URL: http://stacks.iop.org/0022-3719/20/i=4/a=005.

[65] A Gro. “Ab Initio Molecular Dynamics Simulations of the Adsorption of H2 on Palladium Surfaces”. In: *ChemPhysChem* 11.7 (2010), pp. 1374–1381. ISSN: 1439-7641. DOI: 10.1002/cphc.200900818. URL: http://dx.doi.org/10.1002/cphc.200900818.

[66] S Hata et al. “Short range order and its transformation to long range order in Ni_4Mo”. In: *Acta Materialia* 46.3 (1998), pp. 881 –892. ISSN: 1359-6454. DOI: 10.1016/S1359-6454(97)00314-5. URL: http://www.sciencedirect.com/science/article/pii/S1359645497003145.

[67] F. J. Higuera and J. Jimnez. “Boltzmann Approach to Lattice Gas Simulations”. In: *Europhysics Letters* 9.7 (1989), p. 663. URL: http://stacks.iop.org/0295-5075/9/i=7/a=009.

[68] H Horner and H Wagner. "A model calculation for the alpha-alpha' phase transition in metal-hydrogen systems". In: *Journal of Physics C: Solid State Physics* 7.18 (1974), p. 3305. URL: http://stacks.iop.org/0022-3719/7/i=18/a=014.

[69] D. K. Hsu and R. G. Leisure. "Elastic constants of palladium and beta-phase palladium hydride between 4 and 300 K". In: *Phys. Rev. B* 20 (4 1979), pp. 1339–1344. DOI: 10.1103/PhysRevB.20.1339. URL: http://link.aps.org/doi/10.1103/PhysRevB.20.1339.

[70] K Irikura. "Experimental Vibrational Zero-Point Energies: Diatomic Molecules". In: *Journal of Physical and Chemical Reference Data, Volume 36, Issue 2, pp. 389-397* 38.3 (2007), pp. 749–749. DOI: 10.1063/1.3167794. URL: http://link.aip.org/link/?JPR/38/749/1.

[71] L.E. Isaeva et al. "Dynamic stability of palladium hydride: An ab initio study". In: *International Journal of Hydrogen Energy* 36.1 (2011), pp. 1254 –1258. ISSN: 0360-3199. DOI: 10.1016/j.ijhydene.2010.06.130. URL: http://www.sciencedirect.com/science/article/pii/S0360319910014540.

[72] J K Jacobs and F D Manchester. "The 50K transition in palladium hydrogen alloys. II. Specific heat and thermal relaxation". In: *Journal of Physics F: Metal Physics* 7.1 (1977), p. 23. URL: http://stacks.iop.org/0305-4608/7/i=1/a=013.

[74] HC Jamieson, GC Weatherly, and FD Manchester. "Beta-Alpha-Phase Transformation in Palladium-Hydrogen Alloys". English. In: *Journal of the Less Common Metals* 50.1 (1976), 85–102. ISSN: 0022-5088. DOI: {10.1016/0022-5088(76)90255-1}.

[75] E T Jaynes. "Gibbs vs Boltzmann Entropies". In: *American Journal of Physics* 33.5 (1965), p. 391. URL: http://link.aip.org/link/?AJPIAS/33/391/1.

[76] D. E. Jiang and Emily A. Carter. "Diffusion of interstitial hydrogen into and through bcc Fe from first principles". In: *Phys. Rev. B* 70 (6 2004), p. 064102. DOI: 10.1103/PhysRevB.70.064102. URL: http://link.aps.org/doi/10.1103/PhysRevB.70.064102.

[77] M. Johansson et al. “Hydrogen adsorption on palladium and palladium hydride at 1 bar”. In: *Surface Science* 604.78 (2010), pp. 718 –729. ISSN: 0039-6028. DOI: http://dx.doi.org/10.1016/j.susc.2010.01.023. URL: http://www.sciencedirect.com/science/article/pii/S0039602810000385.

[80] H. Katsuta, R.J. Farraro, and R.B. McLellan. “The diffusivity of Hydrogen in palladium”. In: *Acta Metallurgica* 27.7 (1979), pp. 1111 –1114. ISSN: 0001-6160. DOI: 10.1016/0001-6160(79)90128-7. URL: http://www.sciencedirect.com/science/article/pii/0001616079901287.

[82] M. Kemali et al. “Inelastic Neutron Scattering Measurements and Ab Initio Calculations of Hydrogen in Single-Crystal Palladium”. In: *Phys. Rev. Lett.* 84 (7 2000), pp. 1531–1534. DOI: 10.1103/PhysRevLett.84.1531. URL: http://link.aps.org/doi/10.1103/PhysRevLett.84.1531.

[83] A. Kerrache et al. “Monte-Carlo simulation of order-disorder kinetics in 2D and fcc binary alloys”. In: *Computational Materials Science* 17.2-4 (2000), pp. 324 –330. ISSN: 0927-0256. DOI: DOI:10.1016/S0927-0256(00)00046-X. URL: http://www.sciencedirect.com/science/article/pii/S092702560000046X.

[85] B Klein and R Cohen. “Anharmonicity and the inverse isotope effect in the palladium-hydrogen system”. In: *Phys. Rev. B* 45 (21 1992), pp. 12405–12414. DOI: 10.1103/PhysRevB.45.12405. URL: http://link.aps.org/doi/10.1103/PhysRevB.45.12405.

[86] P Kowalczyk and J. M. D MacElroy. “Equilibrium Properties of Dense Hydrogen Isotope Gases Based on the Theory of Simple Fluids”. In: *The Journal of Physical Chemistry B* 110.30 (2006), pp. 14971–14975. DOI: 10.1021/jp062593r. eprint: http://pubs.acs.org/doi/pdf/10.1021/jp062593r. URL: http://pubs.acs.org/doi/abs/10.1021/jp062593r.

[88] U.D. Kulkarni. “Monte Carlo simulation of ordering transformations in NiMo-based alloys”. In: *Acta Materialia* 52.9 (2004), pp. 2721 –2732. ISSN: 1359-6454. DOI: 10.1016/j.actamat.2004.02.020. URL: http://www.sciencedirect.com/science/article/pii/S1359645404001065.

[89] H Kurokawa et al. “Monte Carlo simulation of hydrogen absorption in palladium and palladium-silver alloys”. In: *Catalysis Today* 82 (2003), pp. 233 – 240. ISSN: 0920-5861. DOI: 10.1016/S0920-5861(03)00237-2. URL: http://www.sciencedirect.com/science/article/pii/S0920586103002372.

[91] J. R. Lacher. “The Statistics of the Hydrogen-Palladium System”. In: *Mathematical Proceedings of the Cambridge Philosophical Society* 33 (04 Sept. 1937), pp. 518–523. ISSN: 1469-8064. DOI: 10.1017/S0305004100077641. URL: http://journals.cambridge.org/article_S0305004100077641.

[93] R. Lasser. “Solubility of protium, deuterium, and tritium in the alpha phase of palladium”. In: *Phys. Rev. B* 29 (8 1984), pp. 4765–4768. DOI: 10.1103/PhysRevB.29.4765. URL: http://link.aps.org/doi/10.1103/PhysRevB.29.4765.

[94] R. Lasser and K Klatt. “Solubility of hydrogen isotopes in palladium”. In: *Phys. Rev. B* 28.2 (1983), pp. 748–758. DOI: 10.1103/PhysRevB.28.748.

[96] F.A. Lewis. “The Palladium-Hydrogen System A Survey of Hydride Formation and the Effects of Hydrogen Contained within the Metal Lattices”. In: *Platinum Metals Review* (1982).

[97] Y. Lin. “Atomistic modeling of nano-materials: From classical to ab initio simulations in different timescales”. PhD thesis. Rice University, 2008.

[98] T Luo and J Lloyd. “Grand Canonical Monte Carlo Simulation of Hydrogen Adsorption in Different Carbon Nano Structures”. In: *International Journal of Energy for a Clean Environment* 10.1-4 (2009), pp. 37–56. ISSN: 2150-3621.

[101] F.D. Manchester. “Lattice gas aspects of metal-hydrogen system”. In: *Journal of the Less Common Metals* 49.0 (1976). Hydrogen in metals, pp. 1 –12. ISSN: 0022-5088. DOI: 10.1016/0022-5088(76)90021-7. URL: http://www.sciencedirect.com/science/article/pii/0022508876900217.

[103] W. Maysenholder. “On the Determination of Interaction Parameters from Correlations in Binary Alloys”. In: *physica status solidi (b)* 139.2 (1987), pp. 399–408. ISSN: 1521-3951. DOI: 10.1002/pssb.2221390207. URL: http://dx.doi.org/10.1002/pssb.2221390207.

[104] B. C. McAlister and B. P. Grady. "Simulation of Small-Angle X-ray Scattering from Single-Particle Systems". In: *Journal of Applied Crystallography* 31.4 (1998), pp. 594–599. DOI: 10.1107/S0021889898002192. URL: http://dx.doi.org/10.1107/S0021889898002192.

[105] R. A. McKee. "Site blocking and correlated defect motion in tracer and chemical diffusion". In: *Phys. Rev. B* 21 (10 1980), pp. 4269–4281. DOI: 10.1103/PhysRevB.21.4269. URL: http://link.aps.org/doi/10.1103/PhysRevB.21.4269.

[106] M. W. McKergow et al. "Interatomic Potentials and Lattice Distortions in PdD0.8*". In: *Zeitschrift fr Physikalische Chemie* 2 (), 159169. DOI: 10.1524/zpch.1985.146.2.159. URL: http://www.degruyter.com/view/j/zpch.1985.146.issue-2/zpch.1985.146.2.159/zpch.1985.146.2.159.xml.

[108] H. Mehrer, A. Seeger, and E. Steiner. "The Relationship between Correlation Factor and Isotope Effect of Diffusion in Crystals". In: *physica status solidi (b)* 73.1 (1976), pp. 131–140. ISSN: 1521-3951. DOI: 10.1002/pssb.2220730110. URL: http://dx.doi.org/10.1002/pssb.2220730110.

[109] H Meirovitch. "Computer simulation study of hysteresis and free energy in the fcc Ising antiferromagnet". In: *Phys. Rev. B* 30 (5 1984), pp. 2866–2874. DOI: 10.1103/PhysRevB.30.2866. URL: http://link.aps.org/doi/10.1103/PhysRevB.30.2866.

[110] H Meirovitch. "Methods for estimating entropy with computer simulation: the simple cubic Ising lattice". In: *Journal of Physics A: Mathematical and General* 16.4 (1983), p. 839. URL: http://stacks.iop.org/0305-4470/16/i=4/a=020.

[112] T Mohri and W. A. Oates. "CVM-based calculation of the Pd-H Phase Diagram in the High Temperature Region". In: *Material Transactions V13* (2002).

[113] T Mohri and W. A. Oates. "Theoretical investigation of PdH phase equilibria by the cluster variation method". In: *Journal of Alloys and Compounds* 330332.0 (2002). Proceedings of the International Symposium on Metal-Hydrogen Systems, Fundamentals and Applications (MH2000), pp. 14 –19. ISSN: 0925-8388. DOI: 10.1016/S0925-8388(01)01663-2. URL: http://www.sciencedirect.com/science/article/pii/S0925838801016632.

[114] S. C. Moss and P Clapp. "Correlation Functions of Disordered Binary Alloys. III". In: *Phys. Rev.* 171 (3 1968), pp. 764–777. DOI: 10.1103/PhysRev.171.764. URL: http://link.aps.org/doi/10.1103/PhysRev.171.764.

[115] F. Muguet and P Bassez-Muguet. "Ab initio computations of one and two hydrogen or deuterium atoms in the palladium tetrahedral site". In: *Journal of Fusion Energy* (1990).

[116] M. Muller and J.J. de Pablo. "Simulation Techniques for Calculating Free Energies". In: *Computer Simulations in Condensed Matter Systems: From Materials to Chemical Biology Volume 1*. Ed. by Mauro Ferrario, Giovanni Ciccotti, and Kurt Binder. Vol. 703. Lecture Notes in Physics. Springer Berlin Heidelberg, 2006, pp. 67–126. ISBN: 978-3-540-35270-9. DOI: 10.1007/3-540-35273-2_3. URL: http://dx.doi.org/10.1007/3-540-35273-2_3.

[117] S. Muller. "First-Principles Based Multiscale Modelling of Alloys". In: *Multiscale Simulation Methods in Molecular Science* (2009).

[118] G.E. Murch and R.J. Thorn. "Computer simulation of the chemical potential". In: *Conference on computer simulation for materials applications* (1976).

[119] G. Nelin. "A Neutron Diffraction Study of Palladium Hydride". In: *physica status solidi (b)* 45.2 (1971), pp. 527–536. ISSN: 1521-3951. DOI: 10.1002/pssb.2220450215. URL: http://dx.doi.org/10.1002/pssb.2220450215.

[120] J. Nicol. "Inelastic neutron scattering studies of the interaction of hydrogen with palladium black". In: *Surface Science* 197.12 (1988), pp. 67 –80. ISSN: 0039-6028. DOI: 10.1016/0039-6028(88)90573-0. URL: http://www.sciencedirect.com/science/article/pii/0039602888905730.

[121] M Nilsson and S Rasmussen. "Cellular Automata for Simulating Molecular Self-Assembly." In: *DMCS*. 2003, pp. 31–42.

[123] M. Noureddine et al. "Study of quenched impurities effect on order-disorder phase transition by Monte-Carlo method". In: *Moroccan Journal of Condensed Matter* 9.0 (2011).

[124] W. A. Oates and T. Flanagan. "The Reaction of Hydrogen Atoms with Palladium and its Alloys". In: *Canadian Journal of Chemistry* 53.5 (1975), pp. 694–701. DOI: 10.1139/v75-097. eprint: http://www.nrcresearchpress.com/doi/pdf/10.1139/v75-097. URL: http://www.nrcresearchpress.com/doi/abs/10.1139/v75-097.

[125] W. A. Oates and Ted B Flanagan. "Thermodynamic properties of regular interstitial solutions". In: *Journal of Materials Science* 16.12 (1981), pp. 3235–3243.

[126] W. A. Oates and A. M. Stoneham. "Strain-induced interaction energies between hydrogen atoms in palladium". In: *Journal of Physics F: Metal Physics* 13.11 (1983), p. 2427. URL: http://stacks.iop.org/0305-4608/13/i=11/a=023.

[127] W. A. Oates and H. Wenzl. "On the formation and ordering of superabundant vacancies in palladium due to hydrogen absorption". In: *Scripta Metallurgica et Materialia* 33.2 (1995), pp. 185 –193. ISSN: 0956-716X. DOI: http://dx.doi.org/10.1016/0956-716X(95)00159-S. URL: http://www.sciencedirect.com/science/article/pii/0956716X9500159S.

[128] W. A. Oates et al. "The effect of isotopic substitution on the thermodynamic properties of palladium-hydrogen alloys". In: *Journal of Physics and Chemistry of Solids* 47.4 (1986), pp. 429 –434. ISSN: 0022-3697. DOI: 10.1016/0022-3697(86)90036-3. URL: http://www.sciencedirect.com/science/article/pii/0022369786900363.

[130] P Orondo. "Basic Physics Model for PdH Thermodynamics". In: *preprint* (unknown).

[131] T. M. Ortiz, B. A. Meyer, and A. Razani. "Empirical Correlation of Equilibrium Separation Factors in the Pd-H2/D2 System with Temperature and Composition". In: *Journal of Chemical and Engineering Data* 45.1 (2000), pp. 120–123. DOI: 10.1021/je990199z. eprint: http://pubs.acs.org/doi/pdf/10.1021/je990199z. URL: http://pubs.acs.org/doi/abs/10.1021/je990199z.

[132] E. Pantos and J Bordas. "Supercomputer simulation of small angle x-ray scattering, electron micrographs and x-ray diffraction patterns of macromolecular structure". In: *J.Pure and Appl. Chem. 66: 77-82* (1994).

[134] A. Pendzig and W. Dieterich. "Constant Pressure Simulations of Lattice Gas Models". In: *J Chemical Physics* (1996). DOI: 10.1063/1.473438.

[135] J.K. Percus. "Free energy, entropy, and lattice gas representations". In: *Physica A: Statistical Mechanics and its Applications* 283.34 (2000), pp. 369 –387. ISSN: 0378-4371. DOI: 10.1016/S0378-4371(00)00118-7. URL: http://www.sciencedirect.com/science/article/pii/S0378437100001187.

[136] D.J. Picton et al. "The influence of H-H interactions on the phase diagram of PdH". In: *Journal of the Less Common Metals* 88.1 (1982). International Symposium on the Properties and Applications of Metal Hydrides, pp. 133 – 140. ISSN: 0022-5088. DOI: 10.1016/0022-5088(82)90023-6. URL: http://www.sciencedirect.com/science/article/pii/0022508882900236.

[138] D K Ross. "Strong anisotropy in the inelastic neutron scattering from PdH at high energy transfer". In: *Phys. Rev. B* (1998).

[139] J. M. Rowe et al. "Isotope Effects in the PdH System: Lattice Dynamics of $PdT_{0.7}$". In: *Phys. Rev. Lett.* 57 (23 1986), pp. 2955–2958. DOI: 10.1103/PhysRevLett.57.2955. URL: http://link.aps.org/doi/10.1103/PhysRevLett.57.2955.

[140] J. M. Rowe et al. "Lattice Dynamics of a Single Crystal of $PdD_{0.63}$". In: *Phys. Rev. Lett.* 33 (21 1974), pp. 1297–1300. DOI: 10.1103/PhysRevLett.33.1297. URL: http://link.aps.org/doi/10.1103/PhysRevLett.33.1297.

[141] J. M. Rowe et al. "Neutron Quasielastic Scattering Study of Hydrogen Diffusion in a Single Crystal of Palladium". In: *Phys. Rev. Lett.* 29 (18 1972), pp. 1250–1253. DOI: 10.1103/PhysRevLett.29.1250. URL: http://link.aps.org/doi/10.1103/PhysRevLett.29.1250.

[142] M. Ruda, E.A. Crespo, and S. Ramos de Debiaggi. "Atomistic modeling of H absorption in Pd nanoparticles". In: *Journal of Alloys and Compounds* 495.2 (2010). 15th International Symposium on Metastable, Amorphous and Nanostructured Materials, pp. 471 –475. ISSN: 0925-8388. DOI: 10.1016/j.jallcom.2009.10.064. URL: http://www.sciencedirect.com/science/article/pii/S0925838809020404.

[143] J. J. Rush, J. M. Rowe, and D. Richter. "Dynamics of dilute H in Beta-phase palladium deuteride: A novel mass defect". In: *Phys. Rev. B* 31 (9 1985), pp. 6102–6103. DOI: 10.1103/PhysRevB.31.6102. URL: http://link.aps.org/doi/10.1103/PhysRevB.31.6102.

[144] Y Sakamoto et al. “Calorimetric enthalpies for palladium - hydrogen (deuterium) systems at H(D) contents up to about [H]([D])/[Pd] = 0.86”. In: *Journal of Physics: Condensed Matter* 8.18 (1996), p. 3229. URL: http://stacks.iop.org/0953-8984/8/i=18/a=015.

[145] E. Salomons. “Elastic interaction of hydrogen in palladium studied by molecular-dynamics simulation”. In: *Phys. Rev. B* 42 (2 1990), pp. 1183–1188. DOI: 10.1103/PhysRevB.42.1183. URL: http://link.aps.org/doi/10.1103/PhysRevB.42.1183.

[147] J. M. Sanchez and D. de Fontaine. “Ordering in fcc lattices with first- and second-neighbor interactions”. In: *Phys. Rev. B* 21 (1 1980), pp. 216–228. DOI: 10.1103/PhysRevB.21.216. URL: http://link.aps.org/doi/10.1103/PhysRevB.21.216.

[148] J. M. Sanchez, V. Pierron-Bohnes, and F. Mejía-Lira. “Reciprocal-space analysis of short-range-order intensities by the cluster-variation method”. In: *Phys. Rev. B* 51.6 (1995), pp. 3429–3437. DOI: 10.1103/PhysRevB.51.3429.

[149] K Sato, S Takizawa, and T Mohri. “On-the-Fly Kinetic Monte Carlo Simulation of Atomic Diffusion in L10 Structure.” In: *Materials Transactions, Vol. 52, No. 3* (2011).

[150] A.B. Sazonov and .P. Magomedbekov. “Concentration dependence of the separation factor of hydrogen isotopes in ternary and pseudoternary systems H2-H-X-Y-H”. English. In: *Atomic Energy* 87.1 (1999), pp. 519–525. ISSN: 1063-4258. DOI: 10.1007/BF02673212. URL: http://dx.doi.org/10.1007/BF02673212.

[152] V. F. Sears and S. A. Shelley. “Debye-Waller factor for elemental crystals”. In: *Acta Crystallographica Section A* 47.4 (1991), pp. 441–446. DOI: 10.1107/S0108767391002970. URL: http://dx.doi.org/10.1107/S0108767391002970.

[153] M. Shamsuddin. “Hydrogen interaction in palladium alloys”. In: *Journal of the Less Common Metals* 154.2 (1989), pp. 285 –294. ISSN: 0022-5088. DOI: 10.1016/0022-5088(89)90214-2. URL: http://www.sciencedirect.com/science/article/pii/0022508889902142.

[154] N Shohoji. “Statistical thermodynamic aspects of hydrogen in metals”. In: *Surface and Coatings Technology* 28.3 (1986), pp. 365–382.

[155] G Sicking, P Albers, and E Magomedbekov. "Hydrogen isotope exchange and separation in gas-solid phase systems". In: *Journal of the Less Common Metals* 89.2 (1983), pp. 373 –391. ISSN: 0022-5088. DOI: 10.1016/0022-5088(83)90347-8. URL: http://www.sciencedirect.com/science/article/pii/0022508883903478.

[156] M Sluiter. "Introducing distant interactions in the cluster variation method". In: *Computational Materials Science* 2.2 (1994), pp. 293 –300. ISSN: 0927-0256. DOI: 10.1016/0927-0256(94)90111-2. URL: http://www.sciencedirect.com/science/article/pii/0927025694901112.

[157] S.Matar. "Intermetallic hydrides: A review with ab initio aspects". In: *Progress in Solid State Chemistry* (2010).

[158] L.I Smirnov and D.A Pronchenko. "Chemical potential and phase diagrams of hydrogen in palladium". In: *International Journal of Hydrogen Energy* 27.78 (2002). Proceedings of the Selected Papers of the Third International Con ference on Hydrogen Treatment of Materials, HTM-2001, pp. 825 –828. ISSN: 0360-3199. DOI: 10.1016/S0360-3199(01)00105-7. URL: http://www.sciencedirect.com/science/article/pii/S0360319901001057.

[159] B. Smit and D. Frenkel. "Calculation of the chemical potential in the Gibbs ensemble". In: *Molecular Physics* 68.4 (1989), pp. 951–958. DOI: 10.1080/00268978900102651. eprint: http://www.tandfonline.com/doi/pdf/10.1080/00268978900102651. URL: http://www.tandfonline.com/doi/abs/10.1080/00268978900102651.

[160] W Smith and M Lisal. "Direct Monte Carlo simulation methods for nonreacting and reacting systems at fixed total internal energy or enthalpy". In: *Physical Review E 66* (2002).

[161] M Tkacz and A Litwiniuk. "Useful equations of state of hydrogen and deuterium". In: *Journal of Alloys and Compounds* (2002).

[162] J. Tobochnik, H. Gould, and J. Machta. "Understanding temperature and chemical potential using computer simulations". In: *Am. J. Phys* (2005). DOI: 10.1119/1.1834923. URL: http://arxiv.org/abs/physics/0411161v1.

[164] A. van de Walle and G. Ceder. "First-principles computation of the vibrational entropy of ordered and disordered Pd_3V". In: *Phys. Rev. B* 61 (9 2000), pp. 5972–5978. DOI: 10.1103/PhysRevB.61.5972. URL: http://link.aps.org/doi/10.1103/PhysRevB.61.5972.

[166] C. T. White et al. “D-D (H-H) Interactions within the Interstices of Pd”. In: *Japanese Journal of Applied Physics* 30.Part 1, No. 1 (1991), pp. 182–189. DOI: 10.1143/JJAP.30.182. URL: http://jjap.jsap.jp/link?JJAP/30/182/.

[169] E. Wicke, H. Brodowsky, and H. Zuchner. “Hydrogen in palladium and palladium alloys”. English. In: *Hydrogen in Metals II*. Ed. by Georg Alefeld and Johann Vlkl. Vol. 29. Topics in Applied Physics. Springer Berlin Heidelberg, 1978, pp. 73–155. ISBN: 978-3-540-08883-7. DOI: 10.1007/3-540-08883-0_19. URL: http://dx.doi.org/10.1007/3-540-08883-0_19.

[171] T. Wieder. “A generalized Debye scattering formula and the Hankel transform”. In: *Zeitschrift Naturforschung Teil A* 54 (1999), pp. 124–130.

[172] T. Wieder. “The Debye scattering formula in n dimensions”. In: *Journal of Mathematical and Computational Science* 2 (2012), pp. 1086–1090.

[174] E. Wintersberger et al. “Algorithms for the calculation of X-ray diffraction patterns from finite element data”. In: *Journal of Applied Crystallography* 43.6 (2010), pp. 1287–1299. DOI: 10.1107/S0021889810032802. URL: http://dx.doi.org/10.1107/S0021889810032802.

[175] R. Wolf et al. “Pressure-composition isotherms for palladium hydride”. In: *Phys. Rev. B* 48 (17 1993), pp. 12415–12418. DOI: 10.1103/PhysRevB.48.12415. URL: http://link.aps.org/doi/10.1103/PhysRevB.48.12415.

[176] K. Wyrzykowski and B. Baranowski. “Pressure-concentration isotherms of PdHx thin films up to 0.2 GPa of gaseous Hydrogen”. In: *Journal of the Less Common Metals* 141.1 (1988), pp. 73 –81. ISSN: 0022-5088. DOI: 10.1016/0022-5088(88)90212-3. URL: http://www.sciencedirect.com/science/article/pii/0022508888902123.

[177] W. Yen-Chang and J. Chen andS. Fang. “Determination of Curie Temperature, Short Range Order Parameter and Number of Nearest Neighbors of Palladium Atomes to Iron Atoms in Paladium-Iron Alloys by Resistivity Measurement”. In: *Chinese Journal of Physics, vol. 11, Issue 2, p.13* (1973).

[178] X.W. Zhou et al. “An embedded-atom method interatomic potential for Pd-H alloys”. In: *Journal of Materials Research* 23 (03 Mar. 2008), pp. 704–718. ISSN: 2044-5326. DOI: 10.1557/JMR.2008.0090. URL: http://journals.cambridge.org/article_S0884291400028016.

[179] H Zuchner. “Ewald Wicke and his work on metal-hydrogen systems”. In: *Journal of Alloys and Compounds* 332.0 (2002). Proceedings of the International Symposium on Metal-Hydrogen Systems, Fundamentals and Applications (MH2000), pp. 2 –7. ISSN: 0925-8388. DOI: 10.1016/S0925-8388(01)01516-X. URL: http://www.sciencedirect.com/science/article/pii/S092583880101516X.